FACULTY
OF MECHANICAL
ENGINEERING
CTU IN PRAGUE

Department of Automotive, Combustion Engine and Railway Engineering

MASTER'S THESIS

FUEL SYSTEM FOR A GAS ENGINE WITH A SCAVENGED PRECHAMBER

PALIVOVÁ TRAŤ PRO PLYNOVÝ MOTOR S NEPŘÍMÝM ZÁŽEHEM S VYPLACHOVANOU PŘEDKOMŮRKOU

Štěpán Kyjovský

STUDY PROGRAMME

N2301 Mechanical Engineering

BRANCH OF STUDY

2301T047 Transportation, Aerospace and Handling Technology

SUPERVISOR

Ing. Jiří Vávra, Ph.D.

Prague, 2021

MASTER'S THESIS ASSIGNMENT

I. Personal and study details

Student's name: **Kyjovský Štěpán** Personal ID number: **459573**

Faculty / Institute: **Faculty of Mechanical Engineering**

Department / Institute: **Department of Automotive, Combustion Engine and Railway Engineering**

Study program: **Mechanical Engineering**

Branch of study: **Transportation, Aerospace and Handling Technology**

II. Master's thesis details

Master's thesis title in English:

Fuel System for a Gas Engine with a Scavenged Prechamber

Master's thesis title in Czech:

Palivová trať pro plynový motor s nepřímým zážehem s vyplachovanou předkomůrkou

Guidelines:

For a single cylinder research engine, design a fuel system for a supply of gaseous fuel to the actively scavenged prechamber. Design a holder for the solenoid injectors to the prechamber fuel supply and to the engine intake manifold. In the GT-Suite software, create a mathematical model of the fuel system and perform a design optimization to minimize pressure pulsations. Create the design documentation of the new component implementation into an existing fuel system. Based on the available experimental and simulation data from the prechamber engine, perform an analysis of the combustion system performance. Compare various modelling approaches.

Bibliography / sources:

SAE digital library and available software at the U12120

Name and workplace of master's thesis supervisor:

Ing. Jiří Vávra, Ph.D., Department of Automotive, Combustion Engine and Railway Engineering, FME

Name and workplace of second master's thesis supervisor or consultant:

Date of master's thesis assignment: **14.04.2021** Deadline for master's thesis submission: **14.07.2021**

Assignment valid until: **19.09.2021**

Ing. Jiří Vávra, Ph.D. Supervisor's signature	doc. Ing. Oldřich Vítek, Ph.D. Head of department's signature	prof. Ing. Michael Valášek, DrSc. Dean's signature

III. Assignment receipt

The student acknowledges that the master's thesis is an individual work. The student must produce his thesis without the assistance of others, with the exception of provided consultations. Within the master's thesis, the author must state the names of consultants and include a list of references.

.	
Date of assignment receipt	Student's signature

Declaration

I declare that this thesis has been composed solely by myself and that it has not been submitted, in whole or in part, in any previous application for a degree. Except where states otherwise by reference or acknowledgment, the work presented is entirely my own.

Prague, July 7, 2021

…….....

Štěpán Kyjovský

Acknowledgment

I would like to thank my supervisor for continuous support and guidance during the composition of this thesis. I would also like to thank all the advisors for the offered consultations. Lastly, I express everlasting gratitude to those who endured me along the way.

Abstract

First part of the thesis presents construction of a fuel system intended for a fuel delivery to both the scavenged prechamber and the inlet manifold of a single cylinder research engine. Multiple alternatives are described. Steps are taken towards minimizing the pressure oscillations in the fuel system based on results of a 1D model built in GT-Suite. Second part of this paper aims at processing available experimental and simulation data with the goal of assessing the single cylinder research engine performance. Furthermore, the behaviour of the prechamber template in GT-suite is discussed.

Key words: *Prechamber, scavenged, gas engine, fuel system*

Anotace

V první části práce pojednává o konstrukčním řešení palivové tratě pro přívod paliva do aktivně vyplachované předkomůrky a sacího potrubí zkušebního jednoválce. V textu je uvedeno a porovnáno několik variant. Součástí návrhu jsou opatření pro minimalizaci tlakových pulzací v systému, které jsou navrženy na základě výsledků 1D modelu v prostředí GT-Suite. Druhá část práce za pomoci programu GT-Suite zpracovává dostupné výsledky experimentů a simulací provedených na zkušebním jednoválci s cílem zanalyzovat děje ve spalovacím prostoru. Dodatečně je rozebráno chování modelu předkomůrky v prostředí GT-Suite.

Klíčová slova: *Předkomůrka, vyplachovaná, plynový motor, palivová trať, palivový systém*

Contents

Nomenclature

aTDC	After Top Dead Center
bTDC	Before Top Dead Center
CAD [deg]	Crank Angle Degree
CA2 [deg]	Crank angle of 2% burned mass
$CA2_{MC}$ [deg]	CA2 in main chamber
CA10-90 [deg]	Burn duration between 10% and 90% burned mass
CA50 [deg]	Crank angle of 50% burned mass
$CA50_{MC}$ [deg]	CA50 in main chamber
$CA50_{PC}$ [deg]	CA50 in pre-chamber
CCV	Cycle-to-cycle Variation
CI	Compression Ignition
CNG	Compressed Natural Gas
CTU	Czech Technical University
EGR	Exhaust Gas Recirculation
FLC	Full Load Curve
HRR	Heat Release Rate
IMEP [bar]	Indicated Mean Effective Pressure
ISEC [MJ/kWh]	Indicated Specific Energy Consumption
l_R [mm]	Distance between damping vessel and pressure regulator
l_{PFI} [mm]	Distance between damping vessel and fuel rail
LDTE	Light Duty Truck Engine
LHV	Lower Heating Value
LTC	Low Temperature Combustion
$m_{burnCYL}$ [mg]	Fuel burned in main chamber
m_{burnPC} [mg]	Fuel burned in pre-chamber
m_{error} [mg]	Difference between predicted fuel mass and integrated fuel mass flow rate in the pre-chamber
m_{fuelIN} [mg]	Fuel delivered into cylinder
$m_{fuelOUT}$ [mg]	Fuel leaving cylinder
$m_{fuel\ lines}$ [mg]	Fuel trapped in the fuel lines upstream of the pre-chamber and downstream of the check-valve
$m_{fuel\ lines\ compression}$	Fuel forced in the fuel lines during compression
$m_{fuel\ lines\ combustion}$	Fuel forced in the fuel lines during pre-chamber combustion
MBT	Maximum Brake Torque
p_{avg} [bar]	Average pressure
$p_{clearance}$ [bar]	Pressure in the clearance volume between check-valve and injector
p_{cyl} [bar]	Cylinder pressure
p_M [bar]	Pressure upstream of the mass flow controller

p_{Om} [bar]	Pressure downstream of the mass flow controller
PC	Pre-chamber
PFI	Port Fuel Injection
RPM [1/min]	Revolution per Minute
SCR	Selective catalytic reduction
SCRE	Single Cylinder Research Engine
SI	Spark Ignition
TDC	Top Dead Center
TPA	Three Pressure Analysis
V_M	Damping vessel in the PFI fuel line
V_{PC}	Damping vessel in the pre-chamber fuel line
V_{TDC} [mm^3]	Clearance Volume
$\Delta Cyl - PC$ [bar]	Difference between main chamber and pre-chamber pressure
$\Delta m_{burnCYL}$ [mg]	Difference in main chamber burned fuel between models with and without a fuel system
Δm_{burnPC} [mg]	Difference in pre-chamber burned fuel between models with and without a fuel system
Δm_{error} [mg]	Difference in m_{error} between models with and without a fuel system
Δp [kPa]	Difference between maximum and minimum pressure in a single cycle
Δp_{cr} [bar]	Check-valve Cracking pressure
λ [-]	Equivalence ratio
σIMEP [-]	Variation of IMEP

1 Introduction

With the recent development in multiple societies around the world the importance of environment protection rises in the eyes of the public. Subsequent answer to this value transformation is the ever increasingly stringent regulation affecting various fields of human efforts. Since the focus of this thesis is an automotive sized internal combustion engine only emissions from transportation will be further discussed in some level of detail.

It is widely accepted that transportation is one of the significant sources of greenhouse gas and pollutant emissions. The latter of which is especially prevalent in areas with high population density and intensity of human activities.

Publicly available sources [1] estimate that road transportation amounts to 21% (2017) of total CO2 emissions in the EU of which around 60% is attributed to cars. Adding up to almost 15% of CO2 emissions in the EU being emitted by light commercial vehicles (cars and vans, 12% and 2,5% of total CO2 emissions respectively). Similar numbers could be stated for the USA [2].

In the EU this is being targeted by setting the $95g\ CO_2/km$ limit for cars. As of 2019 the average CO2 emissions for new cars were $122g\ CO_2/km$ [1] indicating that further significant improvement is required to meet this target.

Similarly, pollutant emissions have been thoroughly monitored and regulated in past years and despite the favourable trend of decrease (Figure 1) in production across all monitored air pollutants attributed to the transportation sector, the road transport is still noteworthy producer of pollutant emissions, especially NOx (around 30%)[3].

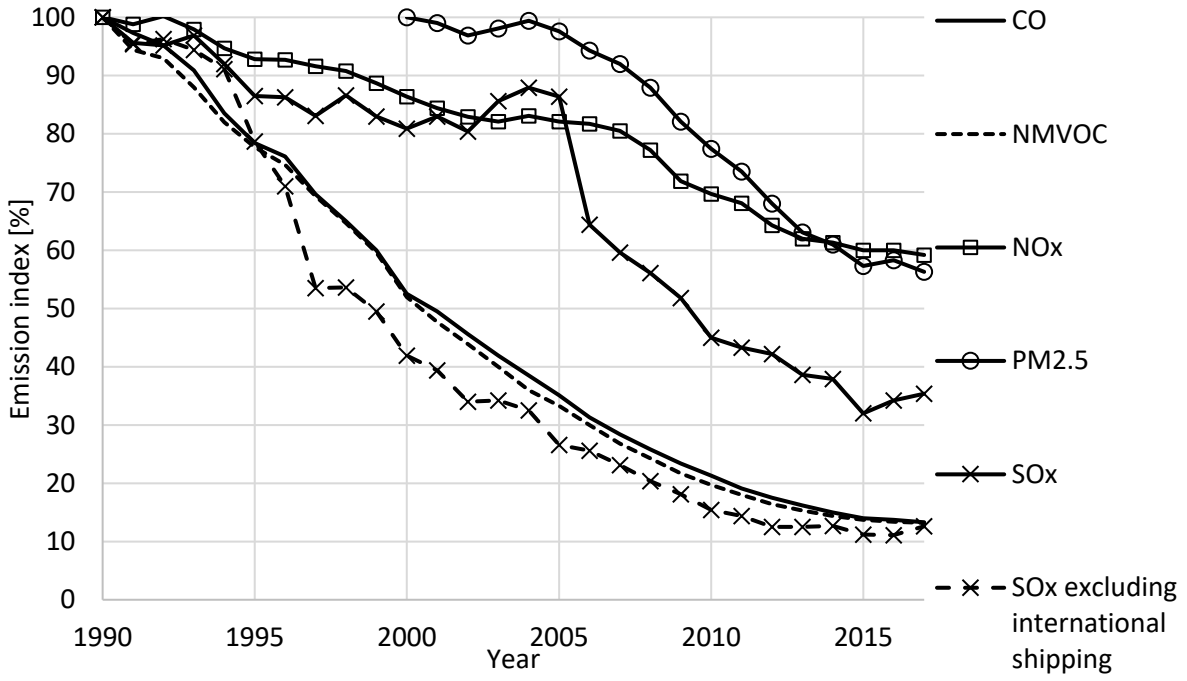

Figure 1 – Trends in emissions of air pollutants from transport [3]

Namely NOx has become the principal pollutant from road transportation since its real world emissions (for diesel passenger vehicles) haven't been able to keep up with the regulations even in a qualitative manner (Figure 2). Only recent diesel passenger vehicles equipped with SCR systems are able to effectively lower real driving NOx emissions [4].

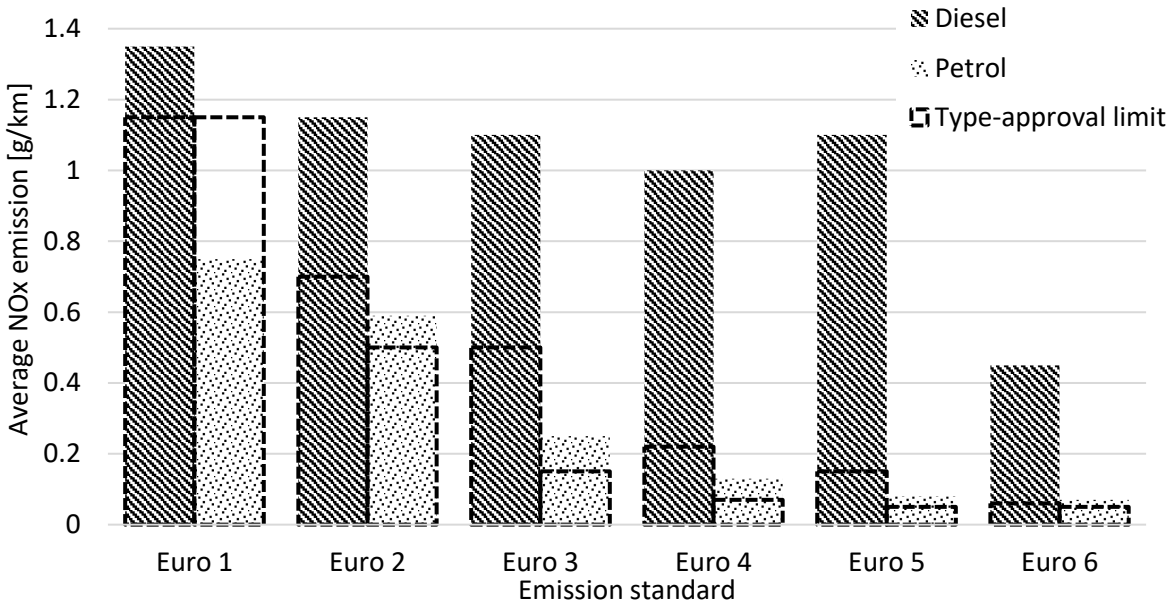

Figure 2 – Remotely measured NOx emissions of Euro 1 to Euro 6 petrol and diesel passenger vehicles [4]

From the information briefly reported above it is apparent there is a strong demand to lower both pollutant and greenhouse gas emissions associated with the road transportation, establishing justification for further research of internal combustion engines.

One concept possibly addressing both these partially contradicting requirements is a Low Temperature Combustion (LTC). Appropriately lowering the temperatures inside the cylinder during the combustion will greatly reduce the production of NOx as well as improve the thermal efficiency through preferable heat ratio values. This is commonly achieved through dilution of the fresh charge with air or EGR. However, mixtures diluted sufficiently to achieve LTC would be difficult to reliably ignite with conventional methods (spark plug), resulting in an increase of CO and unburned hydrocarbons emissions while lowering the efficiency (thus increasing the emissions of CO2).

One possible solution is implementing ignition system capable of producing more energy than a conventional spark plug. This thesis considers an engine equipped with one such system – a prechamber. The focus of this thesis is developing a fuel system to meter fuel directly inside such prechamber. The work will be carried out on an existing single cylinder research engine currently equipped with a passive (without direct fuel supply) prechamber.

2 Turbulent Jet Ignition

The idea of a prechamber dates back to Harry Ricardo and up until recently the automotive industry utilized it in compression-ignition engines (commonly referred to as indirect injection). Outside of automotive industry (and CI engines) prechambers are employed in large natural gas engines. Recently multiple research activities investigated application of prechambers in more compact SI engines such as those in cars.

Nonetheless, the underlying premise remains similar amongst all concepts. The combustion chamber is divided into two sub volumes connected with one or more orifices – the main chamber and the prechamber (occupying approximately 95% and 5% of total volume respectively). During compression a fraction of the air fuel mixture (a few percent) is trapped in the prechamber where it is later ignited (in this case) with a spark plug. Subsequent combustion in the prechamber forces hot gases – containing largely unburned fuel and active radicals – into the main chamber through the connecting orifices. As the flame protrudes into the main chamber rapid burning is initiated, further assisted by the previously exhausted gasses [5,6,7]. This concept has been commonly referred to as a turbulent jet ignition or torch ignition.

There are two major advantages justifying application of such an undoubtedly complicated system. Firstly, the energy released by this system is several orders of magnitude higher than that of a conventional spark plug. Thus, allowing combustion of difficult to ignite mixtures. However, this is only possible if differing quality of mixtures is achievable in the two chambers requiring additional fuelling to the prechamber. Secondly, the jets protrude deep into the main chamber igniting the mixture in multiple locations possibly accelerating the combustion process.

When considering prechamber application in an SI engine two types of prechamber are generally recognized based on how they are supplied with fuel. These two types will be described in greater detail below.

2.1 Passive prechamber

Prechamber layout without its separate fuel delivery is called passive. This kind of a prechamber (Figure 6) depends with its scavenging on the phenomena occurring in the main chamber. All the fuel is delivered into the prechamber through the orifices from the main chamber. Therefore, the equivalence ratio is always similar to that in the main chamber. Since the fuel inside the prechamber itself is ignited with the use of conventional spark plug it is evident that passive prechamber can’t be utilized in lean burn concepts (leaner beyond the capability of a spark plug).

However, the advantages stated above are still applicable to passive prechamber concepts. It is only its operating range that is limited. As the jets protruding from the prechamber ignite multiple locations inside the main chamber, the passive prechamber can provide considerable acceleration of the combustion process. This can be beneficial in knock limited operating conditions as the MBT timing shifts closer to TDC leaving less time for unwanted auto-ignition processes to develop. This is demonstrated on experimental data gathered by Novella et al. [8] presented below (Figure 3). While operating with conventional spark plug the engine was limited by knock under the specified operating conditions (4500RPM, 12.8 bar IMEP) and the combustion was shifted into the expansion (CA50=24° aTDC). All the pre-chambers tested regardless of their respective designs offer reduced combustion duration (by nearly 20 degrees), smaller cycle-to-cycle variation and improved indicated efficiency by almost 10% with respect to the spark plug.

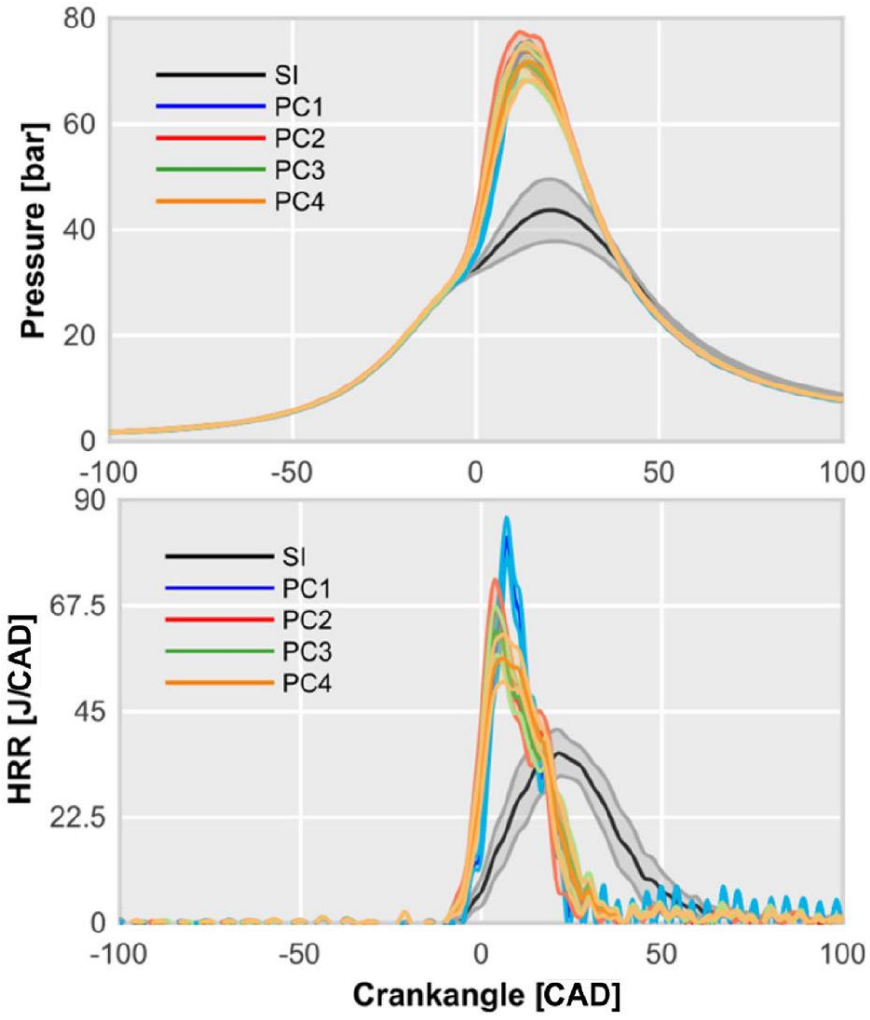

Figure 3 – Measured in-cylinder pressure and estimated HRR profiles comparing conventional spark (SI) plug and different pre-chamber designs (PC1-PC4) on turbocharged automotive SI engine. CCV is illustrated by shaded regions around the plotted average cycle [8]

On the other hand, when operating under less demanding conditions (2000RPM, 6.8 bar IMEP) the difference in CCV becomes insignificant and the difference in the indicated efficiency drops from 10% to less than 4%.

Novella et al. also heavily investigated air and EGR dilution limits of passive prechamber concepts. Notably aiming at achieving $\lambda = 2$ with the goal to lower NOx emissions. From the gathered data (Figure 4) it is apparent that none of the tested prechamber designs were able to achieve that. Moreover, the performance is strongly affected by the specific prechamber designs. Two designs couldn't surpass the lean limit of a conventional spark plug while two designs could still operate at $\lambda = 1.6$.

Arguably most interesting is the captured effect of EGR dilution. None of the prechamber design could match the EGR dilution limits of a conventional spark plug (30%) and with one of the designs no dilution at all was possible.

Detailed description of EGR influence on the phenomena in the prechamber is beyond the scope of this thesis (and is exhaustingly investigated in [8]) but elementary explanation will be provided. Even when operating with no EGR the residual gas fraction in the prechamber is greater than the one in the main chamber due to imperfect scavenging. The stratification of the prechamber mixture further increases the residual gas fraction in the vicinity of the spark gap. Resulting in unfavourable conditions at the time and place of ignition and therefore reaching dilution limits earlier than a system with a spark plug.

The passive prechamber concepts show potential especially, under knock limited operation but lack the capabilities required for achieving LTC.

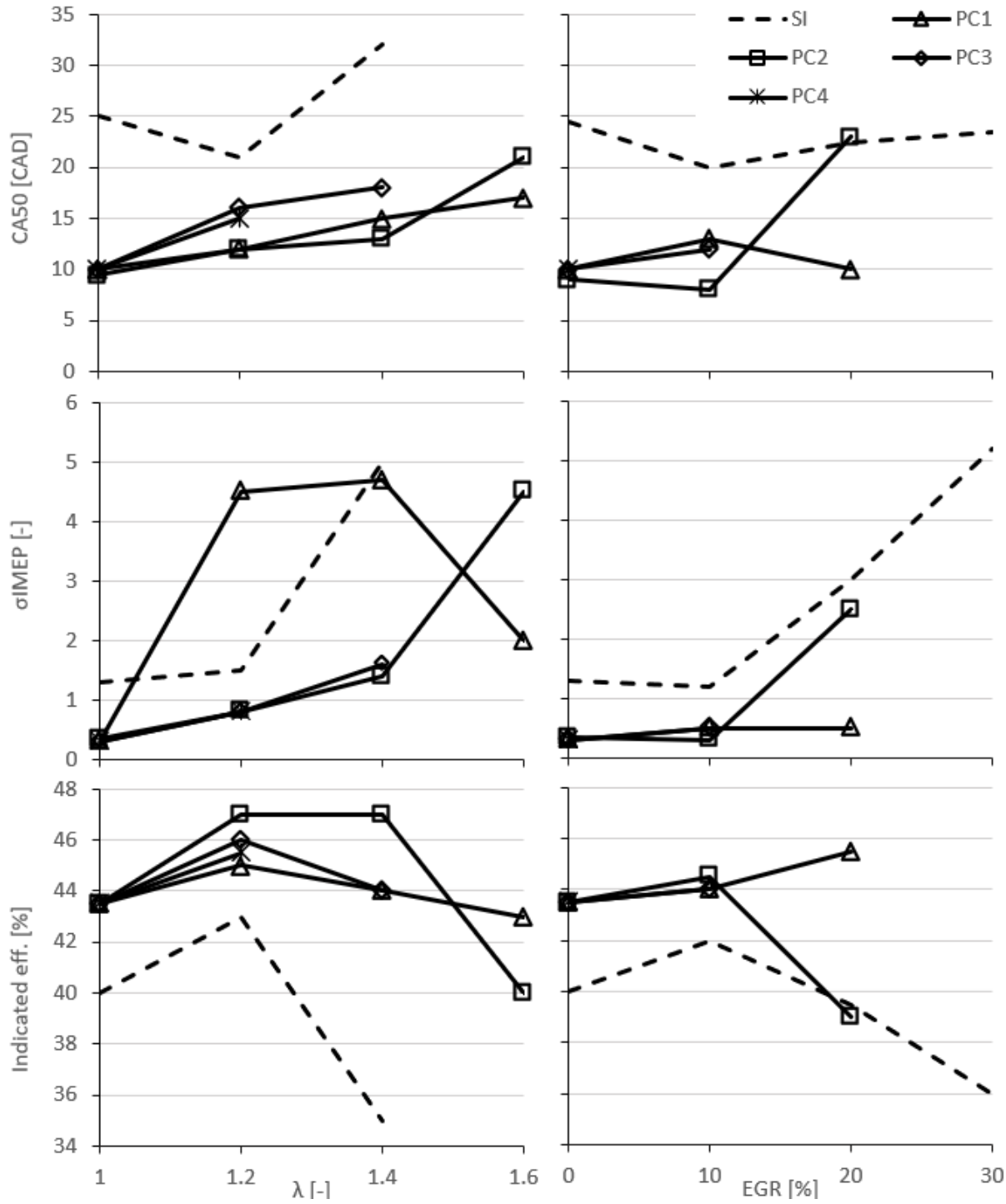

Figure 4 – Measured effect of air and EGR dilution on combustion parameters (4500RPM, 12.8 bar IMEP) [8]

2.2 Active prechamber

Active (or stratified) prechamber aims at limiting the drawbacks present with a passive prechamber at the cost of a greater complexity. It utilizes a separate fuel injection to purge the prechamber of residual burned gases and to establish equivalence ratio independent of the one in the main chamber. Effectively extending the air/EGR dilution limits.

Vávra et al. [9] gathered experimental data (Figure 5) from a light duty truck gas engine utilizing an active prechamber ignition. Demonstrated extension of the lean limit and decrease of NOx emissions in raw exhaust gases was unfortunately accompanied by an increase of unburned methane emissions. Figure 5 also shows the discrepancy between optimum operating points for minimizing NOx emissions and fuel consumption (represented by energy consumption).

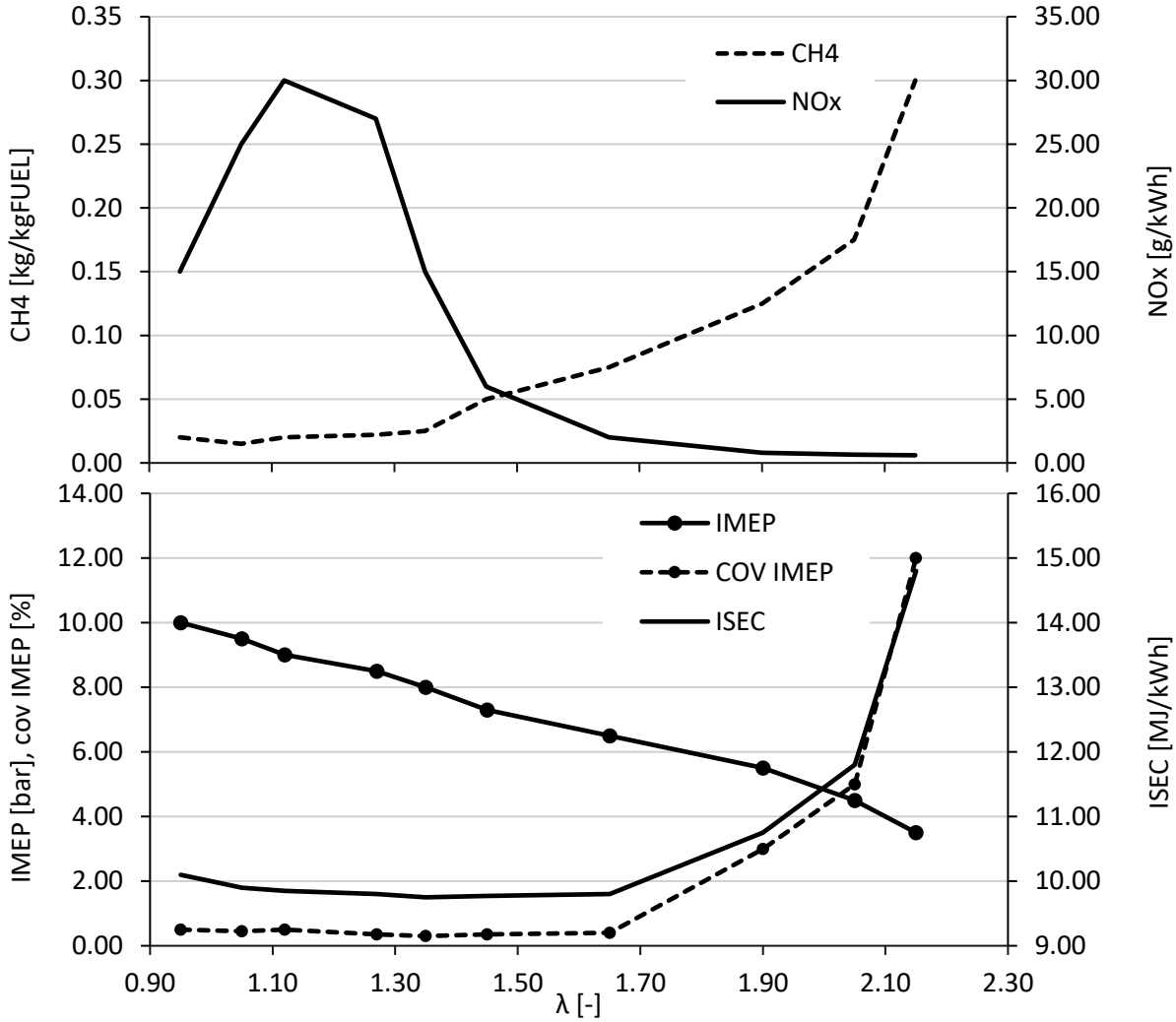

Figure 5 – Effect of lean operation on NOx and unburned methane (EICH4) emissions, indicated specific energy consumption (ISEC), IMEP and coefficient of variation of IMEP (COV IMEP) [9]

The achieved air dilution indicates that LTC is feasible with an active prechamber system. This is further backed by a different experimental investigation by Vávra et al. [10] where significant decrease of peak in-cylinder temperatures is reported (1700K at $\lambda = 1.9$ as opposed to 2500K for stochiometric mixture).

Considering the limited capabilities of the passive prechamber and the promising potential of the active prechamber this thesis will focus on designing a fuel system capable of gaseous fuel delivery into a prechamber as a part of an ongoing effort to convert existing passive prechamber ignition (developed in-house at CTU) into an active one.

3 Experimental setup

All the efforts described, and experimental data used (or presented) in this thesis consider a single cylinder research engine (SCRE) based on a naturally aspirated port injected engine sized for a passenger car application. The parameters of the engine are given in Table 1.

Displacement	375 cm^3
Bore/Stroke	74.5/85.9 mm
Geometric compression ratio	12:1
Valves/cylinder	4

Table 1 – Main engine parameters

Most conventional gaseous and liquid fuels are available at the laboratory including hydrogen. As this thesis focuses on designing gaseous fuel metering system, operation on grid CNG is assumed unless otherwise specified. Table 2 shows measured composition and basic calculated parameters of the CNG. The CNG delivery line is pressurized to 200 bar, the total fuel consumption is measured with a Coriolis flow meter and a pressure regulator is used to adjust the CNG pressure to values required by the low pressure PFI (ca 7 bar).

	$[mol\%]$
Methane	96.093
Ethane	2.602
Propane	0.365
Butane	0.055
Isobutane	0.070
Pentane	0.006
Isopentane	0.010
N_2	0.496
CO_2	0.285

LHV	49,07 MJ/kg
Stochiometric ratio	16.89:1
H/C	3.914

Table 2 – Grid CNG composition and parameters

Currently the engine is able to operate either with a conventional spark plug or a passive prechamber (Figure 6). As the prechamber is retrofitted the compression ratio is reduced (Table 3). Table 3 also includes the proposed active prechamber design for which a fuel system will be designed as a part of this thesis. The active prechamber design will be described later in further detail.

	Spark plug	Passive prechamber	Active prechamber design
Prechamber volume [mm^3]	-	1290	(1550+350)[1]
Fraction of V_{TDC}	-	3.5%	5%
Geometric compression ratio	12:1	11.6:1	11.4:1

Table 3 – CR comparison

[1] Pre-chamber volume plus volume of the fuel delivery lines downstream of the check-valve (Figure 8) as those are directly connected to the pre-chamber volume and act as an additional increase in the clearance volume.

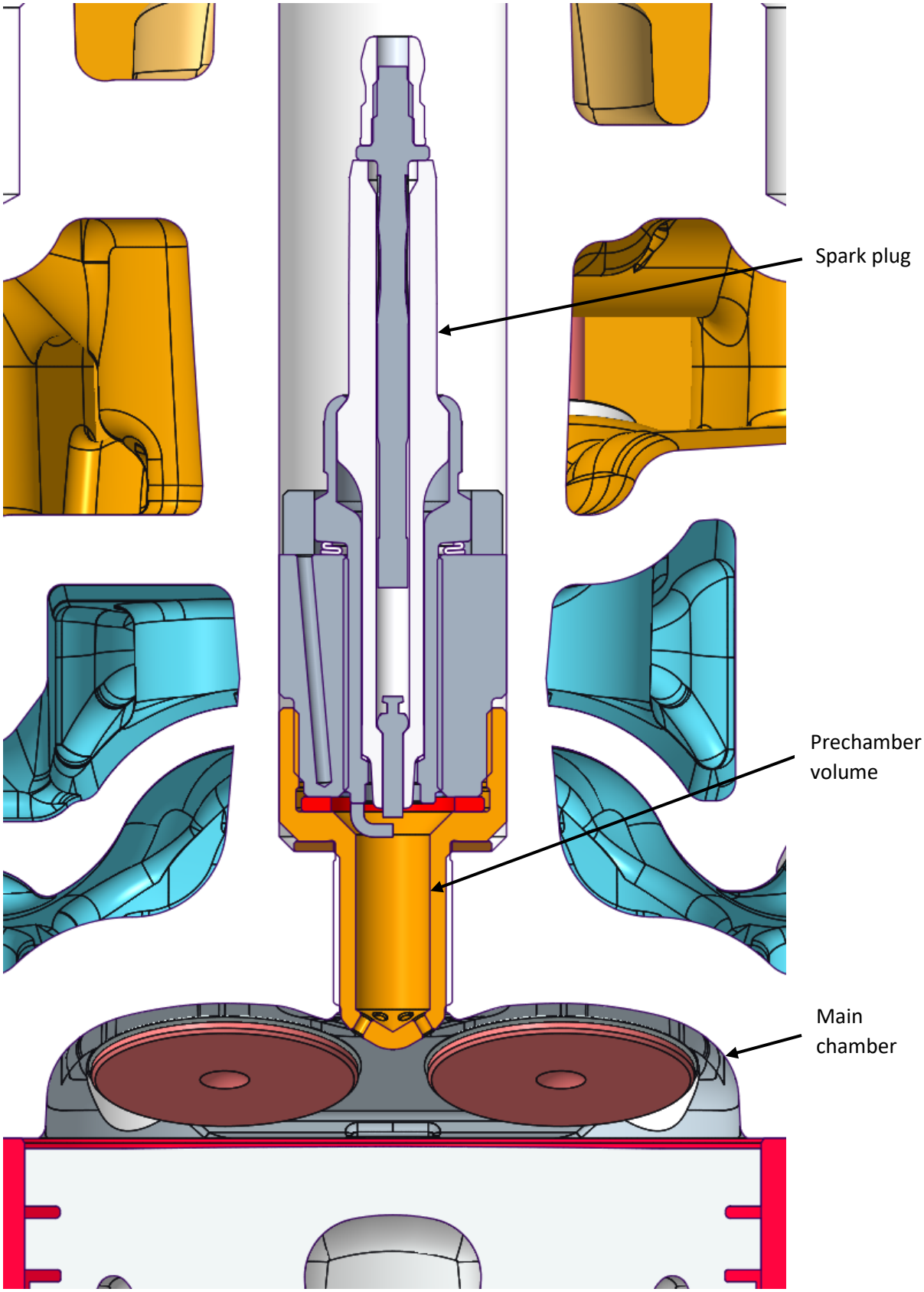

Figure 6 – Passive prechamber

4 Fuel system design

4.1 Active prechamber design

As a prerequisite to this thesis a previously developed active prechamber design is considered. This design is based on the already existing passive prechamber. As the prechamber is retrofitted to a conventional SI engine the space available is limited by the original spark plug bore. This space constraint made implementation of a fuel supply difficult. Top-feed prechamber design concept was investigated originally by the author of this thesis but was deemed too complicated. The design and the spatial constraints are illustrated in Figure 7 for reference.

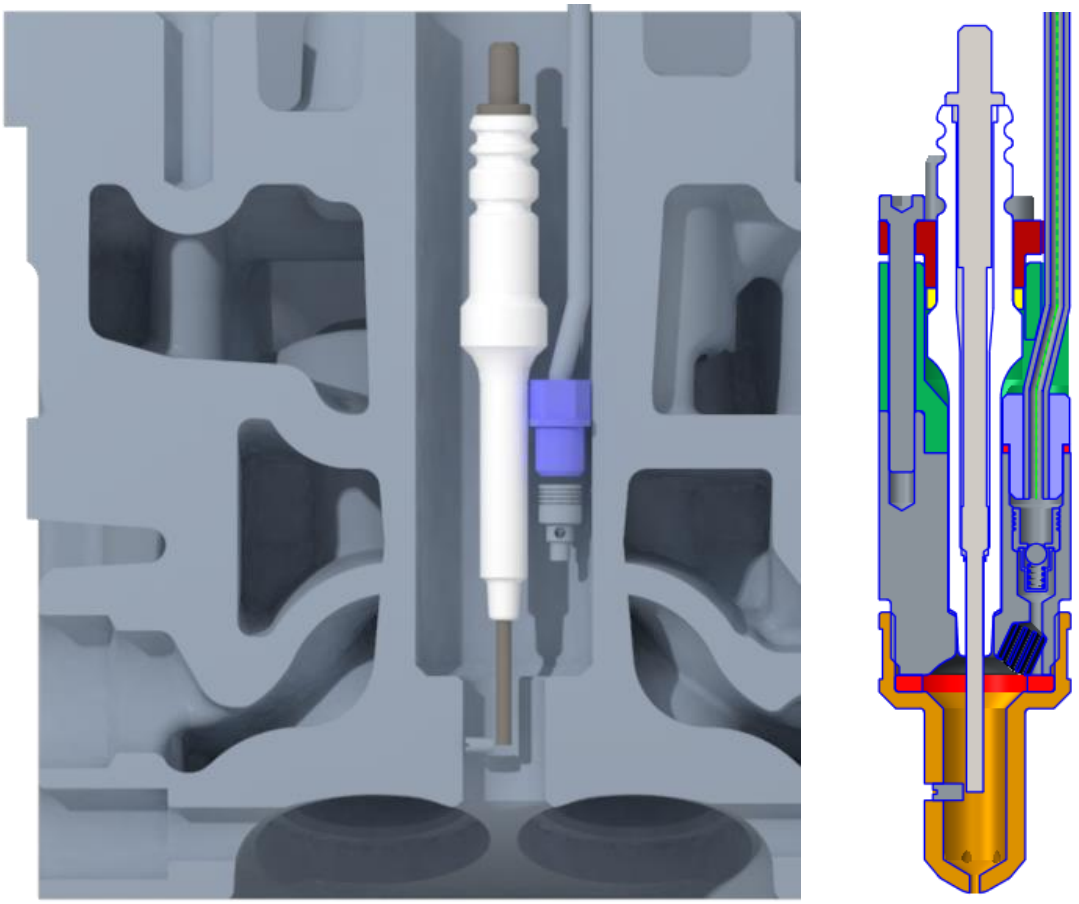

Figure 7 – Top-feed prechamber

As the top-feed design proved to be difficult to realize, modifications to the cylinder head were necessary. Second perpendicular bore connecting the spark plug well with the side of the cylinder head was proposed. This bore would accommodate the fuel supply creating a side-feed design. As this required redesigning of the cooling gallery, bottom of the spark plug well was opened to coolant with the goal to improve prechamber cooling. The design was developed in-house at CTU by Syrovátka and is based on the design already used in [11] – layout of which is apparent in Figure 8. Unfortunately, specifics of the current design can't be published in this thesis.

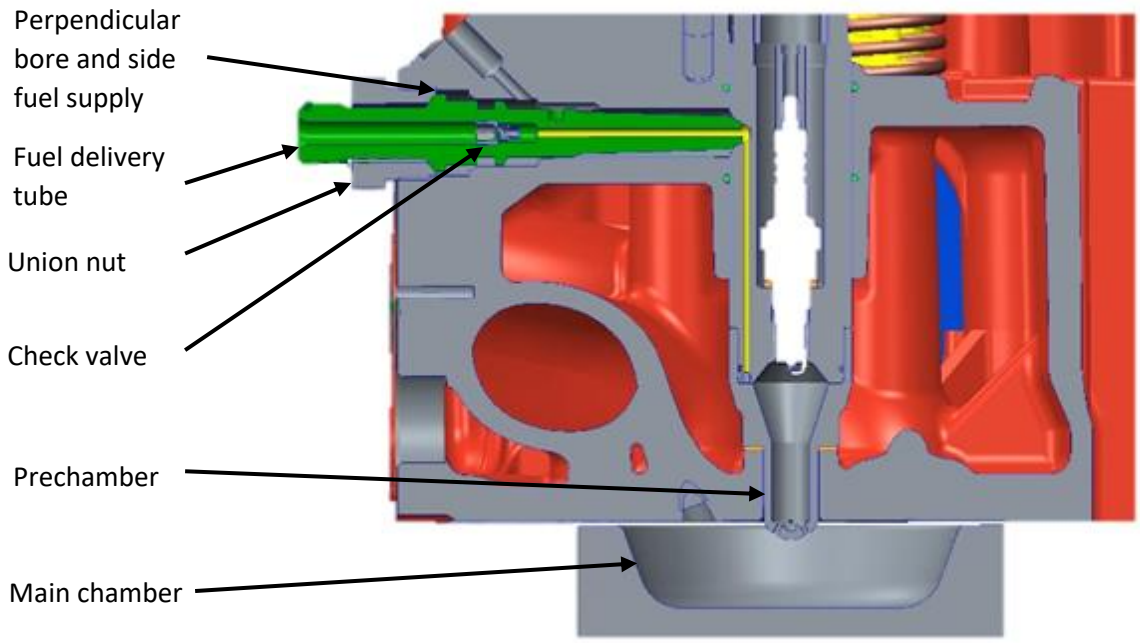

Figure 8 – Layout of the side-feed fuel supply used in [11]

4.2 Fuel system design constraints

Past research conducted at CTU on a light-duty vehicle gas engine with an active prechamber [9,10,11,12] provides basis for the fuel system design. Fuel metering in those experiments was based on a PID mass flow controller (Omega FMA-2610A) and a mechanical check valve (Lee Chek CCFM2550240S; as in Figure 8). The mass flow controller is set to the required fuel delivery rate and the check valve opens at a specific cracking pressure allowing scavenging of the prechamber with fuel. Such system (schematically depicted in Figure 9) is robust but provides limited control – specifically of the injection timing.

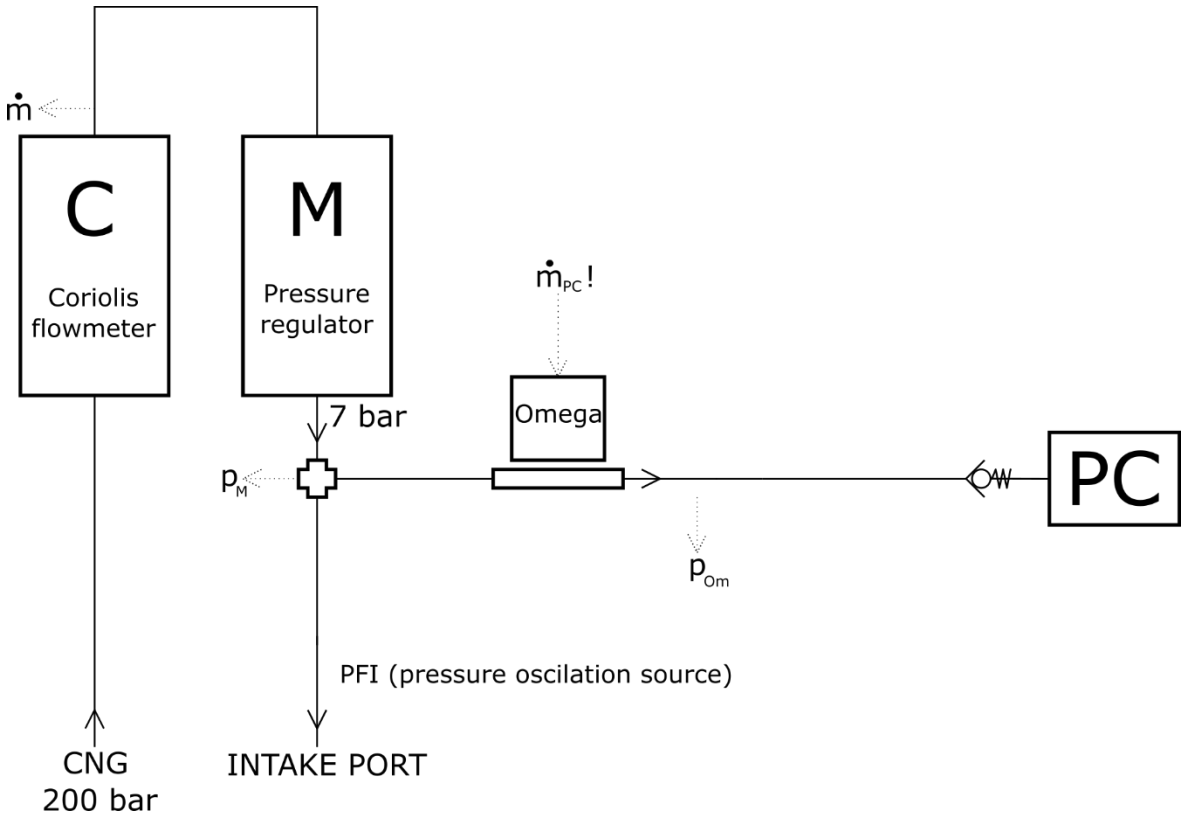

Figure 9 – Diagram of the basic fuel system

Syrovátka et al [12] showed that with this system the cracking pressure is achieved at the beginning of the exhaust stroke and is maintained for around a half of the exhaust stroke. Effectively delivering quarter of the total fuel mass (in PC) during the exhaust stroke, possibly leading to a loss of fuel through the open exhaust valves.

Both the PFI and the check valve are also sources of pressure oscillations. These oscillations are present at both the input and the output of the mass flow controller (p_M and p_{Om} in Figure 9) and make consistent control very difficult. In practice two PID mass flow controllers in series were necessary to achieve reliable control of the mass flow rate.

Meanwhile results of previous in-house CFD simulations (of the SCRE) point at inadequate homogenization of the mixture under certain operating conditions. When comparing two simulations, one with ideal homogenous mixture assumed and other where port fuel

injection phenomena are considered, the resulting engine performance varies. The predicted effect (from CFD) of mixture homogeneity on in-cylinder pressure can be seen in Attachment 1.

Considerations investigated above give rise to basic requirements on the fuel system design

1. Incorporate a solenoid injector into the prechamber fuel delivery line to provide another level of control for both the injected fuel mass and injection timing.
2. Investigate the pressure oscillations in the fuel system with the use of a suitable simulation environment and apply the gained insight on designing damping vessels.
3. Implement a second injector upstream of the current PFI injector to allow for future experimental investigation of homogeneity effects on the engine performance.
4. Integrate all the above elements into the current test bed and the existing active prechamber design.

The diagram from Figure 9 was modified to reflect these design intentions (Figure 10). The existing fuel line will be spliced into two at the output from the pressure regulator (M). The prechamber line will consist of a PID mass flow controller (Omega FMA-2608A), a damping vessel (V_{PC}) and a solenoid injector. The check valve is retained since otherwise the injector would be exposed to the combustion processes in the cylinder.

The main fuel line contains a damping vessel (V_M) as well and supplies fuel either to the intake port (through an already present fuel rail) or to an upstream intake pipe (through an injector holder designed subsequently).

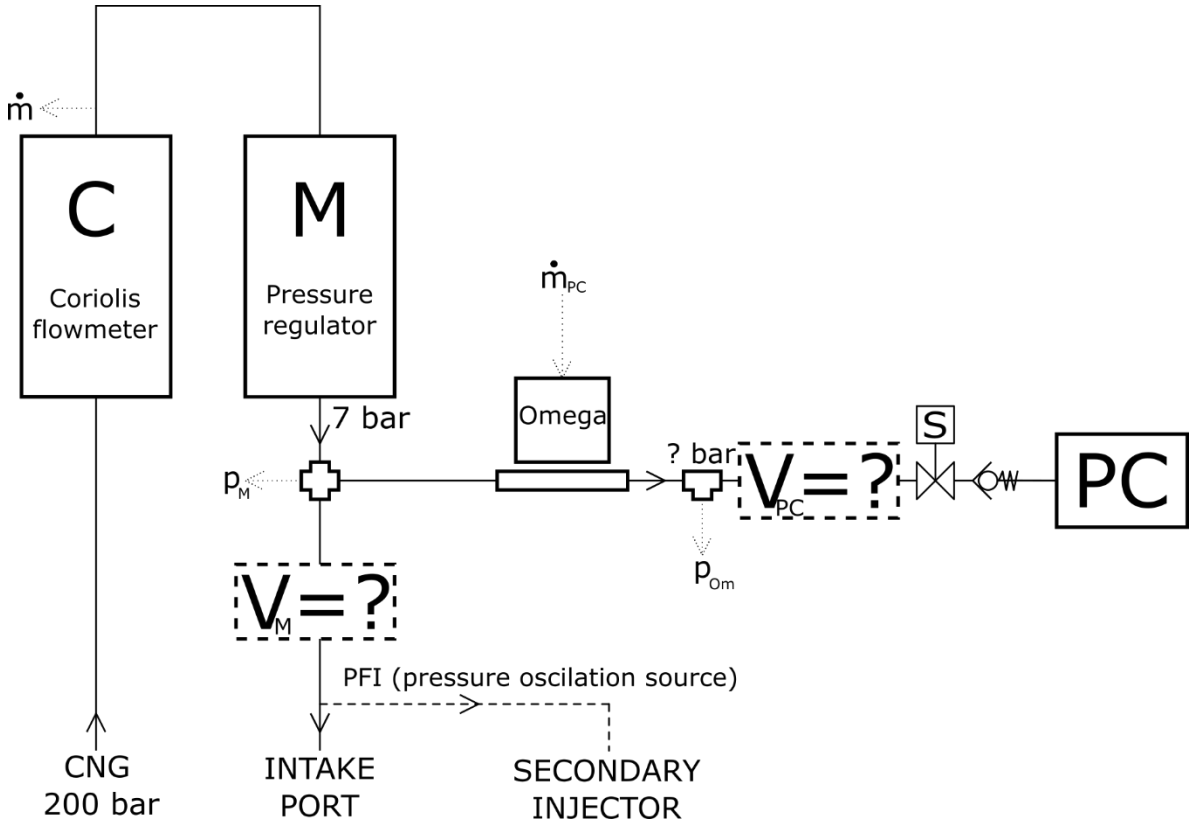

Figure 10 – Complete fuel system diagram

4.3 1-D gas dynamics model of the fuel system

Based on the diagram in Figure 10 a 1-D mathematical model was built using the GT-Suite interface. The yet unknown geometrical dimensions were estimated for this first approximation. The model doesn't consider the pre-chamber volume. It is built up to the connecting orifices (Figure 8) where a boundary condition is applied.

Three boundary conditions are used. The input boundary condition is set to the pressure regulator output (Figure 10, M, 7 bar). For the intake port atmospheric conditions are used and effect of any pressure oscillations present in the intake is neglected for the time being. The pre-chamber boundary values are gathered from past experiments. Unfortunately, measurements taken directly in the prechamber weren't available and in-cylinder values had to be used. As notable pressure differences between the pre-chamber and the main chamber are present only around TDC where no fuel delivery takes place this simplification shouldn't induce any deterioration of the results. The measured pressure is used directly, and the temperature is acquired from a three-pressure-analysis of the data (Section 5.1)

The solenoid injectors are modelled as a pipe (simulating inner injector piping) and an orifice. The timing of the injection is controlled by varying the flow coefficient between 0 and 1. This approach is based on GT-Suite example models. The orifice parameters were tuned so that the injector behaviour is consistent with the manufacturer declared performance and data available from experiments with running engine.

The model includes a mechanical sub model of the check valve (Figure 11). The check valve sub model was built and experimentally verified by Akshay [13].

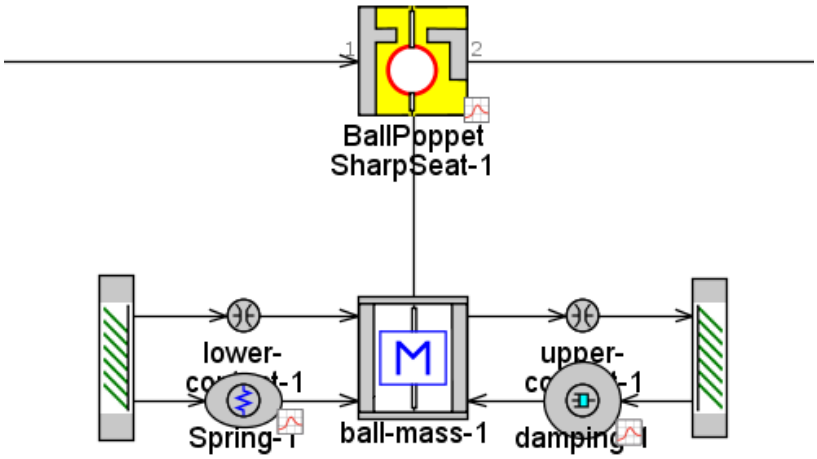

Figure 11 – Check valve GT-Suite model [13]

The complete 1-D model of the fuel system is depicted in Figure 12. Nomenclature and symbols from Figure 10 are included to improve the clarity of the diagram and to highlight all important components of the model.

The notable initially unknown dimensions are the lengths of the connecting hoses and the volumes of the damping vessels. Both of which are a subject of the design efforts described in this thesis. Since this preliminary model will be used to provide input parameters for the later design phases the results will be eventually compared to an updated model based on the finalized fuel system design.

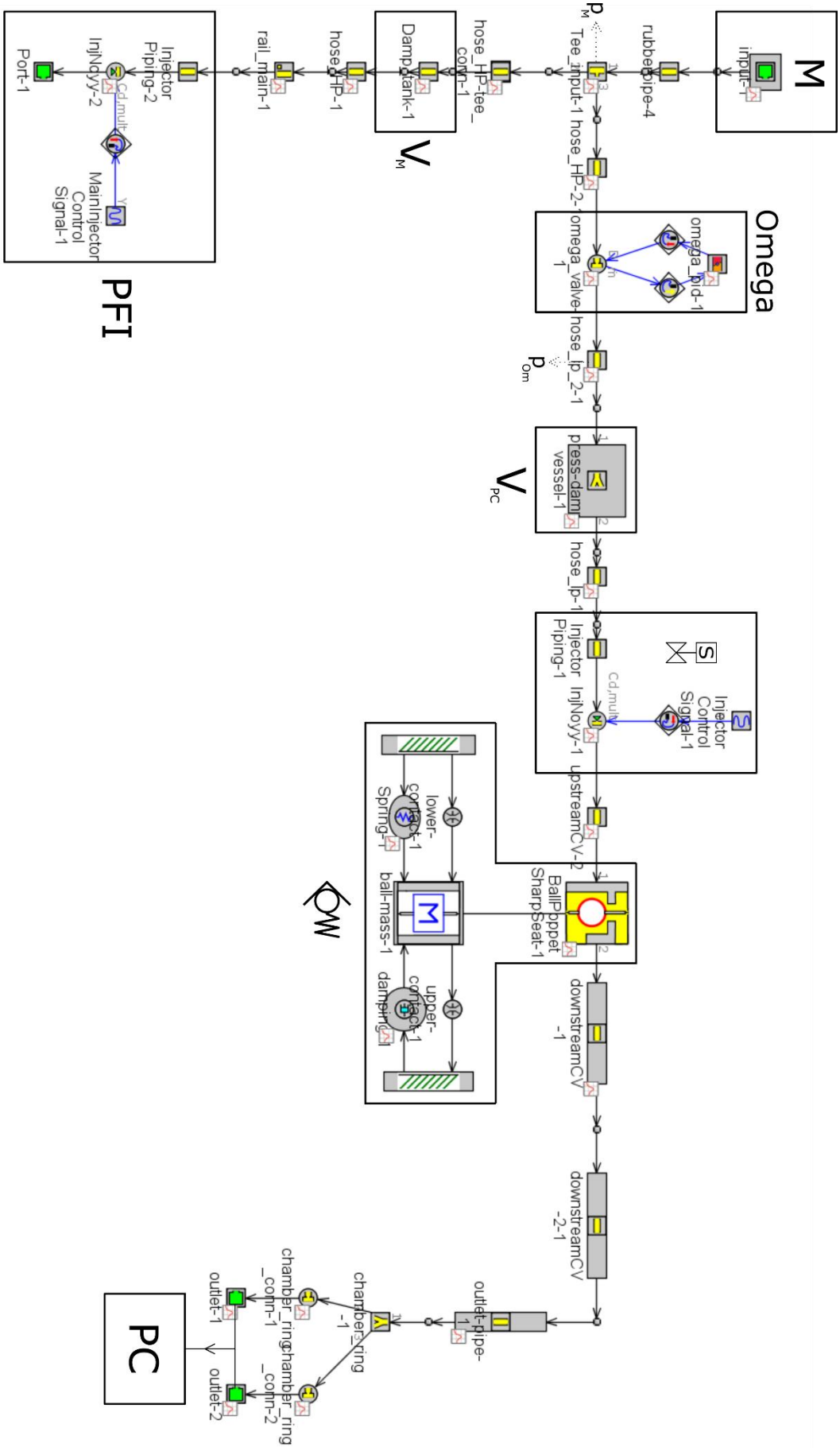

Figure 12 – GT-Power model of the fuel system

4.4 Pre-chamber Injector Holder

4.4.1 Fuel delivery analysis

As briefly described in Section 4.2 the fuel metering into the prechamber using only a check valve was deemed insufficient. It doesn't provide enough control variables to precisely regulate both the delivered fuel mass and the injection timing. The results from the 1-D simulation introduced in Section 4.3 indicate that findings of Syrovátka et al [12] extend to the current setup. The simulation results (Figure 13) show the fuel mass flow rate through the check valve. Two layouts are considered – one with fuel injector upstream of the check valve (Figure 10,14) and one without. The injector opens at the beginning of the intake stroke and closes early in compression. The mass flow controller is set to the same mass flow rate in both cases. The check valve is present in both cases therefore ultimately the fuel delivery is still dependent on achieving the cracking pressure required to open the check valve. However, the solenoid injector provides means of modulating the upstream pressure beyond the settings of the mass flow controller.

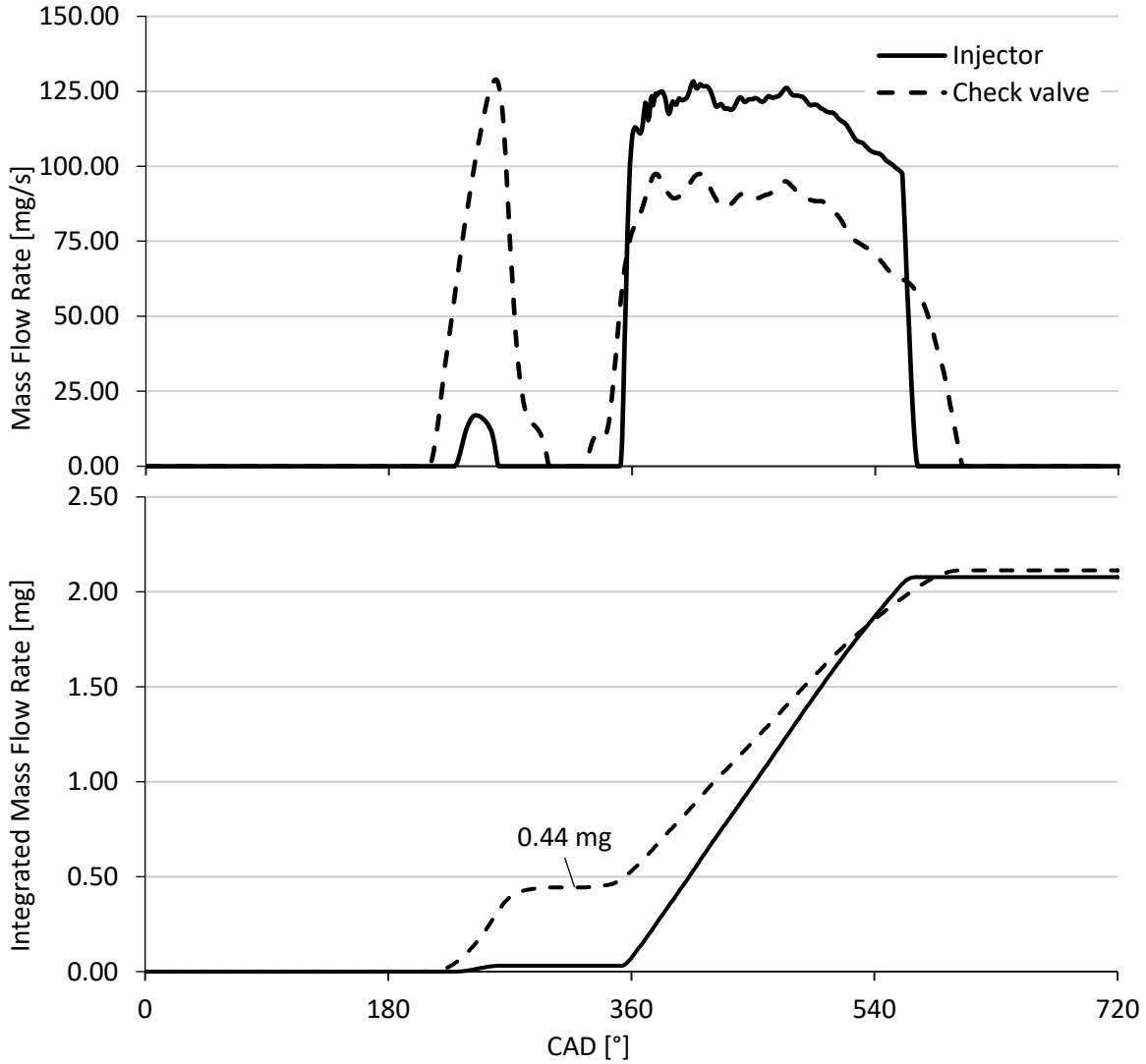

Figure 13 – Comparison of the fuel mass flow through the check valve with and without an upstream injector, operating condition – 2000 RPM, wide open throttle

Without the upstream injector fuel delivery occurs early in the exhaust stroke and this initial injection contains roughly 25% of the total delivered fuel mass. With the upstream injector this early delivery is still present, but the injector is closed at this moment and the fuel flow is restricted. Thus, the fuel flow is limited to any fuel leftover from the last cycle present in the volume between the check valve and the injector. If this clearance volume is sufficiently small the amount of fuel delivered during the exhaust stroke is negligible.

The amount of fuel delivered during exhaust stroke can be further affected by the timing of the injector closing. If the injector closes earlier than the check-valve would by itself, no fuel is delivered in the clearance volume and the pressure drops rapidly to

$$p_{clearance} = p_{cyl} + \Delta p_{cr} \quad (1)$$

This pressure is lower than the pressure sustained in the fuel supply line (which would be maintained in the clearance volume if the check-valve could close by itself) further limiting the amount of fuel delivered during the exhaust stroke.

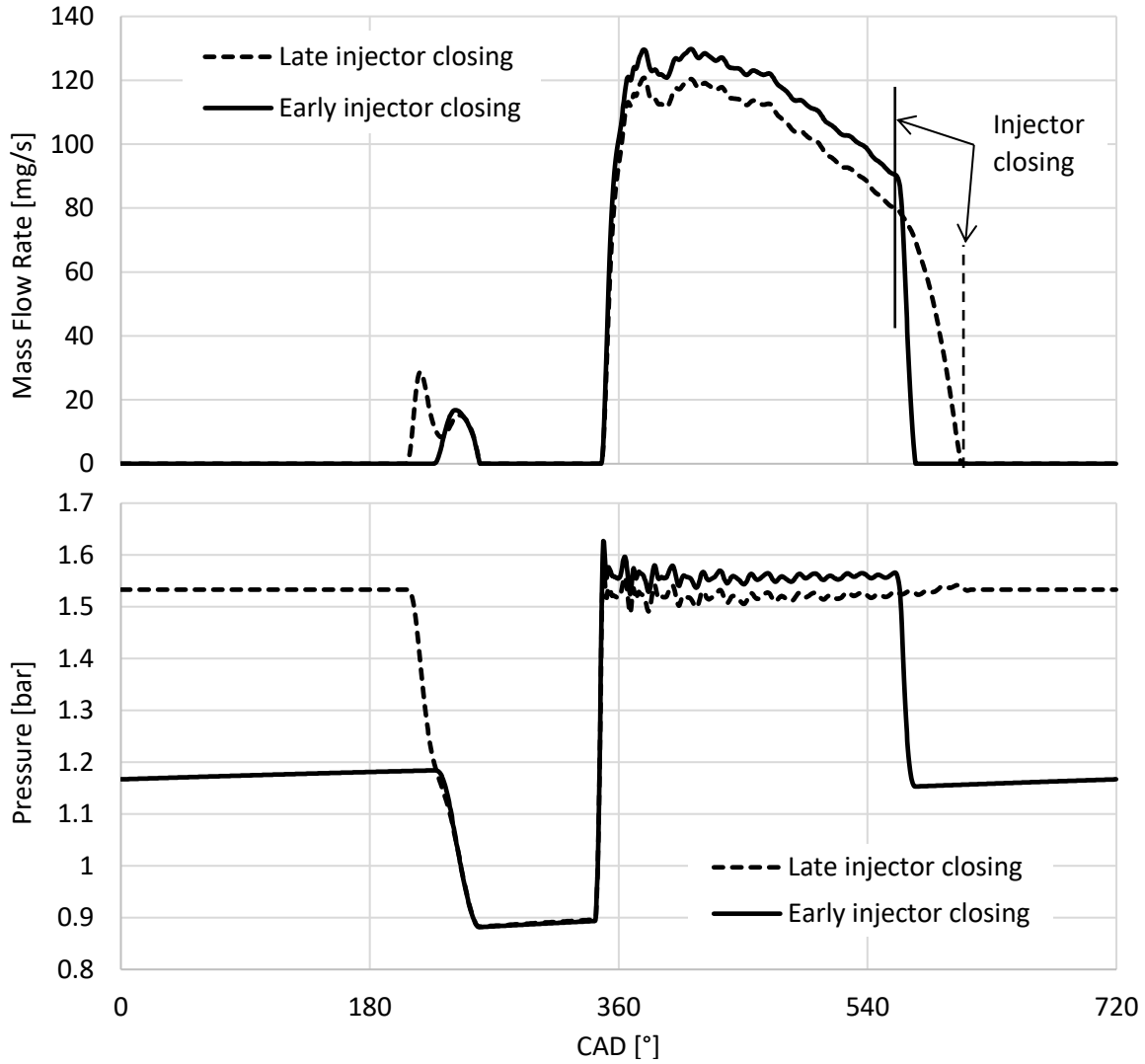

Figure 14 – Effect of injection end timing on the mass flow rate through the check-valve and pressure in the clearance volume.

Simulations results in Figure 14 compare two injector closing timings. The Late injector closing corresponds to injection end at 110° bTDC at which point the check-valve already closed by itself (due to the cylinder pressure increase). The Early injector closing represents the data already presented in Figure 13 and the injector closes at 160°bTDC. The effect on the pressure in the clearance volume and the mass flow through the check-valve is evident. In the case with late injector closing, the amount of fuel delivered during the exhaust stroke nearly doubles. Closing the injector earlier than 160°bTDC offers diminishing returns and some fuel delivery during exhaust is unavoidable with this setup. However, with the described measures it is kept to an acceptable level of 1% of the total delivered fuel mass.

The data do not provide an inconclusive evidence that the fuel delivered during the exhaust stroke is lost but it demonstrates that including a solenoid injector into the pre-chamber fuel system allows for more precise fuel metering.

4.4.2 Pre-chamber Injector Holder Design

To allow for the implementation of the injector an appropriate holder compatible with the current active pre-chamber design is required (Section 4.1).

Elements of the current side fuel supply are utilized. The fuel delivery tube is retained but shortened to accommodate the injector. The check valve is kept to protect the injector (originally PFI) from the combustion process. The union nut is modified to provide a bottom seat for the injector and seat for a pressed-on flange. An O-Ring is added between the union nut and the fuel delivery tube to provide an additional sealing surface. The O-Ring also eases the assembly to the cylinder head since it helps to secure the fuel delivery tube in the union nut.

The two-piece upper part of the holder assembly consists of an upstream injector seat and a flange. The upper assembly is fixed to the union nut flange with two M6 cap head bolts. The two parts are spaced with two aluminium tubes. The axial clearance between the injector and the rest of the assembly is adjusted by a spring washer. An original injector clip mounted backwards is used as a seating surface for the spring washer.

The clearance volume between the injector and the check valve is reduced by the inclusion of an insert. This is done to limit the fuel delivery during the exhaust stroke.

The complete assembly is secured to the cylinder head with M22 thread on the union nut. The union nut is tightened to the head using the hex and the rest of the assembly is put together afterwards. The fuel supply is provided by a pipe thread hose barb.

The final design with all mentioned components is shown in Figure 15. Relevant production and assembly drawings are included in the attachments (2-7).

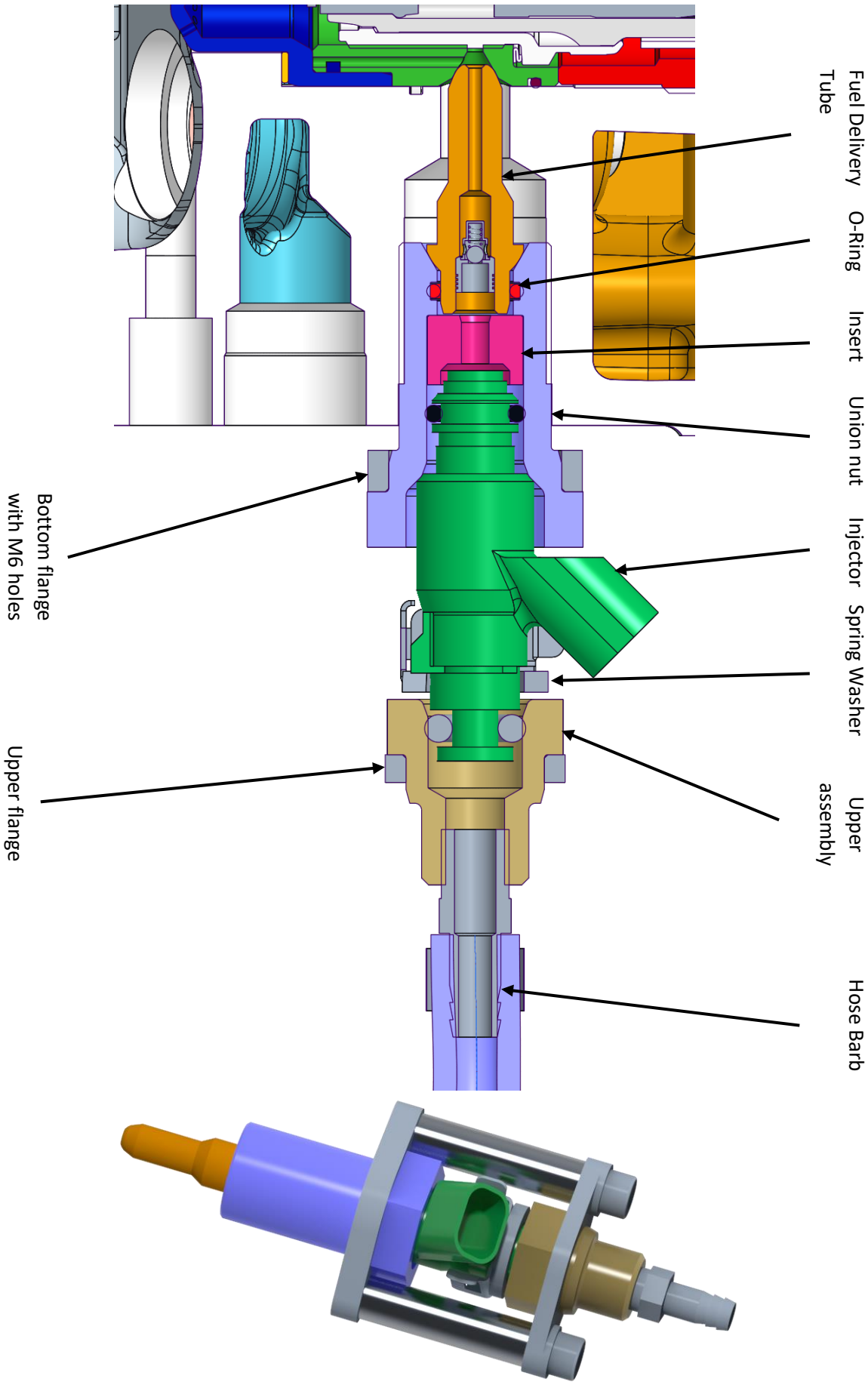

Figure 15 – Injector holder

4.5 Damping vessels

4.5.1 Pressure oscillations analysis

To evaluate the pressure oscillations in the fuel system two measuring points were chosen. These are located at the input and the output of the mass flow controller and are denoted as p_M and p_{Om} (Figure 10,14). A single parameter was chosen as a way to illustrate the effect of changing the design variables on the level of pressure oscillations in the system. This parameter (Δp) is defined as the difference between the maximum and the minimum value of pressure recorded during a single engine cycle at the respective measuring locations (p_M, p_{Om}). Simulation results in Figure 16 display the predicted effect of PFI on pressure at the intake side of the mass flow controller without any damping vessels at 2000RPM. The parameter Δp is indicated and in this case amounts to 0.5 bar.

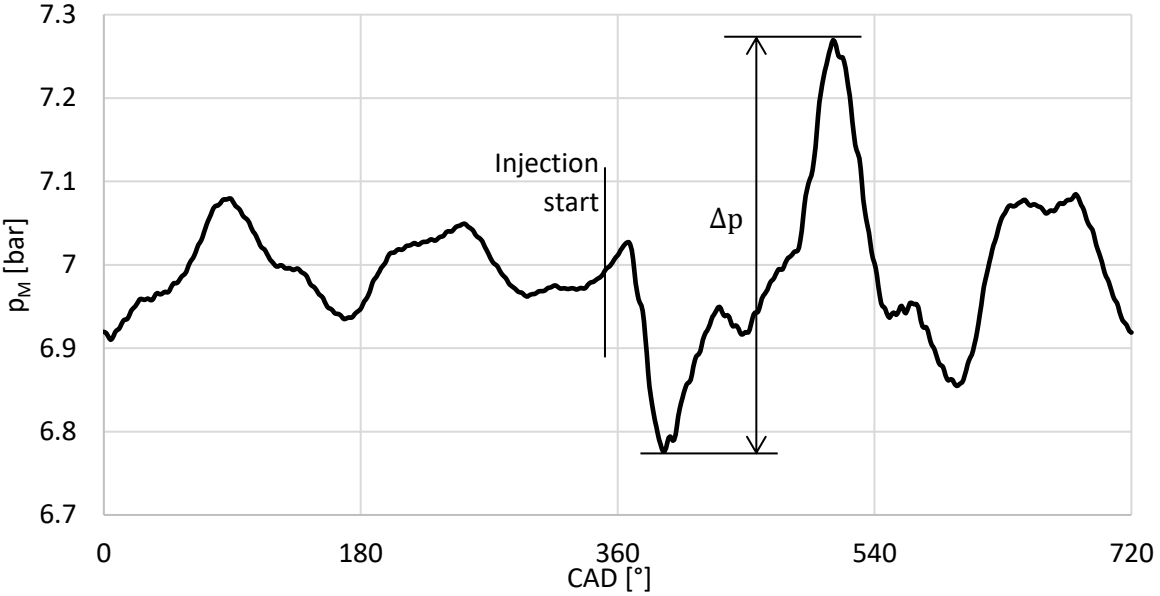

Figure 16 – Pressure at the input of the mass flow controller (p_M), no damping vessels, 2000RPM, PFI injection start 350° aTDC

Similarly results from the output side of the mass flow controller were available and both are reported in Table 4 to provide a benchmark for any modifications. Values of Δp normalized by the average pressure at respective locations are included allowing clearer understanding of the results.

	Δp [bar]	$\frac{\Delta p}{p_{avg}}[-]$
p_M	0.5	8%
p_{Om}	0.13	8%

Table 4 – Initial results, no damping vessels

Damping vessels in a form of an expansion chamber (Figure 10,14) were proposed as a measure to limit the pressure oscillations in the fuel system. With the help of the 1-D numerical model the effect of damping volumes on the parameter Δp can be investigated.

The Figure 17 shows the effect of varying both damping volumes on Δp at respective measuring points such as

$$\Delta p_M = f(V_M) \tag{2}$$

$$\Delta p_{Om} = f(V_{PC}) \tag{3}$$

providing insight into the correct sizing of the damping vessels.

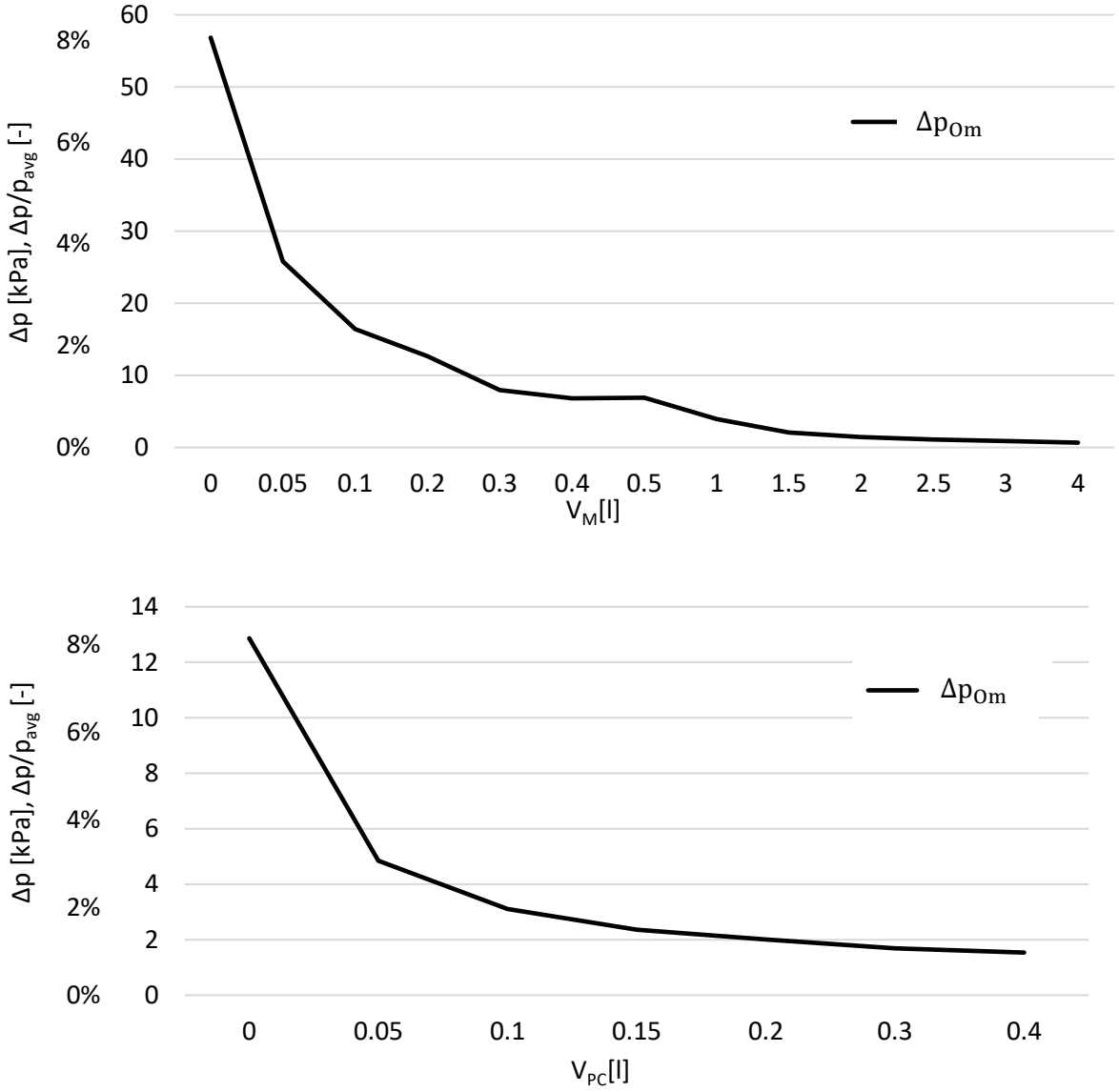

Figure 17 – Effect of varying the damping volumes on the parameter Δp

Both data sets flatten out towards larger volumes. No clear optimum is reached but the changes in Δp appear to be irrelevant past $V_M = 2\ l; V_{PC} = 0.2\ l$. Furthermore, already at $V_M = 0.5\ l$ the normalized value of Δp drops below 1%. Noteworthy results are presented in Table 5.

	V_i [l]	Δp [kPa]	$\frac{\Delta p}{p_{avg}}[-]$
p_M	0.5	6.9	1%
	0.2	12.5	1.8%
p_{Om}	0.4	1.5	1%
	0.2	2	1.25%

Table 5 – Results from analysis in Figure 17

Cross-sensitivity was also investigated in the following manner

$$\Delta p_{Om} = f(V_M) \tag{4}$$

$$\Delta p_M = f(V_{PC}) \tag{5}$$

and no meaningful effect was observed. Impact of the damping volumes (or the lack thereof) on the performance of the mass flow controller is apparent in the model however, these changes do not reflect into the observed parameters. It is likely that such investigation is beyond capabilities of the model as the idealized mass flow controller doesn't allow for enough interaction between the two lines. Therefore, the results of this analysis aren't further presented.

Normalized value of Δp around 1% was established as a design objective. This was achieved with $V_{PC} = 0.4l$ and $V_M = 0.5l$ but the flatness of the curves in Figure 17 meant that this requirement was overly restrictive and would lead to impractically large damping vessels without significant effect on Δp.

Relaxing the design objective to 1.5% would lower the required volumes to $V_{PC} = 0.15l$ and $V_M = 0.25l$ while still leading to a sizable improvement over the initial state (Table 4). As these values were close to each other it was decided that the two damping vessels will be identical to simplify the manufacturing phase. With that in mind $V_M = V_{PC} = 0.2l$ was chosen as an input parameter for the design phase. Simulation results are reiterated in Table 6 and a percentage improvement of Δp over the initial state is included.

	V_i [l]	Δp [kPa]	$\frac{\Delta p}{p_{avg}}[-]$	improvement
p_M	0.2	12.5	1.8%	75%
p_{Om}	0.2	2	1.25%	85%

Table 6 – Results from analysis in Figure 17 for the chosen volumes

4.5.2 Helmholtz resonator

Apart from the expansion chamber a damping vessel in a form of a Helmholtz resonator was investigated. Helmholtz resonator is a volume connected in parallel to the main line (Figure 18). Such solution initially appeared to have a further positive side effect on the level of pressure oscillations in the PFI fuel rail. However, to achieve this beneficial behaviour unrealistic dimensions of the connecting hoses were required. When more reasonable dimensions were considered for the 1-D model this positive side effect all but disappeared

while introducing a high frequency oscillation superimposed over the original pressure signal at the mass flow controller input p_M (Figure 19). Since the Helmholtz resonator provided no improvement at the cost of greater complexity it was abandoned as a concept.

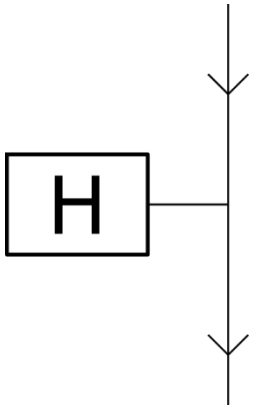

Figure 18 – Diagram of Helmholtz resonator

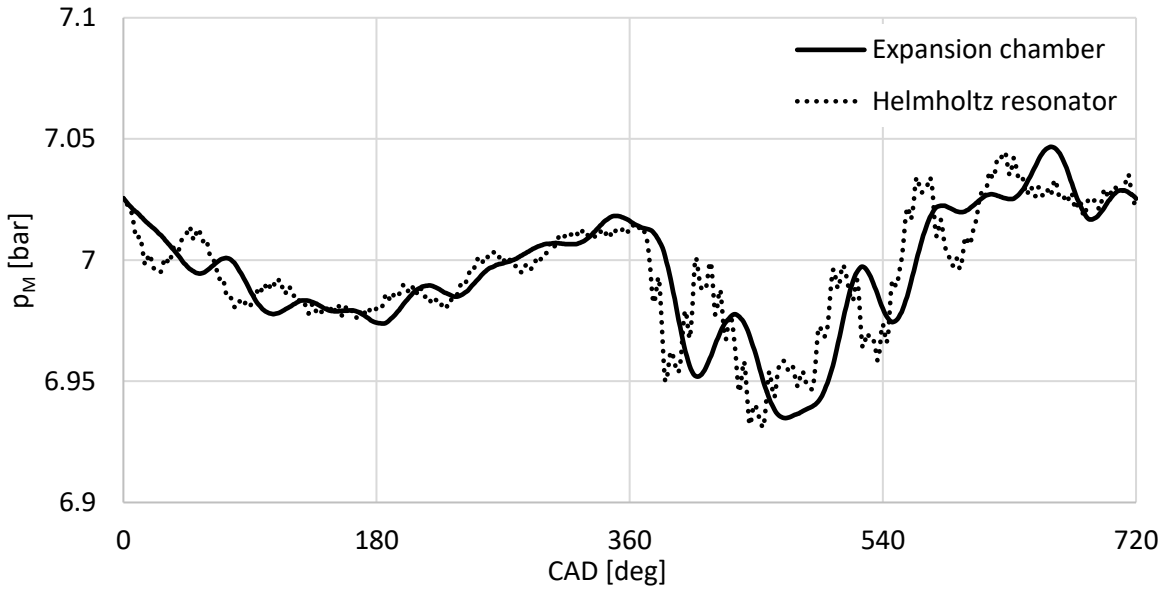

Figure 19 – Comparison between expansion chamber and Helmholtz resonator, mass flow controller input (p_M), 2000 RPM

4.5.3 Speed dependence of the pressure oscillations

In the previous chapters the volume and concept of the damping vessels were decided upon based on the performance at a single operating point (2000 RPM, wide-open-throttle). To validate this design further investigation under different working conditions is necessary. It is reasonable to presume that part load operation can be neglected. As the delivered fuel mass decreases the requirements on the fuel system damping capabilities are reduced. The results of the speed dependency analysis are presented in Figure 20. Cases with no damping volumes and with a Helmholtz resonator on the fuel flow controller input side are included for reference.

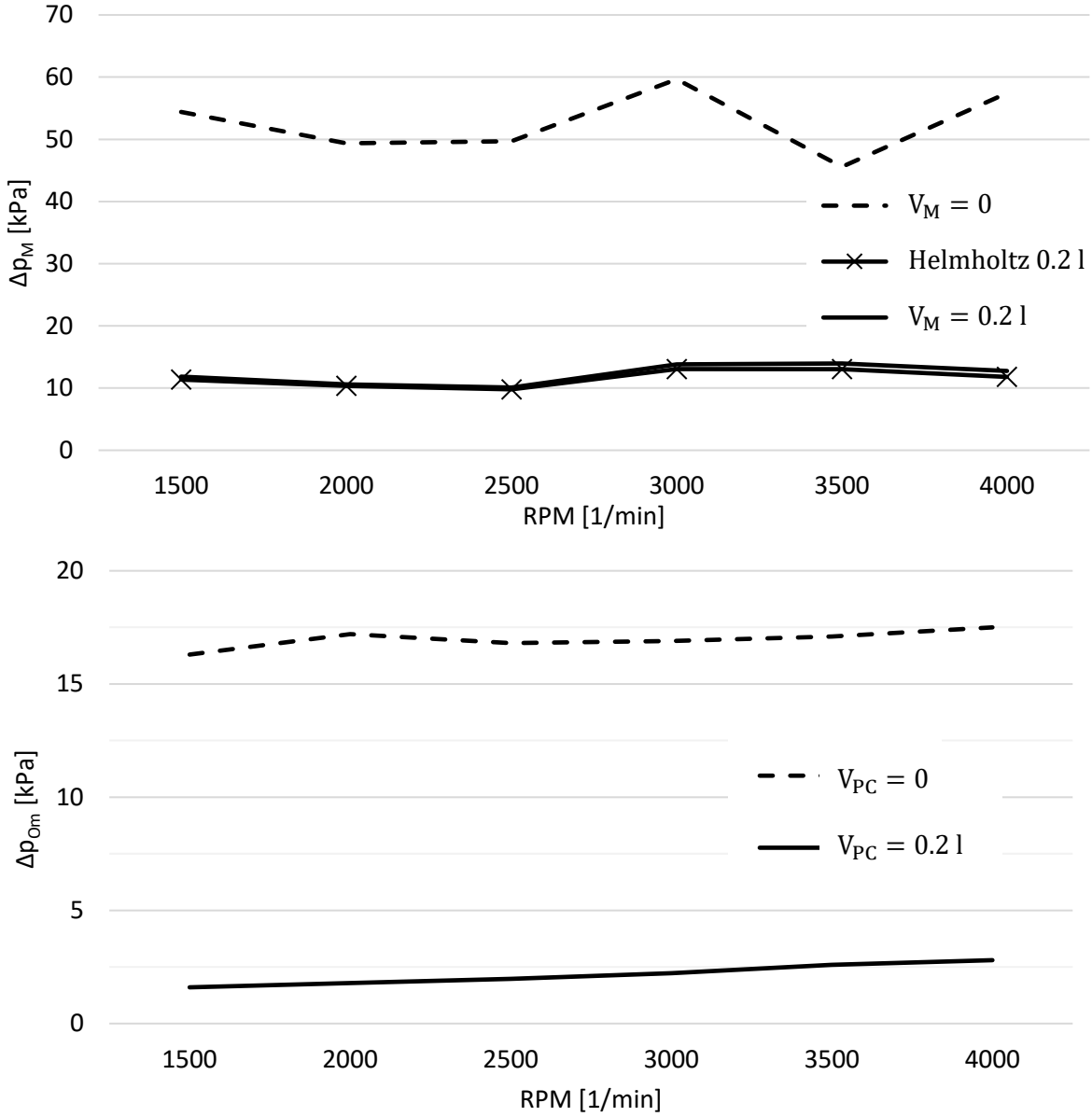

Figure 20 – Speed dependent behaviour of Δp

At the input side of the mass flow controller (p_M) some influence of engine speed on the fuel system behaviour is present but there is no clear indication that the performance of the system deteriorates with engine speed. The observed effect is caused by an interference of the pressure waves travelling through the system i.e. when the rarefaction wave formed by the (PFI) injector opening reaches the damping vessel (relatively large volume with respect to the rest of the fuel system) it is reflected as compression wave back towards the injector. But since the damping vessel isn't large enough the net effect isn't zero and a pressure drop occurs in the damping vessel. This pressure drop induces second rarefaction wave upstream travelling towards the pressure regulator where the wave is reflected back towards the damping vessel. Each wave is reflected multiple times during a cycle and investigating such effect analytically is complicated. The conclusion that unfavourable phasing of these interactions causes the observed variation of Δp is sufficient for the purpose of this thesis.

Figure 21 illustrates the described effect on the simulation results at two operating points. At 3000 RPM the injection occurs at a time when pressure in the system is already low (thanks to the oscillations present in the system). Meanwhile at 2000 RPM the injection starts during a pressure peak. It is apparent that at 3000 RPM the impulses caused by the PFI are in phase with the frequency of the pressure oscillations in the system.

The wave propagation in the system is affected solely by the speed of sound, engine speed and the distances the waves need to cover. Of those only the distances can be realistically affected in the design phase. Injection timing might appear as a plausible parameter as well. But varying the injection timing has no effect on Δp_M since the system just reaches a new equilibrium with a respective phase shift.

Nonetheless, with the proposed damping volume in place the variation is at acceptable levels ($\Delta p/p_{avg}$ change within three tenths of a percentage point, Figure 22). Although, since the lengths of the connecting hoses are yet unknown, it is important to verify these results with the finalized geometry in mind.

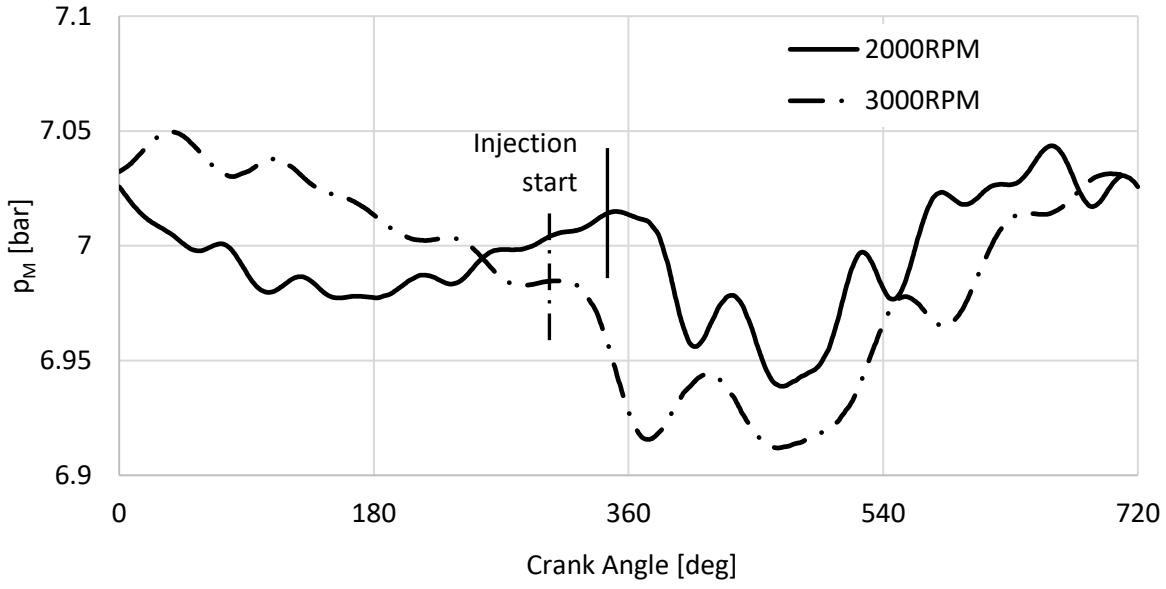

Figure 21 – Pressure at the mass flow controller input for different engine speeds, injection duration 10ms

At the mass flow controller output (p_{Om}) the effect of speed is more distinct. However, the average pressure increases accordingly to cope with the decreasing times available for the fuel delivery into the pre-chamber. Subsequently the effect of speed on the normalized $\Delta p/p_{avg}$ is small (Figure 22) and doesn't limit the system.

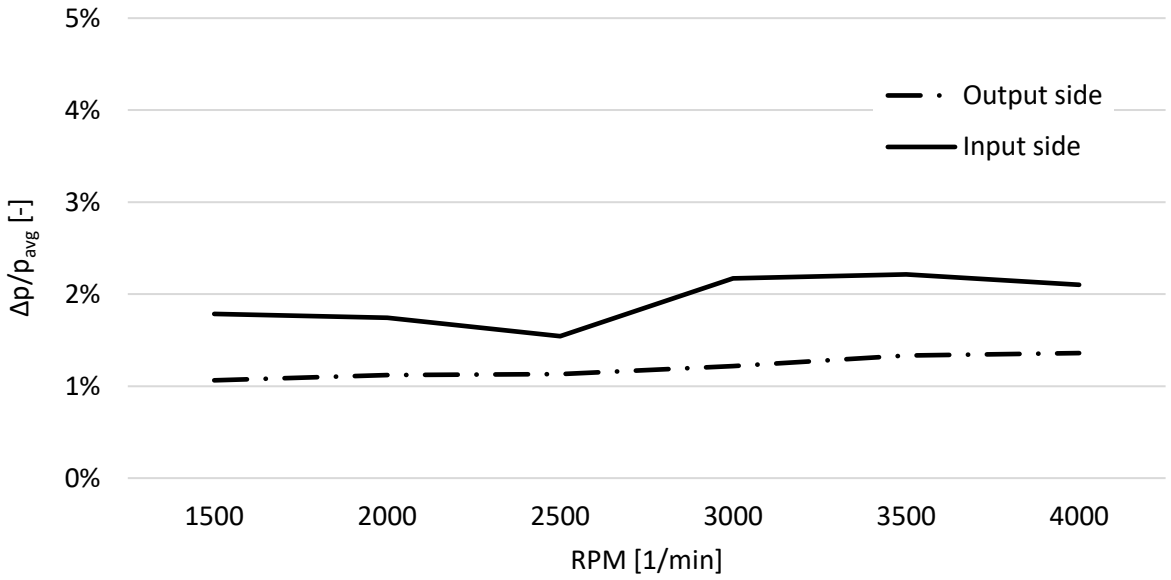

Figure 22 – Speed dependent behaviour of $\Delta p/p_{avg}$

To support the claim that part load conditions pose less stress on the fuel system the dependence of Δp_M on injection duration was investigated. Injection duration of $10\ \mathrm{ms}$ corresponds to the amount of fuel required during engine's full load operation. The end of the injection is set to a constant value. The rail pressure remains the same and the quantity of fuel is modulated only through the injection duration. Results in Figure 23 confirm the assumption that the maximum fuel quantity is the most demanding operating condition.

Based on the simulation results the fuel system with the proposed damping volumes should retain its intended performance under various operating conditions.

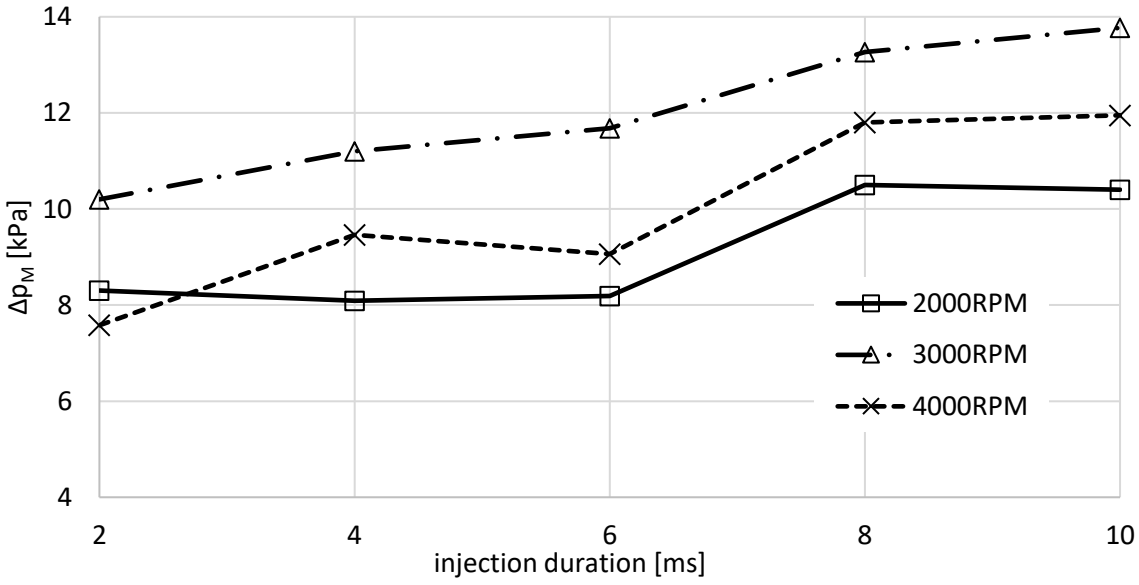

Figure 23 – Effect of injected fuel quantity on Δp_M

4.5.4 Design of the Damping Vessels

As previously mentioned, the two damping vessels will be identical to lower manufacturing costs. For the same reason standardized components need to be utilized. Two different approaches are available.

The first possibility is a welded tank from a stainless-steel pipe, normalized weld-on tank heads and pipe thread nipples (Figure 24). This kind of design includes two long welds that need to be of an excellent quality as any defect would lead to leakage which is unacceptable.

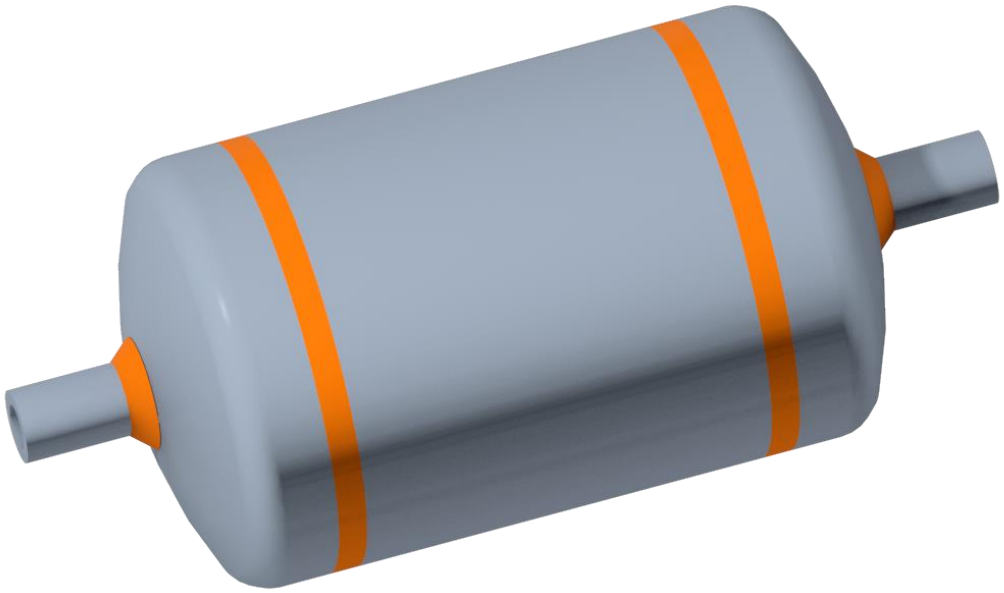

Figure 24 – Welded tank

Alternatively, it is possible to join pipe thread fittings to act as a tank. This is the option that was ultimately decided upon. Since it allows for more rapid manufacturing as all the parts are of-the-shelf and complex welds are avoided.

The tanks are assembled from Class 150 stainless steel pipe thread fittings (AISI 316/EN 1.4401). Class 150 fittings can operate at pressures up to 20 bar. The outer threads are tapered (R) and the inner are parallel (G). To further secure sealing of the components a thread sealant will be used. The tank (Figure 25) consists of 2” threaded pipe nipple acting as the main body and two 2”-½” reducing couplings. Tanks are implemented into the current Swagelok fuel delivery system with Swagelok tube to tapered thread connector (or rather a SuperLok equivalent). The final volume of the tanks is 0.2l.

Assembly drawings of the tanks are included in Attachments 8 and 9.

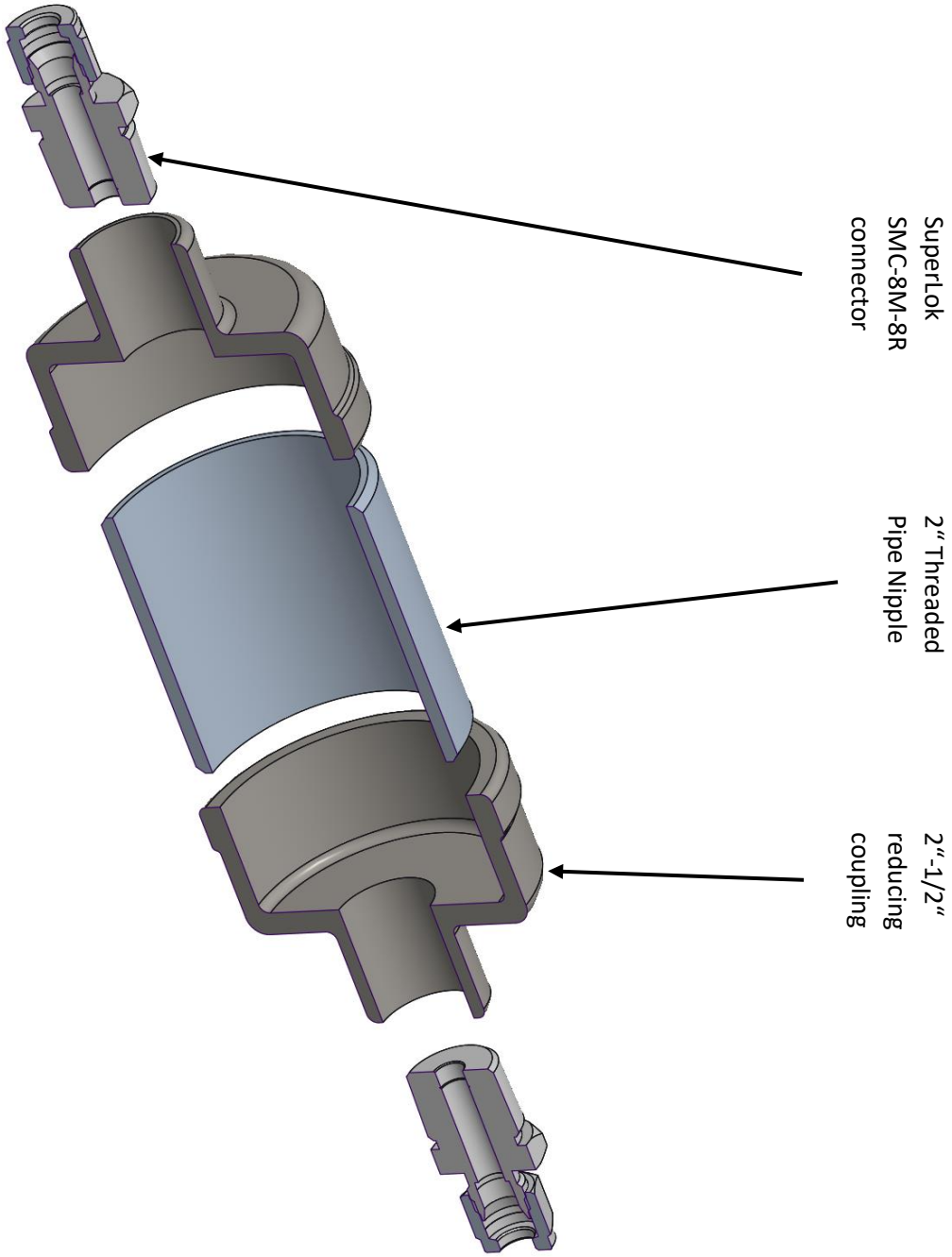

Figure 25 – Tank assembled from pipe fittings

4.6 Secondary injector

As brought up in Section 4.2 results from CTU in-house CFD simulations of the Single Cylinder Research Engine indicate unsatisfactory homogenization of the fuel air mixture which in certain cases leads to large discrepancy in the engine performance (Attachment 1). Including a secondary injector into the ongoing fuel system design would provide a convenient way to experimentally expand on this topic.

4.6.1 Design of the Secondary Injector Holder

The present setup of the test bed is visible in Figure 26. The current fuel injector is positioned conventionally – oriented towards the intake valves. Considering the current intake arrangement, the only reasonable location where a secondary injector might be placed is upstream of the throttle body.

Stainless steel pipe will be inserted in between the throttle body and the air supply hose acting as a base for an appropriate injector holder. Initially a concept similar to the one designed in Section 4.4.2 was investigated where the union nut would be welded onto the intake pipe. This approach was abandoned shortly because of multiple issues. Based on the 1-D simulation (Section 4.3) results the lack of any proper fuel rail would lead to severe pressure oscillations upstream of the injector. Also, no provision for a fuel pressure sensor was available in the vicinity of the injector and the manufacturing of the weldment appeared problematic.

Ultimately after several iterations an injector holder utilizing an original CNG fuel rail was developed. Because the SCRE is based on a 4-cyl engine the fuel rail had to be modified. The rail was shortened leaving us only with a seat for one injector, a provision for the pressure regulator and a fuel supply fitting. The rail was resealed again using brazing. The rail is fastened to a 3D-printed plastic holder with a 3D-printed plastic clamp and an M6 bolt utilizing an already present hole.

Bottom seat for the injector is welded onto the pipe and has a flange pressed onto it. Two threaded M6 holes are used to fasten the plastic rail holder to the bottom part of the assembly.

The whole assembly will be supported by an already present stand to which it will be held with a pipe clamp.

The final design with all mentioned components is shown in Figure 27. Relevant production and assembly drawings are included in the attachments (10-14).

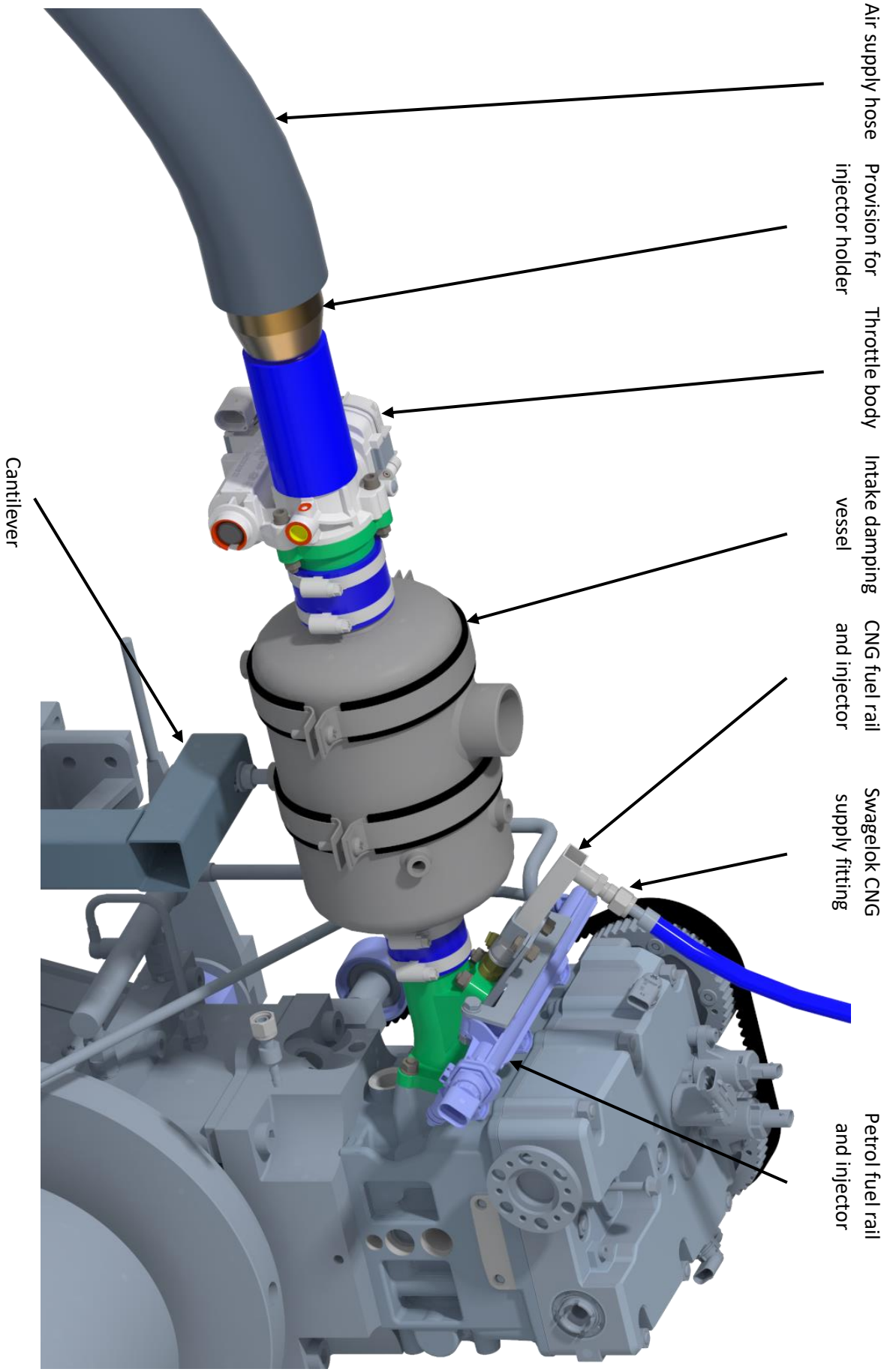

Figure 26 – Intake system of SCRE [14]

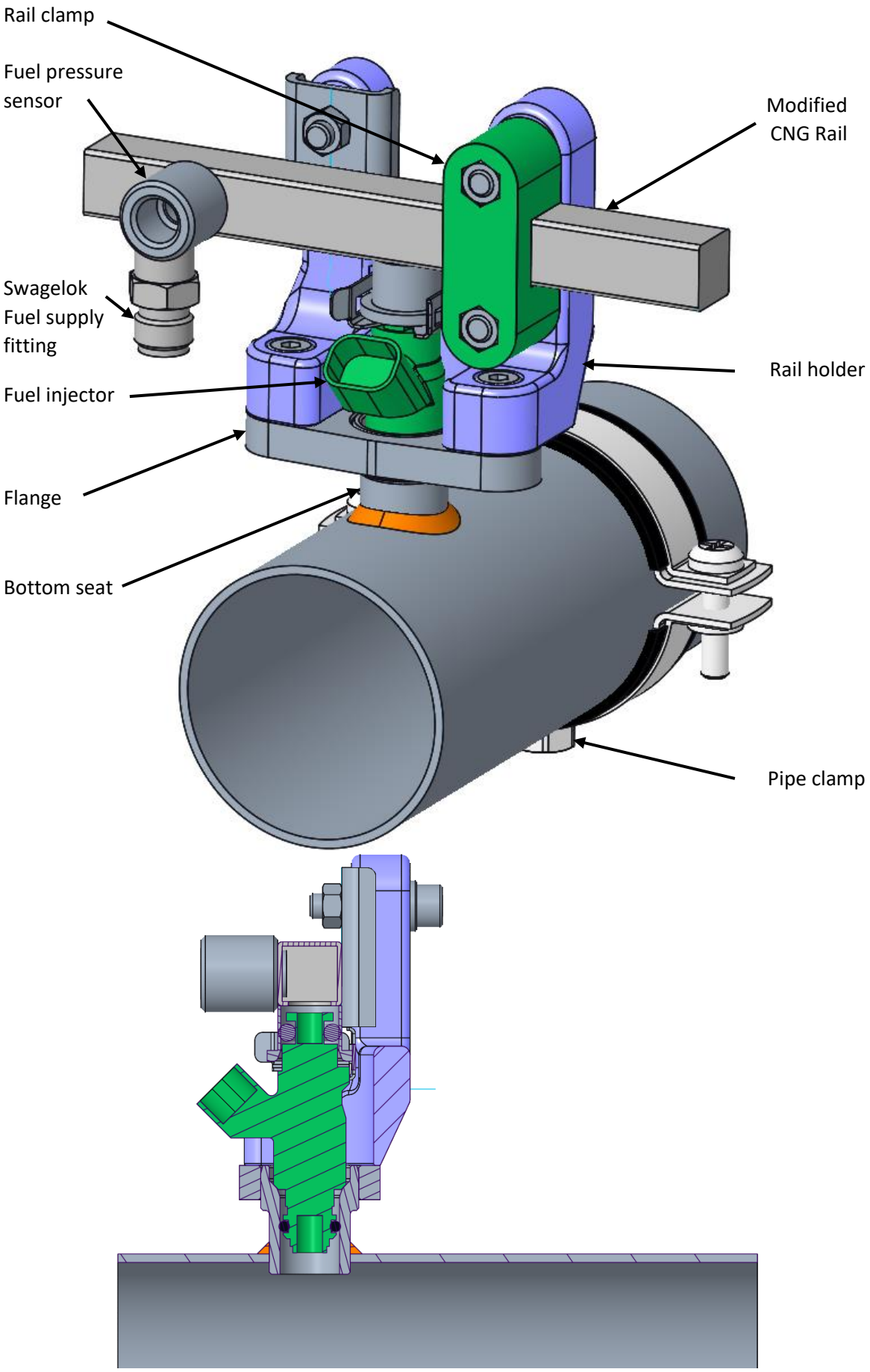

Figure 27 – Secondary Injector Holder

4.7 Fuel System implementation

In the previous Sections several components were investigated and designed separately. At this point it is necessary to connect all these subassemblies into a single fuel system while considering the constraints already presents at the test bed.

Currently the connection between the fuel pressure regulator (Figure 10) and the CNG fuel rail is realized with a rubber ¼" hose (Swagelok PB) and a Swagelok push-on hose end (Figure 26). As this hose is routed to the vicinity of the engine it will be reused as the fuel supply for the proposed fuel system. Since Swagelok type fittings are present in the current fuel system (be it the fuel supply hose or the fuel rail supply fitting), and are the only possible fuel rail connection, these fittings will be at least partially used in the suggested fuel system as well (foreshadowed in Section 4.5.4).

Swagelok (or equivalent i.e. SuperLok) fittings are double ferrule compression type tube fittings. The sealing is achieved in the conical contact between the body and the ferrules which are pressed onto the accordingly sized tube during the assembly without any prior steps (Figure 28). The ease of assembly is especially beneficial in an experimental laboratory where most of the components are one-off prototypes.

Figure 28 – Double ferrule compression fitting (SuperLok) [15]

4.7.1 Design of the Fuel System

The structure of the fuel system is based on Figure 10. The components of the assembly that aren't directly connected to the engine are supported by a U-Section beam inserted into an existing cantilever (Figure 26). The beam is held to the cantilever with two bolts (one hole pre-existing, other drilled on site). The damping vessels are fastened to the beam using pipe clamps and the mass flow controller is bolted down.

The main (and secondary) fuel supply hose utilizes the Swagelok push-on type fittings while the other hoses are attached with pipe thread barbs and secured with Cobra hose clamps. Thread sealant will be applied to the pipe thread connections. A separate hose is required for the secondary injector to limit wear on the fuel rails' supply fittings caused by the repeated assembly. When operation with the secondary injector is required, the main fuel supply hose is disconnected from V_M and the secondary fuel supply hose is connected.

Tee fitting upstream of V_{PC} allows for subsequent implementation of a pressure measuring device that would enable experimental validation of the 1-D simulations' results. Similar measure could be retrofitted upstream of V_M utilizing cross tee fitting (4 ports).

Figure 29 shows the final fuel system assembly with all the subassemblies described. Figure 30 depicts the fuel system assembly in context of the test bed. Further details of used parts and connection are available in the attached drawings (Attachments 15-21).

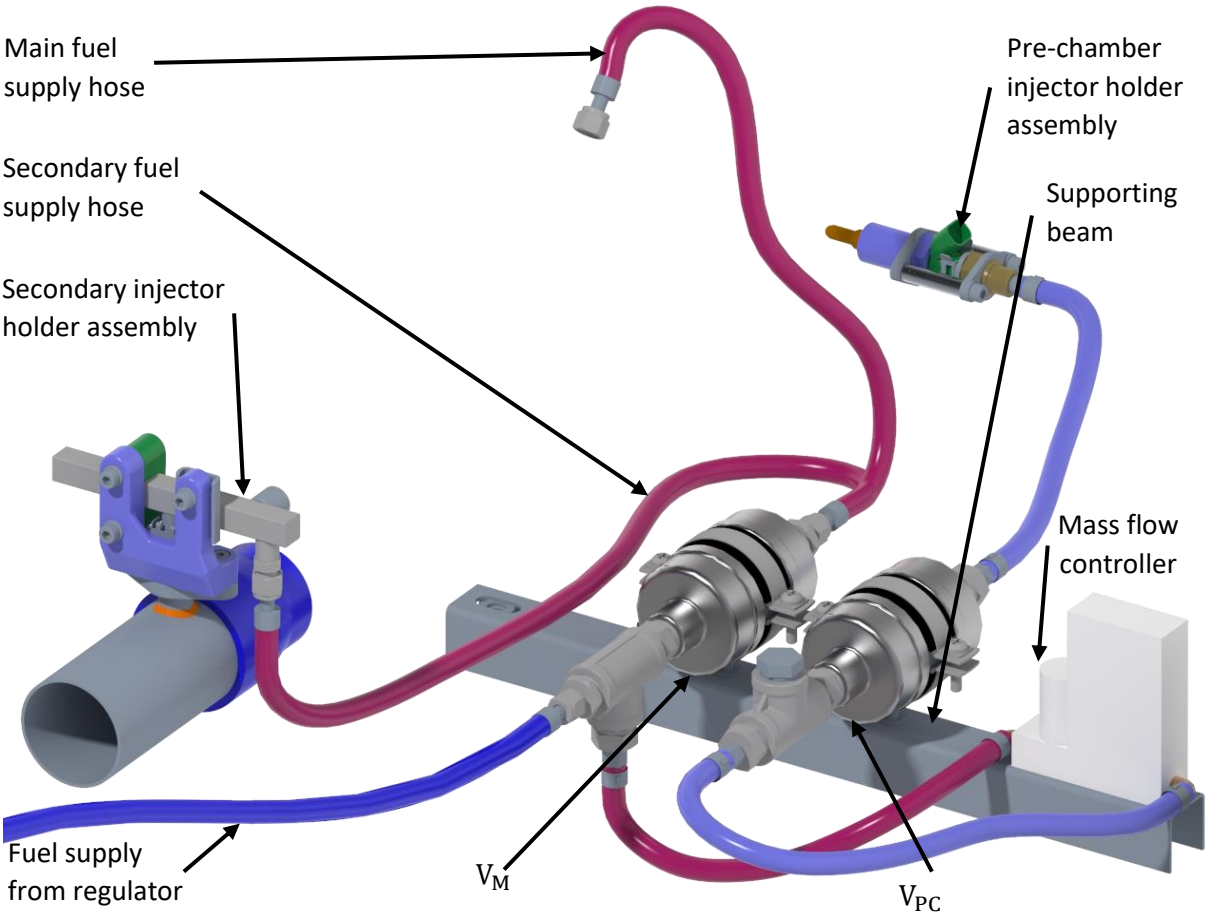

Figure 29 – Fuel system assembly

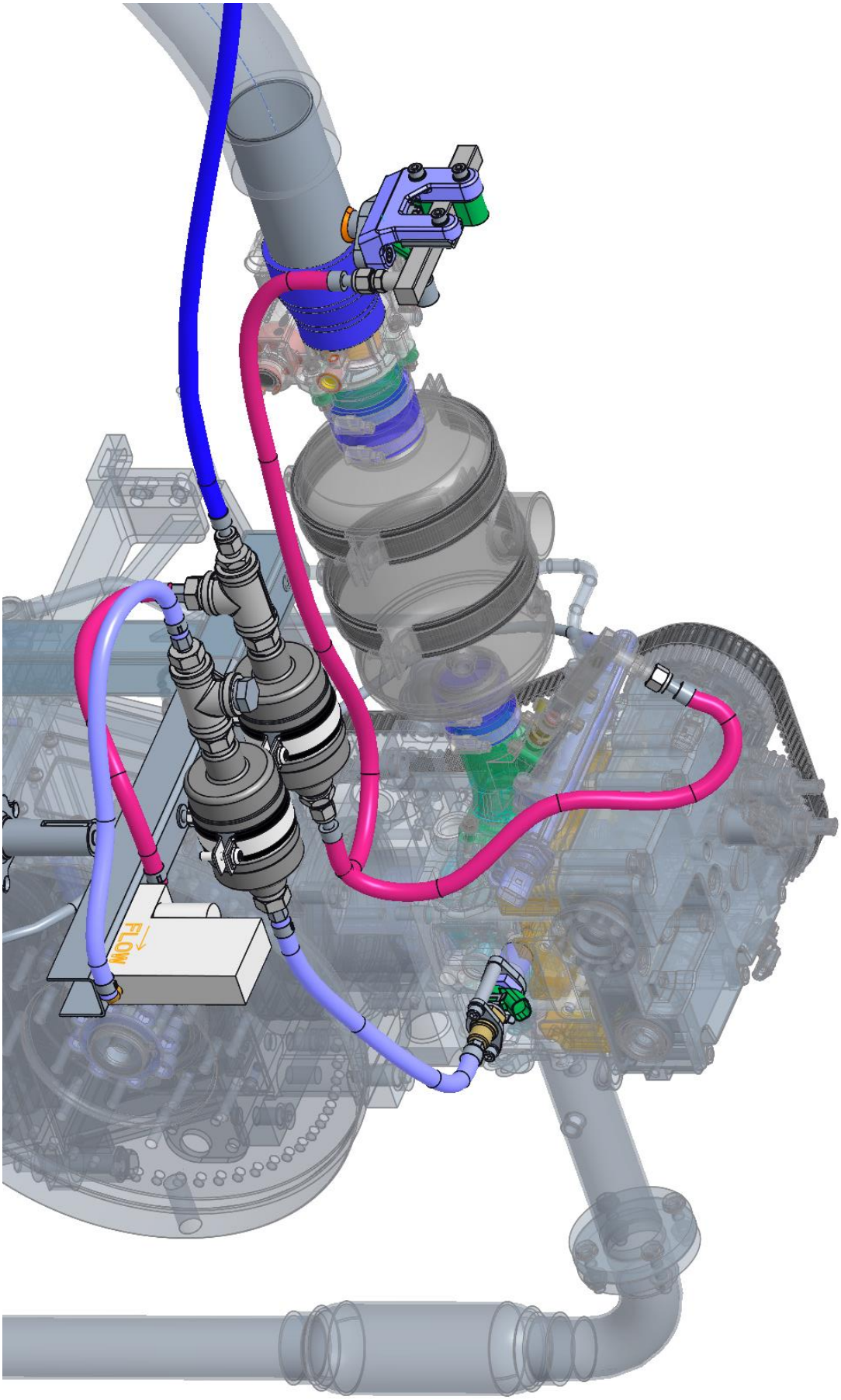

Figure 30 – Fuel system installed in the current setup

4.8 Final simulation results

It is obvious that some of the important geometrical features of the fuel system weren't available in the preliminary design phase (mainly lengths of the connecting hoses). Therefore, as a final step the 1-D model needs to be updated and the decisive simulation results compared to the initial ones. It is also necessary to separately investigate the operation with the secondary injector since the fuel supply hoses and the fuel rails differ.

Results in Figure 31 compare Δp at the mass flow controller input for different stages of development of the 1-D model (and the fuel system itself). Pronounced deterioration of performance is present in the range between 2000 and 2500 RPM for both the finalized setups. While at lower and higher engine speeds the system with the main injector converges to (or even outperforms) the initial results.

Additionally, the results with the secondary injector setup show further increase in Δp. The difference is roughly constant throughout most of the investigated speed range and amounts to couple of kPa.

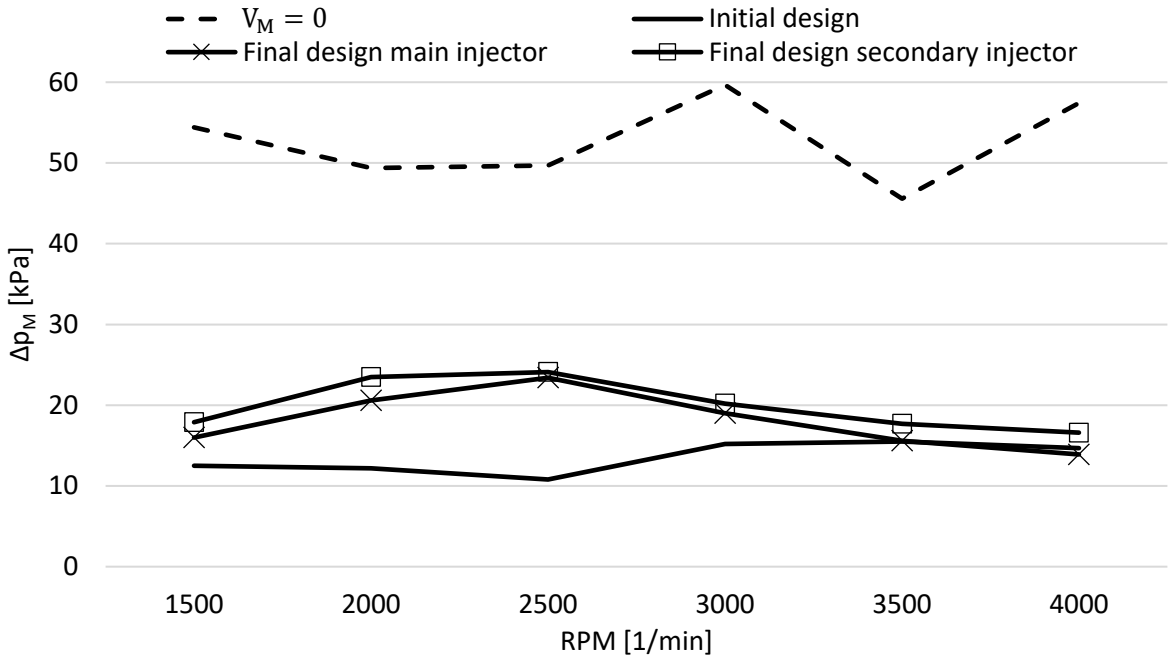

Figure 31 – Comparison of initial and finalized simulation results of Δp_M

Figure 32 shows the predicted percentage improvement of Δp_M over the initial state (no damping vessels, as in Table 6) and the normalized $\Delta p/p_{avg}$ for the finalized geometries. Results of the initial simulation (as in Section 4.5.3) are included for reference. Overall, even in the worst case scenario the performance of the fuel system (quantified by the change of Δp_M) improves by at least 50% and values of the normalized $\Delta p/p_{avg}$ remain around 3% which is well below 5% - a value commonly accepted in much more complex fuel system designs such as a Common Rail Fuel Injection.

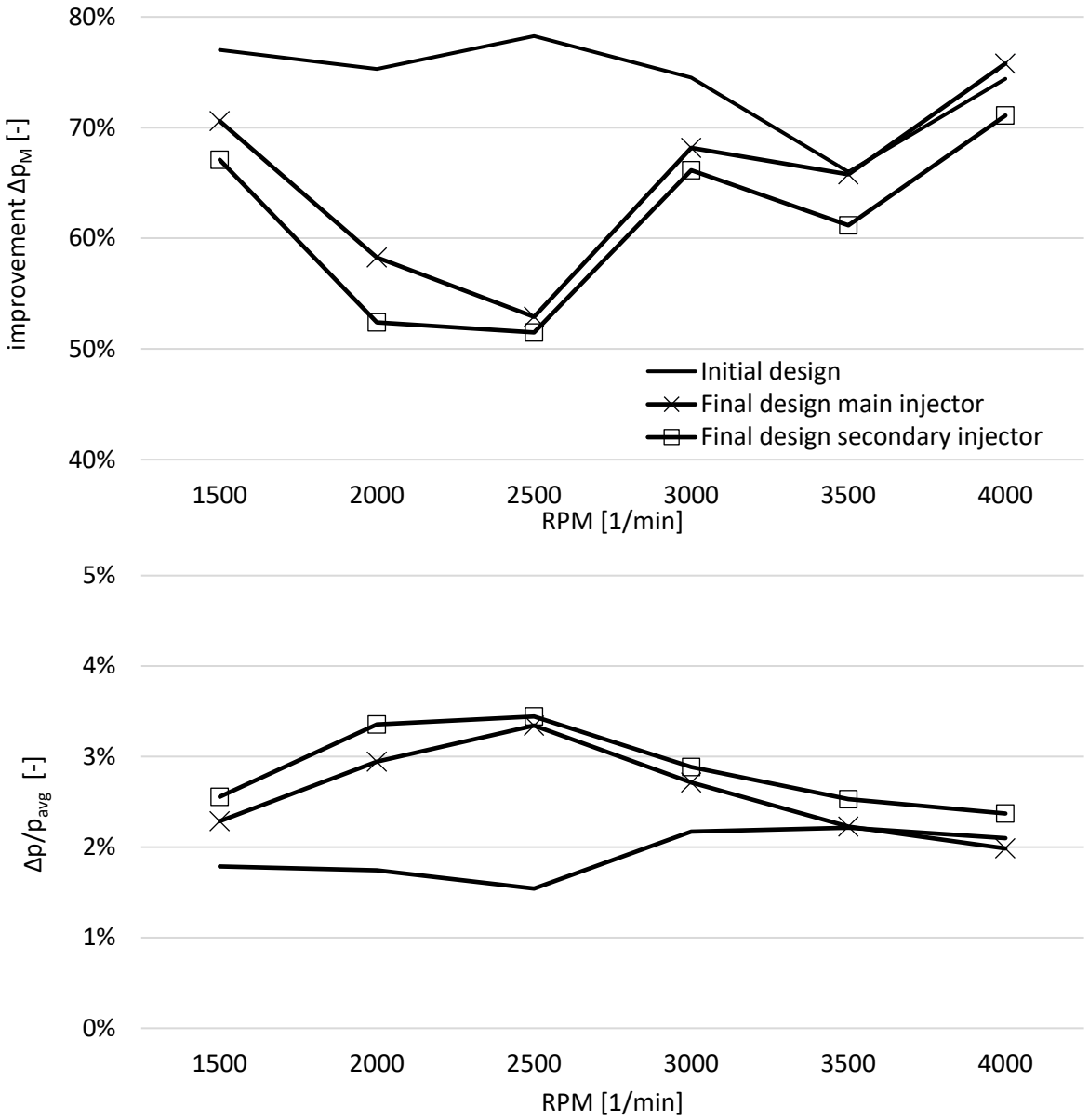

Figure 32 – Predicted improvement of Δp_M and predicted $\Delta p/p_{avg}$ *for the considered designs*

The same comparison for Δp at the mass flow controller output is available in Figure 33. The predicted performance (quantified by Δp_{Om}) is similar between the initial and the final designs as the preliminary geometry downstream of the mass flow controller was estimated well. The results with secondary injector aren't included since no effect was observed (see Section 4.5.1, Cross-sensitivity).

More detailed results are available in Attachment 25 and 26 (only case with main injector).

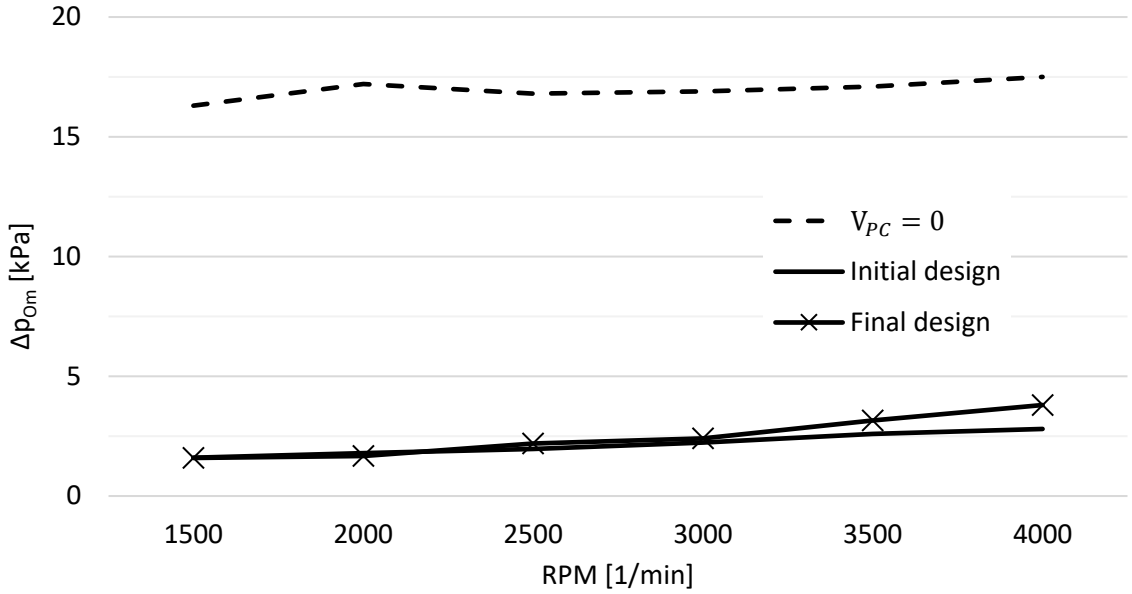

Figure 33 - Comparison of initial and finalized simulation results of Δp_{Om}

4.9 Concluding remarks about the Fuel System design

To understand the reasoning behind the deterioration of the fuel system performance upstream of the mass flow controller it is necessary to reiterate the changes in fuel system dimensions. Two notable differences are present (Table 7, arrangement of the Fuel System per Figure 10):

- the distance between the damping vessel and the fuel rail (l_{PFI}) and
- the distance between the damping vessel and the regulator (l_R)

	Preliminary design	Final design main injector	Final design secondary injector
Damping vessel to Regulator (l_R)	800 mm	1380 mm	1380 mm
Damping vessel to Fuel rail (l_{PFI})	120 mm	500 mm	720 mm

Table 7 – Dimensions differences between the preliminary and final designs

Further investigation into the effect of geometry on the fuel system performance showed that lengthening the distance between the fuel pressure regulator and the damping vessel pushes the resonance described in Section 4.5.1 towards lower engine speeds. Figure 34 confirms that if the original distance l_R is inserted in the finalized 1-D model the resonance returns to the vicinity of 3000 RPM as was the case with the initial results. Δp_M is still larger than in the preliminary case and this difference remains independent of engine speed. Since the location of the resonance was identical to the initial results, it appears that the resonance described in Section 4.5.1 depends mostly on the geometry upstream of the Damping Vessel, as the fuel injection timing (acting as a main source of oscillation) is independent of the geometry and any subsequent (already reflected) pressure waves downstream are small enough to be filtered by the Damping Vessel.

In spite of expectations lowering the distance l_{PFI} had no clear effect on Δp_M and therefore, the increase of Δp_M over the initial design observed in Figure 34 couldn't be attributed to any single design parameter.

Meanwhile increasing the distance l_{PFI} proved to be the reason for slightly differing behaviour between the designs with main and secondary injector. Simulation results show that increasing length of this hose leads to bigger pressure drop in the Damping Vessel with the subsequent effect on Δp_M visible in Figure 31. The slight differences in fuel rails between the two cases had no effect on the results whatsoever.

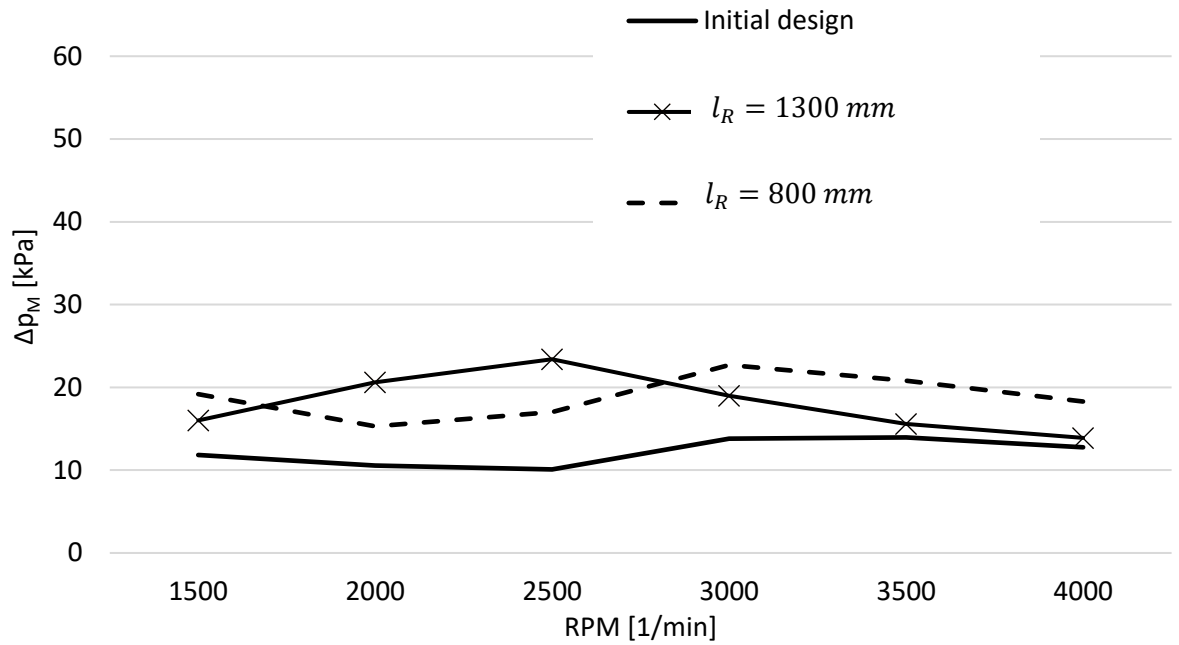

Figure 34 – Effect of the distance from Regulator to Damping Vessel on Δp_M

Overall, the dimensions of the fuel system are more or less dictated by the actual arrangement of components already present at the test bed and major adjustment isn't possible without significant alteration of the current setup. With that in mind the predicted performance of the proposed fuel system is acceptable.

The described effects of dimensions on the fuel system performance provide a reference for possible future modifications of the system if proven necessary.

5 Combined Engine and Fuel System model

In the final phase of this effort it was desirable to couple the 1-D model of the fuel system with the 1-D model of the Single Cylinder Research Engine. This would allow to further numerically verify the behaviour of the fuel system model without the simplifications assumed in Section 4.3 (pressure oscillations in the intake, conditions difference between the pre-chamber and the main chamber). Additionally, such model could be utilized to gain initial control parameters for the pre-chamber injection (timing, mass flow controller setting) and for future predictive pre-chamber models that are currently in-development at CTU.

5.1 Three-Pressure-Analysis with Passive Pre-Chamber

To gain a baseline performance for the engine 1-D model a three-pressure-analysis was carried out (the predicted in-cylinder temperatures are used in the 1-D fuel system model, Section 4.3) based on already available experimental data (gathered with a passive pre-chamber). Majority of the 1-D model used for TPA was also available beforehand (Figure 35).

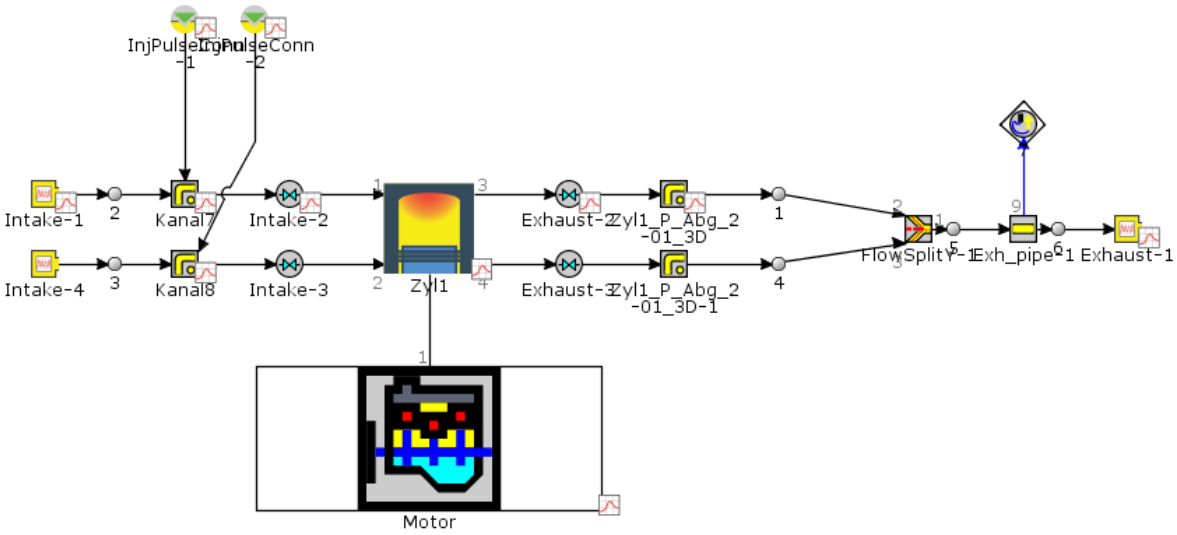

Figure 35 – 1-D GT-Power model for TPA

The in-house model used for TPA was originally developed with spark ignition in mind and some changes were made to reflect the implementation of a pre-chamber. The pre-chamber is introduced in the model through modification of engine parameters (CR, area ratios for the heat transfer model) rather than being modelled directly. Allowing to avoid tuning of the interaction between the main chamber and the pre-chamber and guesstimating the pre-chamber burn rate as, no experimental in-pre-chamber pressure data are available for this engine and the amount of relevant CFD results is limited. The parameters used to include the pre-chamber in the 1-D model are in Table 8.

	Spark plug	Passive prechamber	Active prechamber design
Compression ratio	11.2:1	10.85:1	10.7:1
Head/Bore Area Ratio	1.24	1.35	1.35
Cylinder/Bore Area Ratio	1.357	1.357	1.357

Table 8 – Engine parameters affected by the implementation of a pre-chamber

The evaluated operating points are full load curve from 1000 to 4000 RPM. The injected fuel mass is set to the measured value and the fuel used is defined in Table 2. The used heat transfer model is WoschniClassic rather than the modified WoschniGT model available in GT-Power[2]. Air flow measurements aren't available at the test bed and the air mass per cycle must be calculated from measured pollutant concentrations through lambda (obtained with equation defined by professor Takáts [16]). Data fitting features of GT-Power (like LHV multiplier or Pressure shift) are disabled.

The results in Figure 36 show good agreement between the measured and predicted values (largest difference of IMEP around 2%) with slight qualitative discrepancy of the inducted air mass at 1000 RPM. The predicted burn rates will be used directly in the non-TPA models.

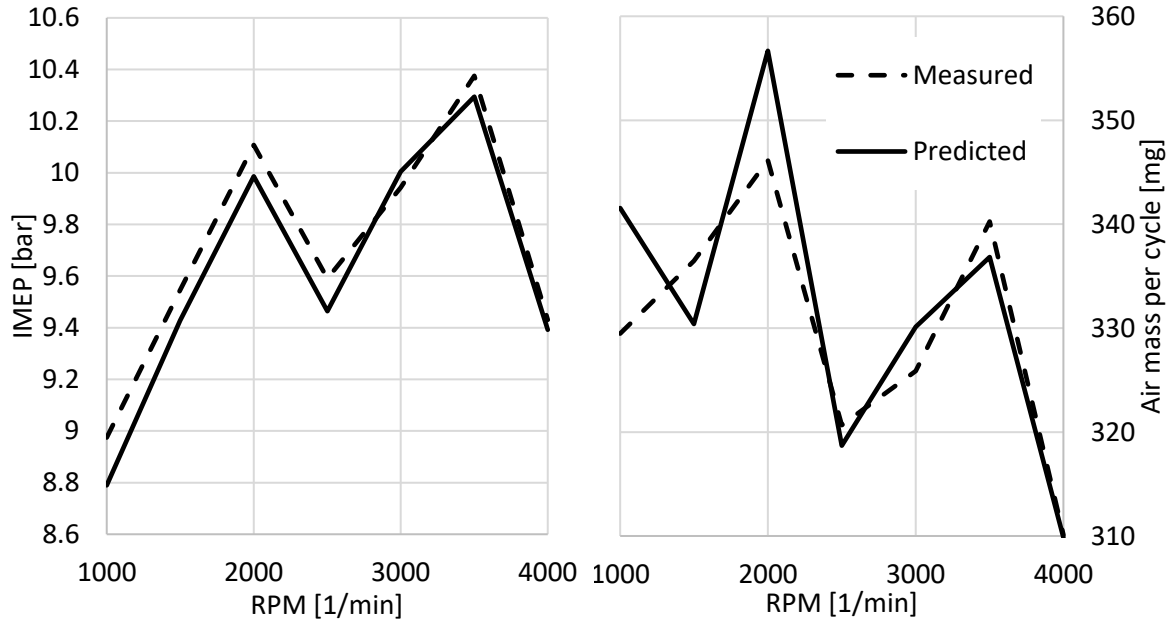

Figure 36 – Comparison of experimental data and TPA results, full load curve, passive pre-chamber

5.2 First attempt

Pre-existent complete SCRE model (including complete exhaust and intake) was updated with the latest geometries (from the available CAD models) and connected with the already presented Fuel System model. The pre-chamber was modelled using the GT-Power template. Burn rate in the pre-chamber is imposed through a Wiebe function and its parameters are

[2] The reasoning will be apparent in later chapters. Other potentially more fitting models (Eichelberg) are available but fine tuning the SCRE 1-D model wasn't a purpose of this thesis.

approximated based on data available from a different active pre-chamber engine (Light Duty Truck Engine – LDTE [9,10,11]) where pressure measurements inside the pre-chamber were available. Burn duration is assumed to be identical. Burned fuel fraction in pre-chamber was obtained from past experiments (LDTE) with motored engine and fuel supplied only into the pre-chamber. The obtained burned fuel fraction is around 30%. CA50 in the pre-chamber is estimated halfway between the main chamber Combustion Start and CA2 (from TPA) which is in line with past data gathered on LDTE (Figure 37).

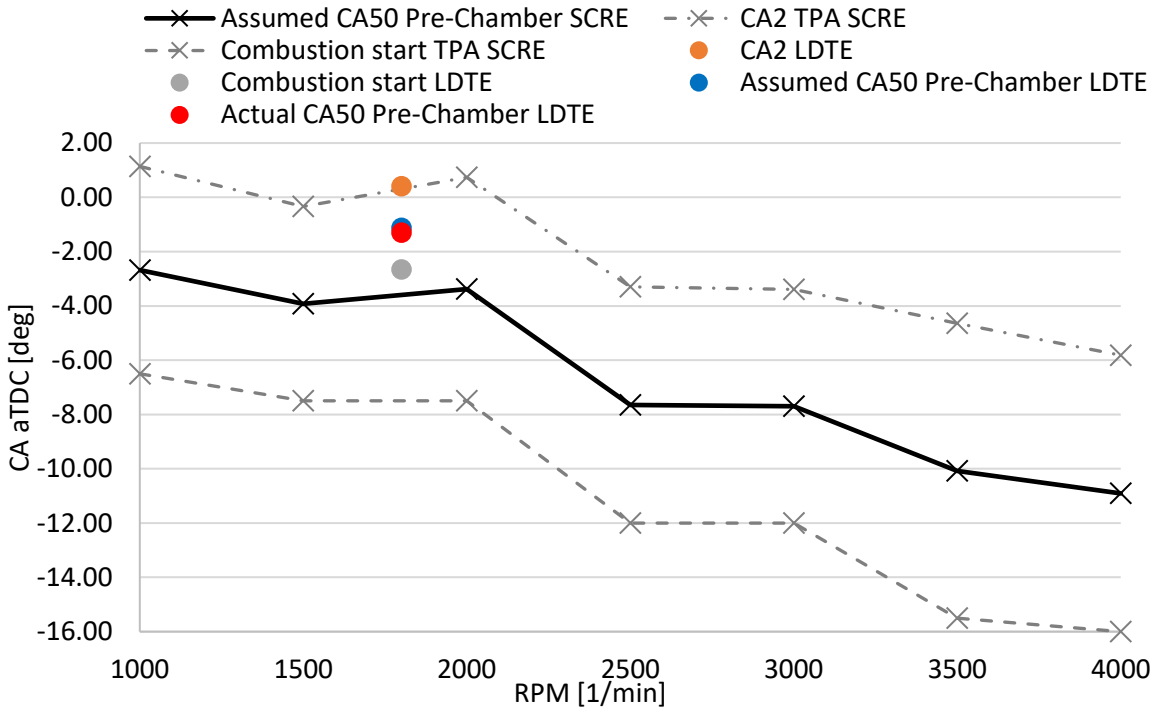

Figure 37 – Assumed CA50 in pre-chamber with respect to the TPA predicted burn characteristics in main chamber, single LDTE operating point for reference

Initial results showed underperforming with poor combustion efficiency. To limit uncertainty in the subsequent analysis the Fuel System was removed from the model, fuel was set to methane and results with only a passive pre-chamber were investigated.

Significant backflow into the pre-chamber during combustion in the main chamber was observed. The backflow contains roughly stochiometric fraction of fuel and this fuel isn't burned (most likely because it is trapped in the pre-chamber during the main chamber combustion) contributing to the lower performance.

Moreover, the predicted fuel mass flow rate back into the pre-chamber doesn't correlate with the predicted fuel mass inside the pre-chamber. If the mass flow rate through the connecting orifice is integrated the resulting values differ (Figure 38). This peculiar behaviour means that fuel leaves the main chamber but doesn't appear in the pre-chamber resulting in an unnatural fuel loss. It seems the pre-chamber template somehow tries to limit fuel concentration after the pre-chamber combustion. This theory is supported by the fact that

the amount of the allowed fuel backflow (observed in the GT-Power predicted fuel mass in pre-chamber) depends on the fraction of fuel burned assumed for the pre-chamber Wiebe curve. The error between the simulation results values and the mass flow integration is affected as well (compare Figure 38 and Figure 39)

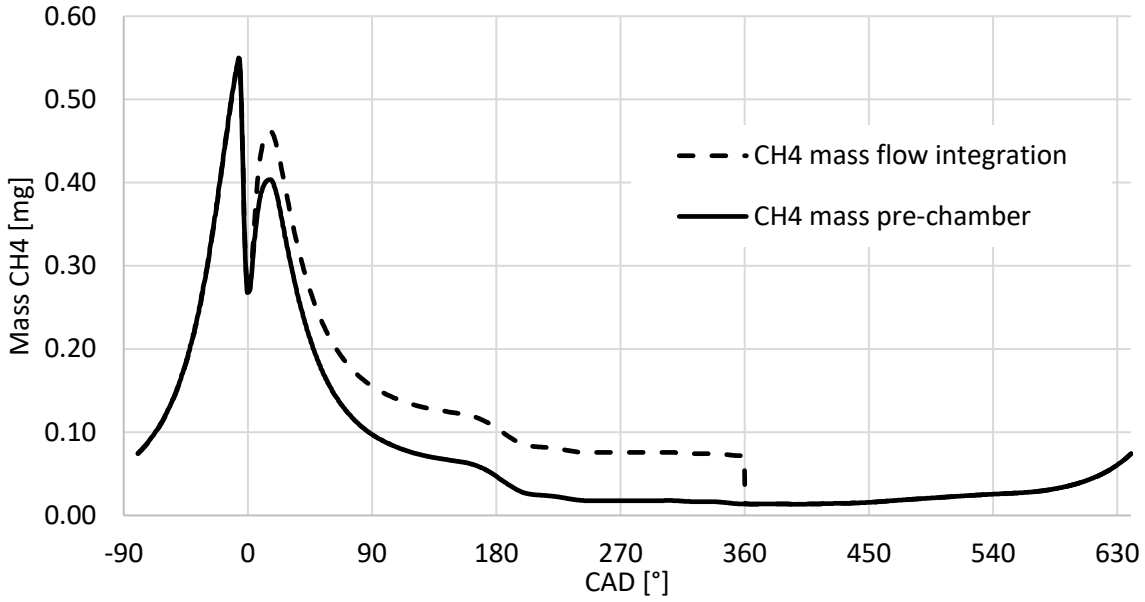

Figure 38 – CH4 mass in pre-chamber predicted and obtained by integration of the mass flow through connecting orifice, pre-chamber Wiebe curve assumed fraction of fuel burned = 0.3

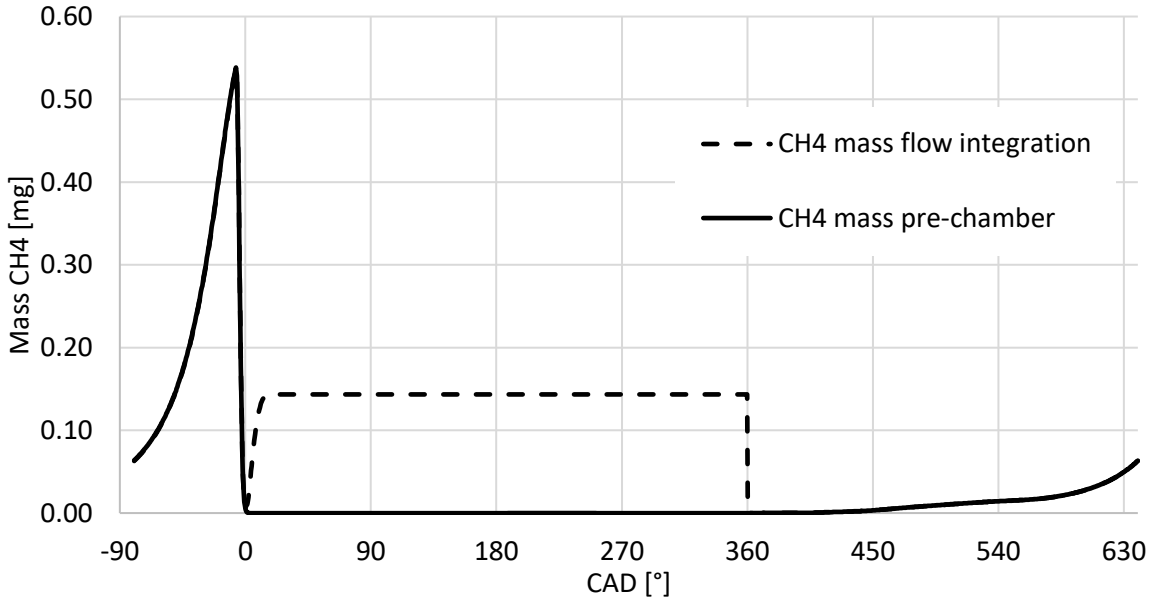

Figure 39 - CH4 mass in pre-chamber predicted and obtained by integration of the mass flow through connecting orifice, pre-chamber Wiebe curve assumed fraction of fuel burned = 1

Most results from this phase are purposefully omitted since their only contribution is that they are incorrect. Also, the GT-Power pre-chamber template is relatively recent and as such its behaviour between different versions varies. Therefore, it is difficult to reproduce some of the initial results. The purpose of this chapter is to maintain temporal coherence and to foreshadow issues investigated in later chapters.

5.3 CFD data comparison

As mentioned previously some results of in-house CFD simulations of SCRE with passive pre-chamber are available. The aim of this chapter is to use this data (that also include inside pre-chamber results) as an input to TPA with the pre-chamber model included (Figure 40) and then tune available parameters to try and replicate the CFD results. Multiple signals are monitored beyond the standard results to observe the pre-chamber fuel mass discrepancy. Also, a new parameter is introduced to further evaluate the quality of the fit. The parameter is the difference between main chamber and pre-chamber pressures since it governs the mass flow between the respective chambers ($\Delta \mathrm{Cyl} - \mathrm{PC}$).

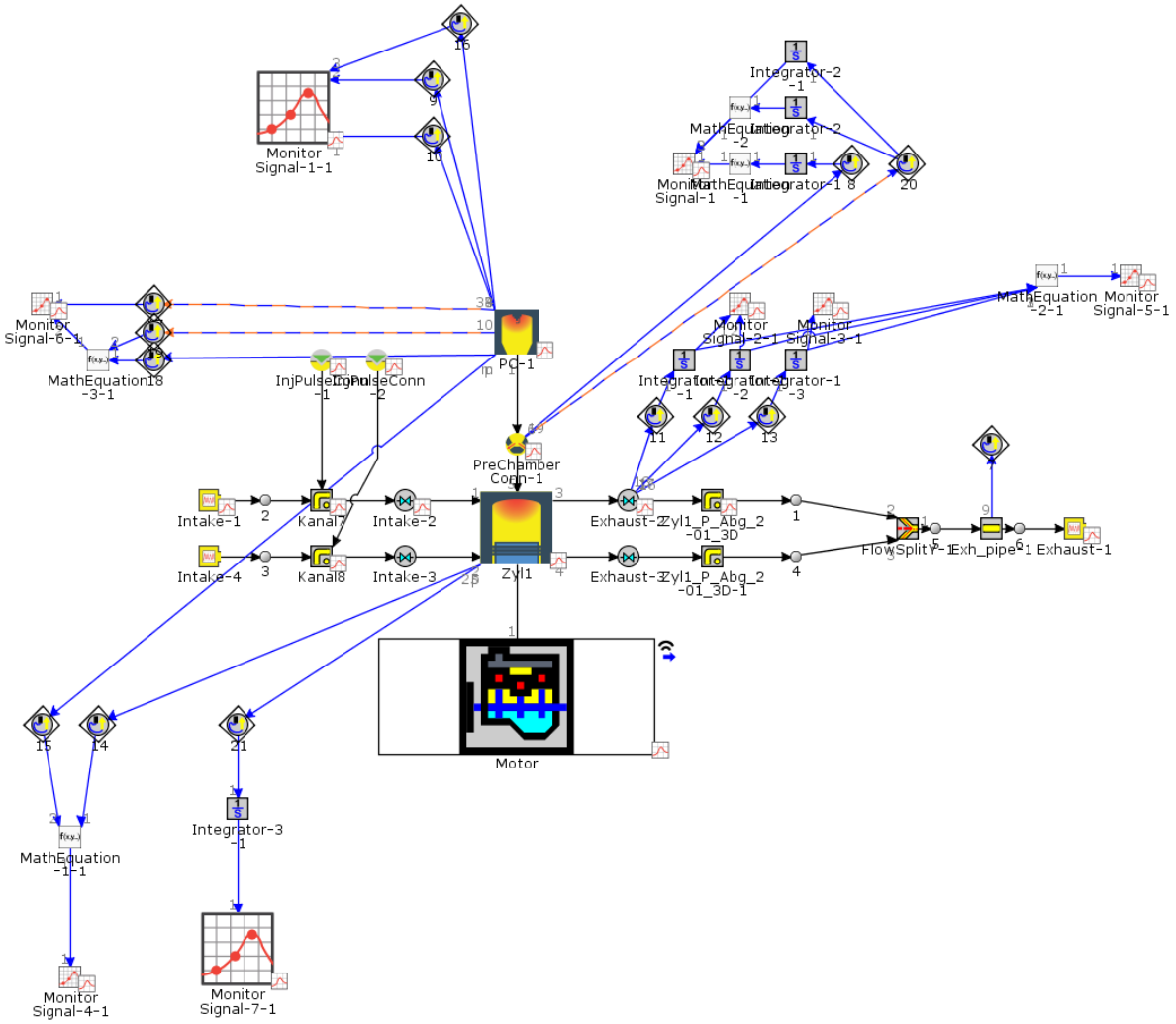

Figure 40 – TPA with pre-chamber included

Single operating point is available – part load condition at 2000RPM fuelled with methane. Qualitatively the CFD results predicted significantly smaller backflow into the pre-chamber, different combustion phasing and different heat transfer rates with respect to the First Attempt model. However, there is no point quantitively comparing these since they were gathered at different operating points.

5.3.1 Fuel fraction burned in Pre-Chamber

The CFD simulation assumes simplified combustion model where all fuel is burned. Therefore, the chemical efficiency inside the pre-chamber can't be investigated. This isn't necessarily an issue since the aforementioned value of 30% (gathered from LDTE) was initially misinterpreted. The value of 30% contains two components. Firstly, the combustion efficiency (fraction of fuel burned for the Wiebe curve) and secondly, (and more importantly) the fuel outflow from the pre-chamber. As the pre-chamber is connected to the main chamber, the combustion initiated at the top of the pre-chamber pushes unburned fuel and active radicals into the main chamber[3].

The effect of fuel outflow is the more important contributor to the final ratio between fuel burned in the pre-chamber and fuel trapped in the pre-chamber (at the beginning of the combustion). 1-D simulation with no combustion present in the main chamber and 0.5mg[4] of fuel delivered directly to the pre-chamber (to reflect how LDTE experiment was setup) shows that large differences in the assumed Wiebe curve fraction of fuel burned have relatively small effect on the ratio of fuel burned to fuel trapped in the pre-chamber (Table 9)[5].

Pre-chamber Wiebe curve Fraction of fuel burned	$\frac{fuel\ burned\ PC}{fuel\ trapped\ PC}$
1	0.3
0.3	0.2

Table 9 – Effect of assumed fraction of fuel burned on the ratio of fuel burned and fuel trapped, no combustion in main chamber

Moreover, with fraction of fuel burned set to 1 the ratio is equal to the expected value of 0.3. Based on these considerations setting the fraction of fuel burned in the pre-chamber to 1 isn't detrimental to the simulation quality. Nonetheless, further experimental investigation would be beneficial to provide greater understanding of this topic.

5.3.2 Combustion phasing

The pre-chamber combustion parameters assumed in Figure 37 are contradicted by the CFD results which indicate that the pre-chamber CA50 comes couple degrees after the main chamber CA2. This means that the pressure peaks in respective chambers are much closer to

[3] This interaction is described in great depth in [6]

[4] Corresponding to pre-chamber fuel mass obtained from CFD results

[5] It is important to note that these results were gathered in v2021 version of GT-Power. This version allows to bias the outflow from pre-chamber towards unburned gases – "Preferential Outflow of Unburned Gases" option. Without this setting the initial outflow succeeding the pre-chamber combustion contains larger amounts of burned gases and the fuel outflow is reduced by roughly 30%. This indicates that larger amount of fuel is eventually burned in the pre-chamber and the importance of Wiebe curve definition increases. Such behaviour however contradicts in-house CFD results and findings by others [6].

each other and significantly smaller backflow into pre-chamber is observed (with respect to Section 5.2).

With the use of TPA the main chamber burn rate is predicted from the CFD results. TPA isn't available for the pre-chamber template and the Wiebe curve parameters need to be calibrated manually. This effort is further hindered by the non-constant mass inside the pre-chamber altering the parameters of the final combustion from the assumed Wiebe curve parameters (Table 10). Fuel mass in the pre-chamber (representing the combined effect of combustion and fuel outflow, Figure 41) and $\Delta\mathrm{Cyl} - \mathrm{PC}$ (to assess correctness of pressure phasing, Figure 42) are the main parameters to evaluate the quality of the fit between the two sets of results.

	Wiebe curve parameters	Predicted burn rate
CA50	11° aTDC	9.3° aTDC
CA10-90	8.5°	8.7°
Exponent	2	?
Burned fuel fraction	1	0.886[6]

Table 10 – Comparison of pre-chamber Wiebe curve parameters and predicted burn rate

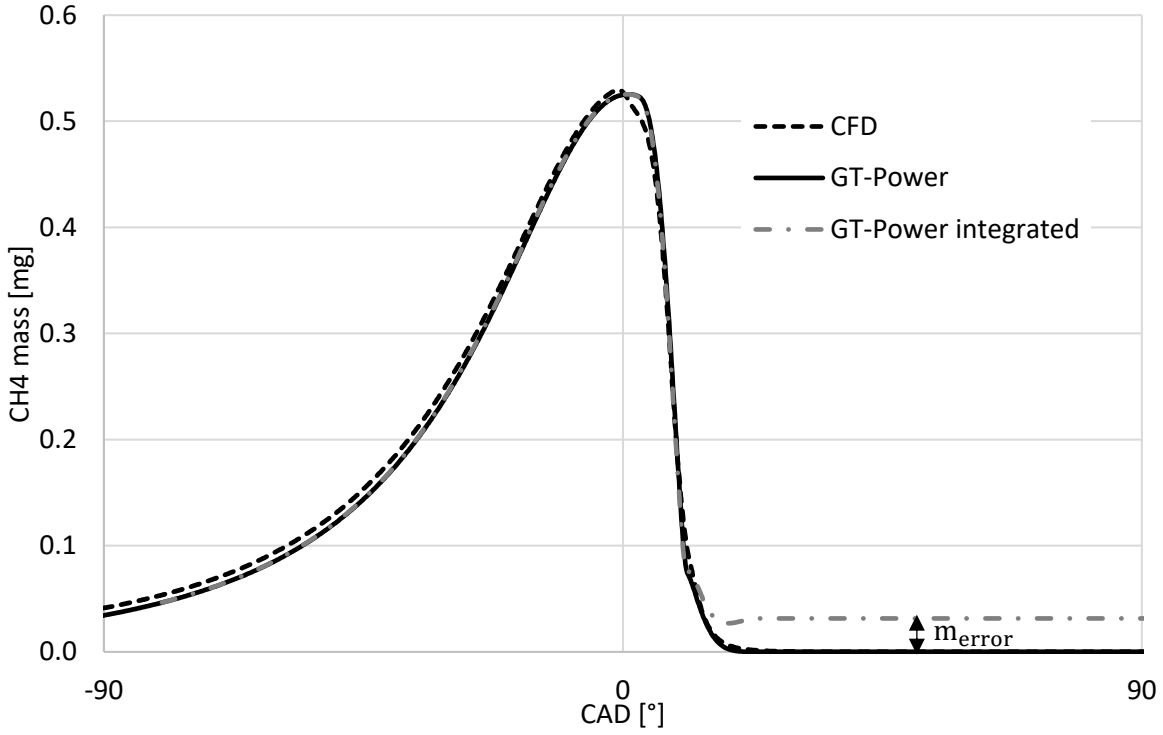

Figure 41 – Methane mass pre-chamber, comparison of CFD, GT-Power and value obtained by integrating mass flow rate through the connecting orifice

[6] Surprisingly GT-Power utilizes the lost m_{error} to calculate burned fuel fraction. See $m_{burnPC}/(m_{burnPC} + m_{error}) = 0.247/(0.247 + 0.0316) = 0.886$ which is equal to the predicted pre-chamber burned fuel fraction in the GT-Power results.

The foreshadowed discrepancy between pre-chamber fuel mass obtained from the predicted mass fractions and from the fuel mass flow rate integration is still present. However, as the amount of backflow was limited the error between the two values lowers as well. The error is down from 0.144mg (Figure 39) to 0.03mg. Applying mass balance to the fuel entering the cylinder, burned and leaving the cylinder like so

$$\mathrm{m_{fuelIN}} - \mathrm{m_{burnCYL}} - \mathrm{m_{burnPC}} - \mathrm{m_{fuelOUT}} = 16.86 - 16.549 - 0.247 - 0.0332 = 0.0315\mathrm{mg} \approx \mathrm{m_{error}} = 0.0316\mathrm{mg} \quad (6)$$

supports the claim that integrated mass flow rate value is indeed correct, and the fuel is lost. This issue was investigated extensively during this effort, was repeatable and no satisfying resolution was discovered. It is possible that the observed behaviour originates in the way the pre-chamber template is implemented in GT-Power.

However, relative to the fuel mass delivered per cycle this amount is sufficiently small (0.2%) to have negligible effect on the engine's performance. As such, this error was deemed acceptable to carry on. But this topic will be likely revisited in the future.

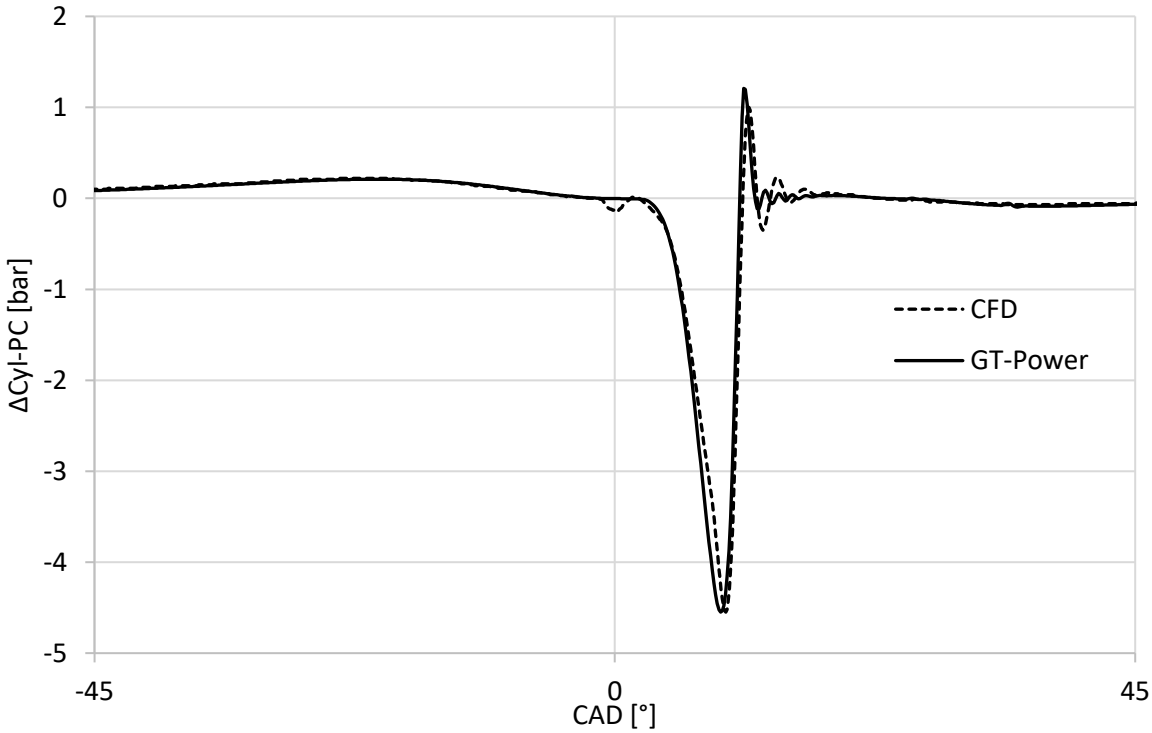

Figure 42 –Predicted difference between cylinder and pre-chamber pressure, comparison of CFD and GT-Power

5.3.3 Pre-chamber heat transfer

It was observed that the pre-chamber heat transfer coefficient model affects the filling of the pre-chamber (more so than reasonable varying of connecting orifice discharge coefficient). GT-Power pre-chamber template allows either assuming the main chamber coefficients or to tune a *Flow* model based on 4 turbulent parameters. Such flow model had to be tuned to

try and fit the heat transfer rates predicted by the CFD. Comparison between the two models and the CFD and their effect on pre-chamber filling is available in Figure 43.

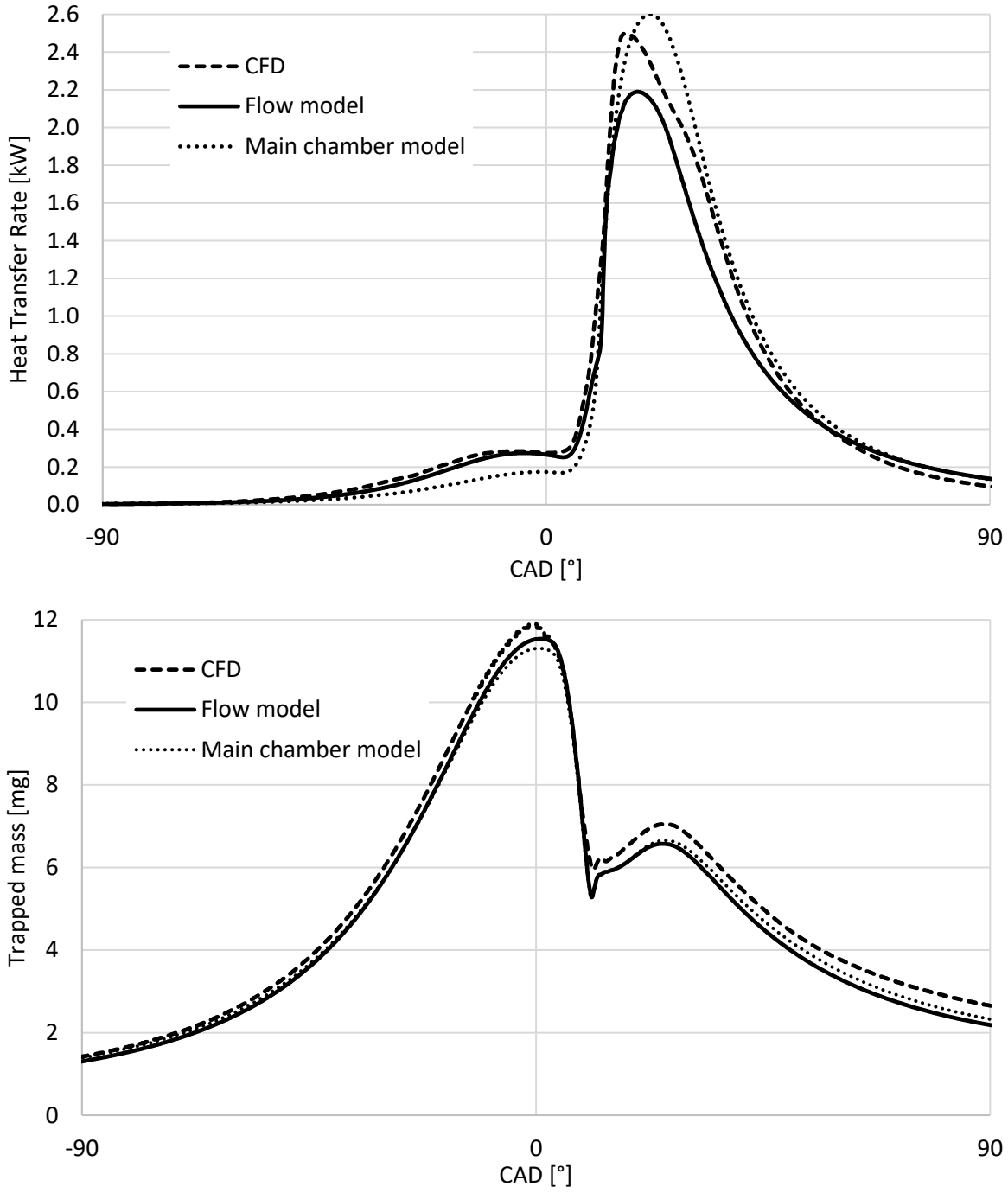

Figure 43 – Comparison of different heat transfer coefficients models and their effect on pre-chamber filling

The Flow model predicted heat transfer rates followed the CFD results more accurately during compression which had some positive effect on the trapped mass in the pre-chamber around TDC. Meanwhile, the main chamber model followed the CFD results well during the expansion but the effect on the trapped mass during expansion was limited. None of the models correlated well with CFD during the combustion. The Flow model is utilized in

subsequent models as the slightly enhanced filling during compression was deemed more significant. However, all the predicted trapped mass around TDC results are within 5%.

5.3.4 Results

The endeavours described in the past chapters led to GT-Power model that could very well reproduce the CFD results. Some of the results were already presented in Figures 43,44 and 45. Further results are presented below.

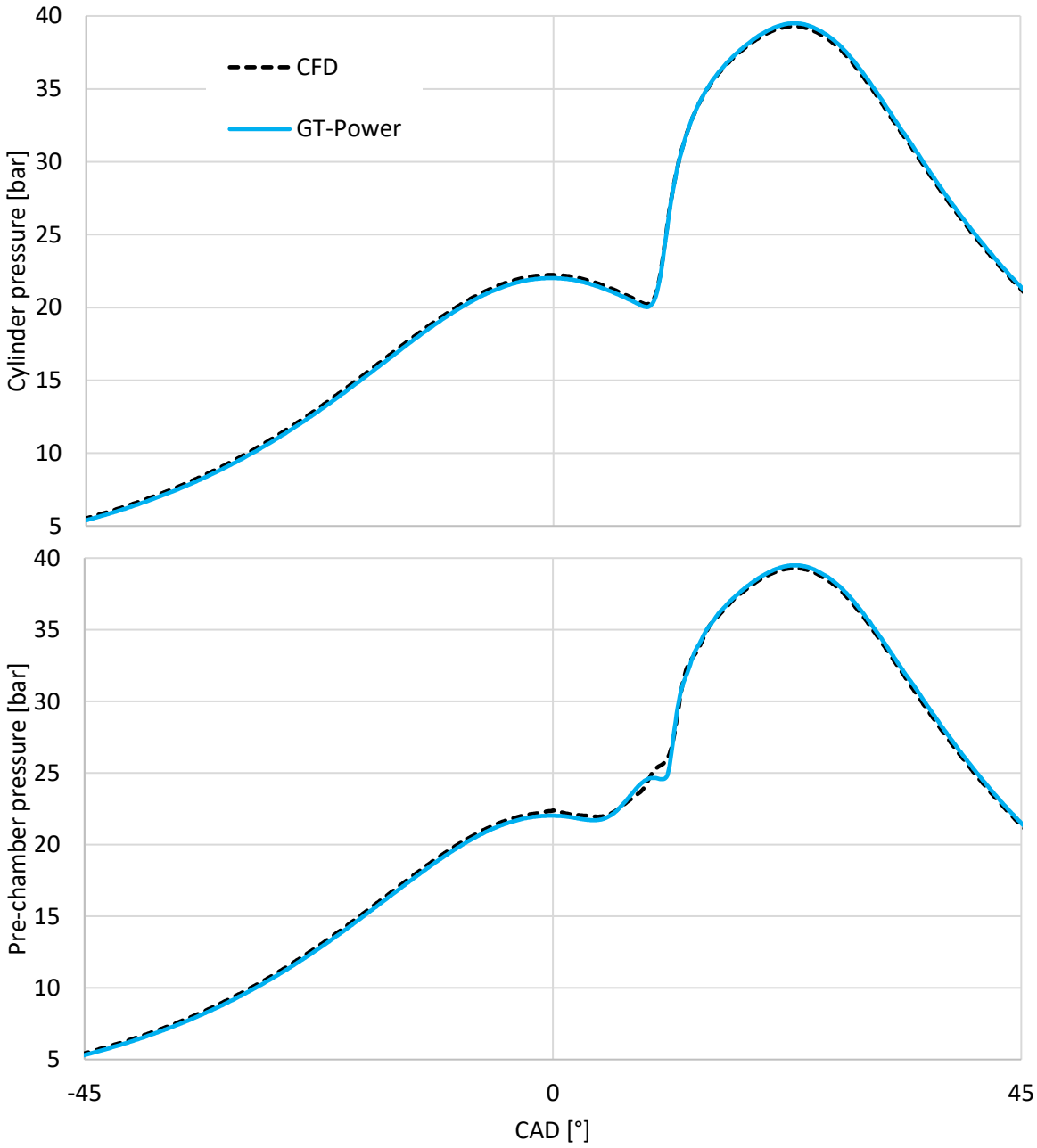

Figure 44 – Comparison of predicted in-cylinder and in-pre-chamber pressure between CFD and GT-Suite

	CFD	GT-Power
IMEP [bar]	8.61	8.77

Table 11 – Predicted IMEP CFD vs GT-Power

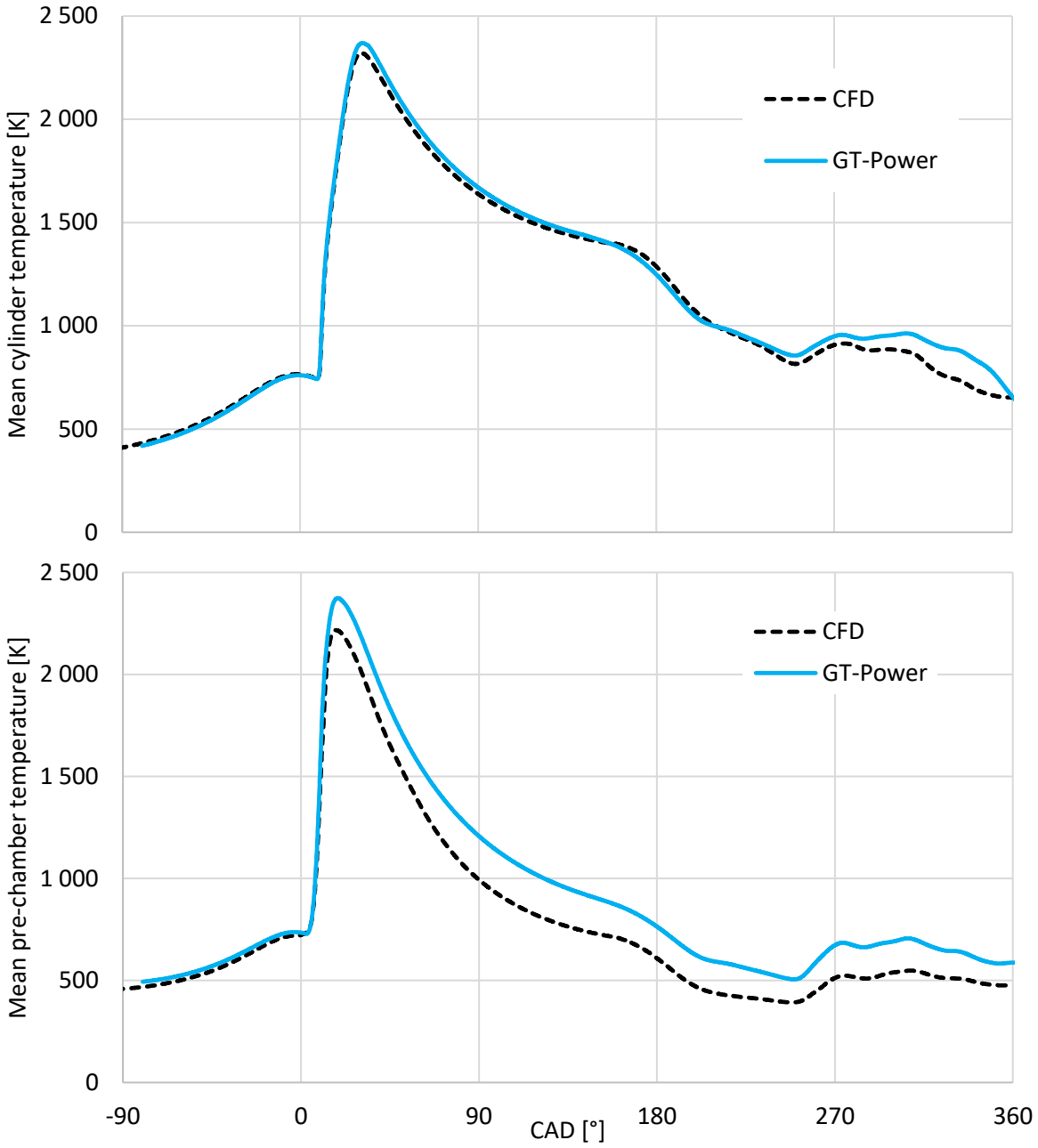

Figure 45 - Comparison of predicted in-cylinder and in-pre-chamber mean temperature between CFD and GT-Suite

All the presented results show good fit with the exception of pre-chamber temperature. The use of Main chamber heat transfer model alleviates the difference slightly due to the larger heat transfer rates during expansion, however the same peak temperature is still reached (as in Figure 45) making it clear that the heat transfer model isn't the underlying cause.

One final note to the results is necessary, comparison of the in-cylinder heat transfer rates showed that the WoschniClassic model correlates slightly better with the CFD results (albeit far from perfectly) than the WoschniGT (Figure 46). WoschniClassic is able to at least somehow react to an increased turbulence caused by the exhaust valve opening and overestimates the Heat Transfer Rates during expansion slightly less with respect to

WoschniGT. If integrated over the cycle total Heat Transfer is identical for both models. It is only the phasing of the heat transfer rates that changes.

Author is aware of the fact that proper prediction of heat transfer rates is difficult even with the use of CFD, however the goal in this chapter was to reproduce the CFD results as closely as possible. Furthermore, rerunning the TPA (from Section 5.1) with WoschniClassic heat transfer model resulted in predicted performance more closely following the experimental results. The results in Section 5.1 are already based on a model utilizing the WoshcniClassic model as was mentioned.

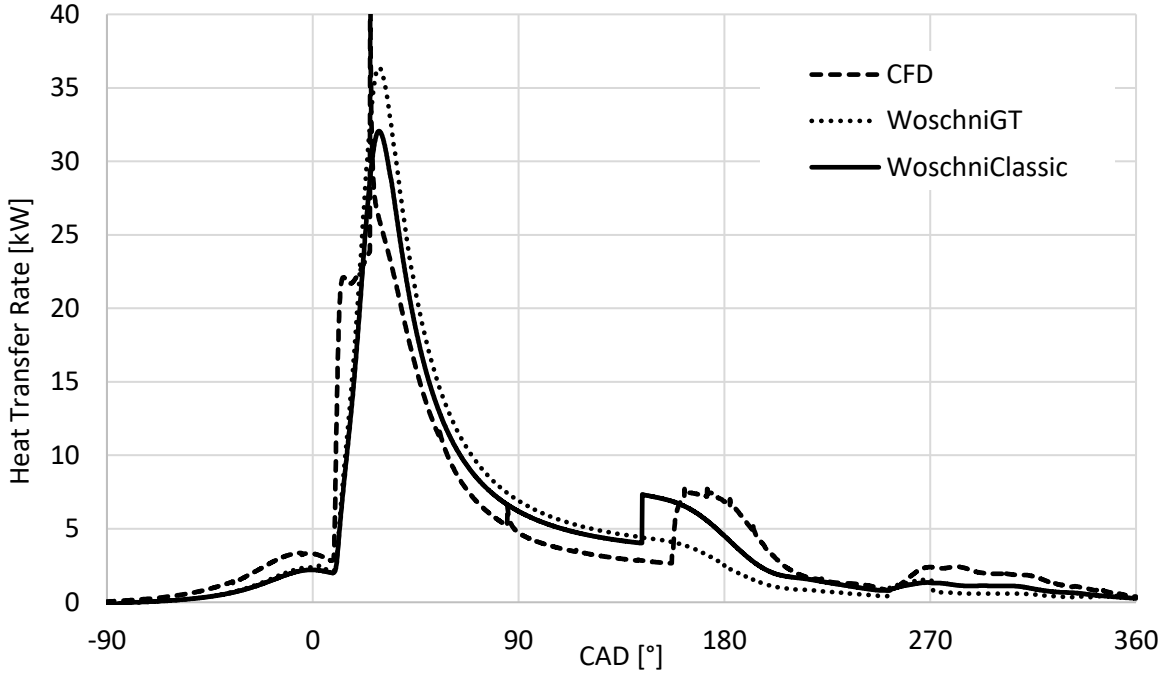

Figure 46 – Comparison of Heat Transfer Rates between different models and CFD

5.4 Extrapolating the pre-chamber burn rates to different operating points

Before a second attempt to build the combined engine model was undertaken, the TPA from Section 5.1 was rerun with the pre-chamber template included (Figure 40) to assess whether the performance of the model would be acceptable when the burn rates obtained in the last chapter are extrapolated to different operating points.

The pre-chamber burn rates at 2000RPM are taken directly from the last chapter results. Despite being a part load case, its load is very close to the FLC (Table 11).

Pre-chamber burn duration was estimated with a linear extrapolation such that CA10-90 at 2000RPM was set to 8.5° (Table 10) and the RPM induced increase proportional to the increase of the main chamber CA10-90 obtained with the model from Section 5.1 (Figure 47).

Pre-chamber CA50 (Figure 47) is based on the difference between $CA50_{MC}$ and $CA50_{PC}$ (6.7° at 2000RPM) and is extrapolated to different engine speeds so that is proportional to the difference between main chamber CA50 and CA2 (obtained in Section 5.1).

$$CA50_{MC} - CA50_{PC} = 6.7 \frac{(CA50_{MC} - CA2_{MC})_{RPM}}{(CA50_{MC} - CA2_{MC})_{2000RPM}} \quad (7)$$

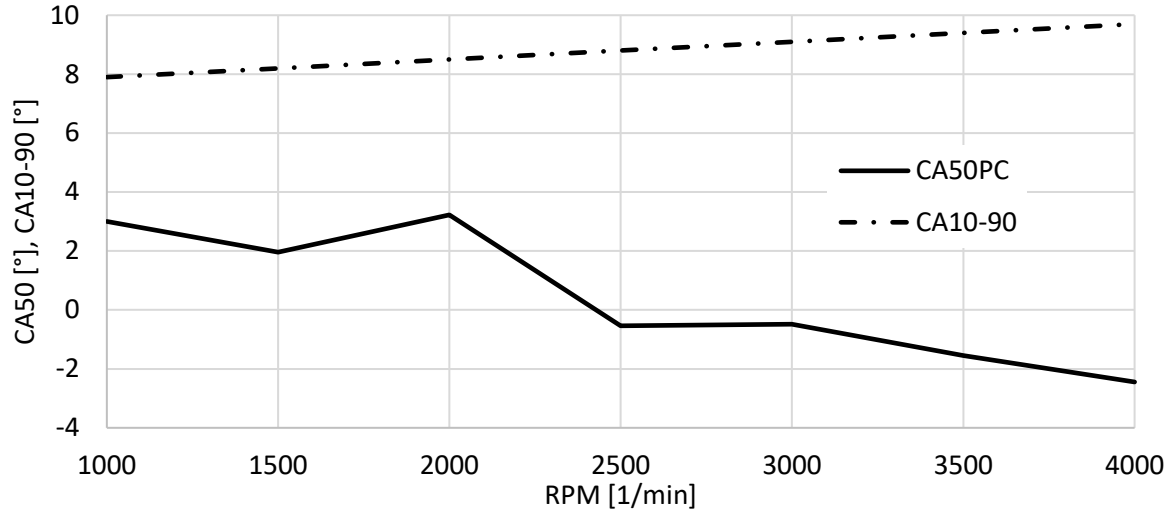

Figure 47 – Extrapolated burn rate parameters for FLC

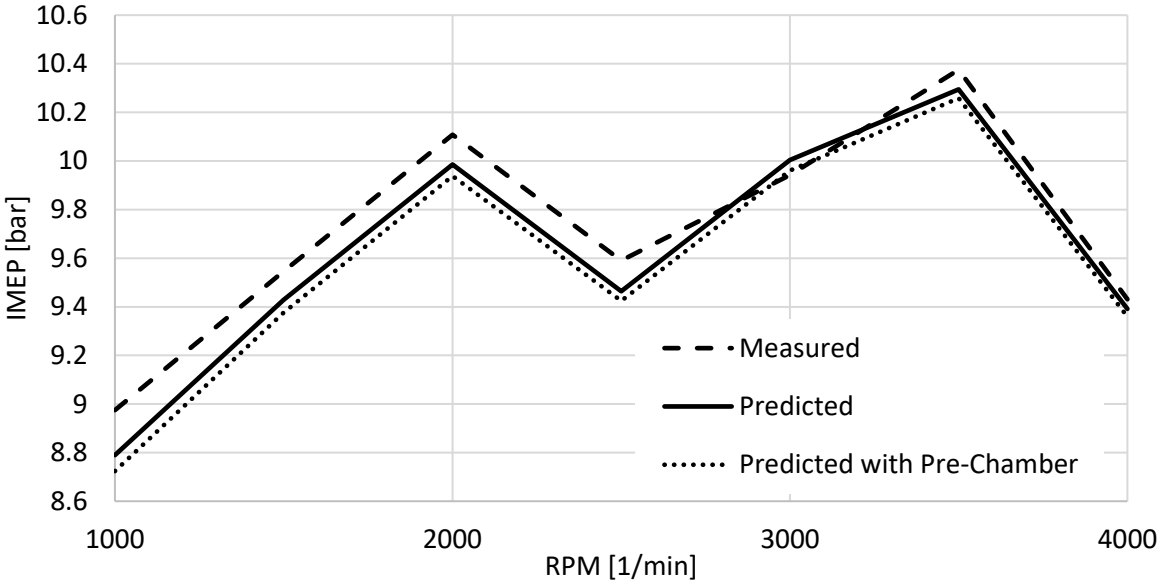

Figure 48 – Comparison of the predicted performance with and without pre-chamber template included in the GT-Power model

The predicted IMEP in Figure 48 shows good agreement between the results from Section 5.1 and those obtained in this chapter. With the pre-chamber parameters based on the insight gained in Section 5.3, including the pre-chamber template in the 1-D model no longer hinders the model's performance and can be therefore included in the simulations without a severe penalty on the quality of the results. However, it needs to be stated that the extrapolation carried out in this chapter is extremely rudimental and it can't provide any deeper understanding of the pre-chamber main chamber coupling. For future efforts it is necessary to implement in-pre-chamber pressure measurements to the current test bed.

5.5 Second attempt

With the acceptable performance obtained from the TPA model with a pre-chamber template included a final attempt to obtain a working combined fuel system + SCRE model was conducted (Attachment 24).

The main fuel injector is now controlled with a PID controller to allow for a close loop lambda control. The principle described in Section 4.3 still stands, the PID controller only controls the length of the period during which the discharge coefficient is set to 1.

Initially the performance was once again validated with the pre-chamber injector closed i.e. in a passive mode with fuel system delivering only into the intake port. The performance is lower to that achieved in Section 5.4 – about 2% throughout the whole speed range (Figure 49).

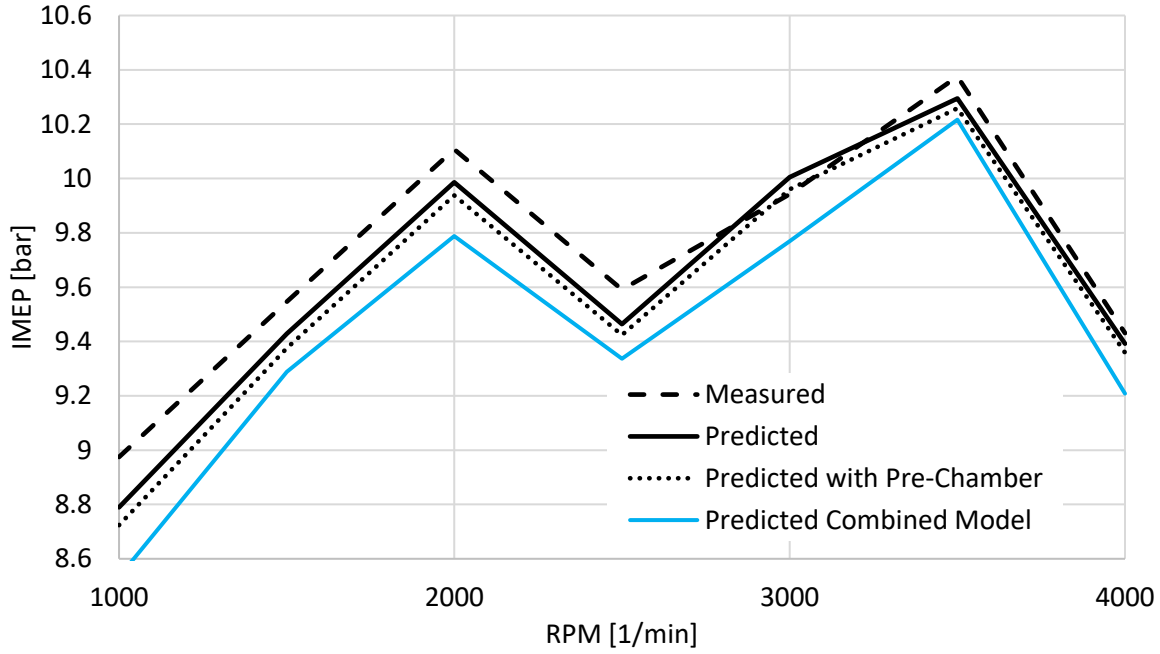

Figure 49 – Predicted performance of the Combined Model, relative to other results

Examination of the results showed that the probable cause is a smaller amount of fuel burned in the main chamber. Multiple sub causes can be found. Firstly, the active pre-chamber is larger in volume (Table 3), trapping and later burning more fuel inside. Secondly, as fuel is forced inside the pre-chamber during compression some of this fuel ends up in the fuel supply lines upstream of the pre-chamber and downstream of the check-valve (see Figure 15, Table 3) where it can't participate in the combustion process and remains until it is scavenged late during power stroke. Further fuel is forced into the fuel lines by the pre-chamber combustion. Lastly, the aforementioned error in the pre-chamber fuel mass

calculation is substantiated by the larger pre-chamber and inclusion of the fuel system[7]. These effects at 1500RPM can be quantified as

$$\Delta m_{burnCYL} - \Delta m_{burnPC} - \Delta m_{error} - m_{fuel\ lines}{}^{8} = 0.38 - 0.11 - 0.06 - 0.19 = 0.02mg \cong 0 \quad (8)$$

Qualitatively this kind of behaviour seems reasonable[9] but it can't be validated without experimental data or CFD results.

Finally, the simulation was run once more with the pre-chamber fuel delivery activated i.e. active mode and the results are compared with the fuel system pressure oscillations results from Section 4.8 (Figure 50,51). Good agreement is obtained between the models (only variant with the main injector is considered). Detailed results are available in Attachment 25 and 26.

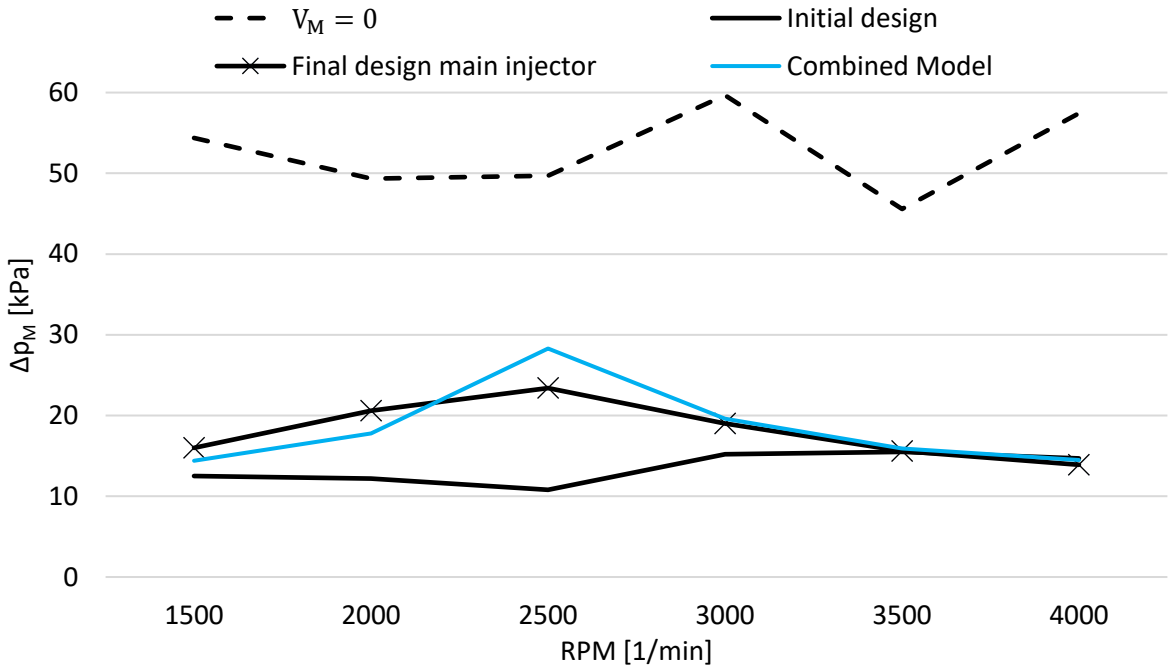

Figure 50 - Δp_M predicted with the Combined Model in comparison to previous results

[7] It appears that the error is present with all orifices connected to the pre-chamber not only the one that connects it to the main chamber. During power stroke the fuel trapped in the fuel lines can be seen flowing back to the pre-chamber through the connecting orifice but no effect on the predicted pre-chamber fuel mass is present. This fuel isn't included in m_{error} in Equation 8 since it is already considered in $m_{fuel\ lines}$.

[8] $m_{fuel\ lines} = m_{fuel\ lines\ compression} + m_{fuel\ lines\ combustion} = 0.16 + 0.03 = 0.19mg$

[9] Apart from the fuel mass error. The amount of fuel forced into the fuel lines by the pre-chamber combustion could be of question as well, but the final value is already small.

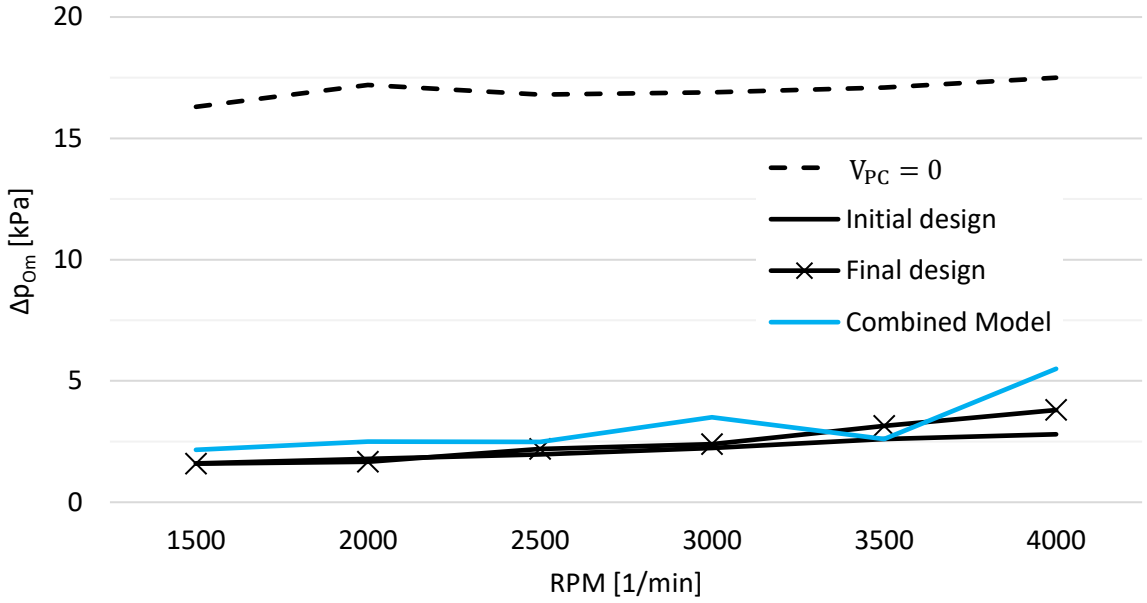

Figure 51 - Δp_{Om} predicted with the Combined Model in comparison to previous results

6 Conclusion

In the first part of this thesis a fuel system for a single cylinder research engine - aimed at simultaneous fuel delivery into an intake port and into an active pre-chamber - was developed. The developed fuel system includes an injector controlling the fuel delivery into the pre-chamber and a secondary port injector to investigate effects of a fuel homogeneity. Pressure oscillations in the system were investigated with the help of a 1-D model and appropriate damping vessels were proposed to limit these oscillations. The system was implemented into an existent test bed without significant alterations of the current setup.

These efforts were completed up to the relevant manufacturing drawings. At this point all that remains is manufacturing, assembly and possible subsequent experimental validation of the predicted pressure oscillations in the system.

Efforts described in the second part of this thesis aimed at combining the developed 1-D Fuel System model with a 1-D engine model. To achieve this the pre-chamber main chamber coupling was investigated on available CFD results and the gained insight was then extrapolated to the considered operating points. Behaviour of the GT-Power pre-chamber template was also inspected, discovering a possible error in the pre-chamber fuel mass calculation. The resulting model demonstrated acceptable performance and was used to further validate the fuel system pressure oscillations predicted in first part of this text. Comprehension gained during the journey to make the Combined Model operational provides valuable experience for future 1-D simulations.

Many assumptions were made during the extrapolation of the CFD results leading to a clear conclusion that in-pre-chamber pressure measurements need to be implemented into the current test bed. Such data are required for better understanding of the pre-chamber related phenomena and for validation of the presented presumptions. If properly validated the developed model could provide added apprehension of the pre-chamber main chamber coupling and the related fuel flows.

References

[1] Road transport: Reducing CO2 emissions from vehicles. European Commission [online]. Brussel, 2017 [Accessed 2021-4-26]. Available from: https://ec.europa.eu/clima/policies/transport/vehicles_en

[2] Fast Facts on Transportation Greenhouse Gas emissions. United States Environmental Protection Agency [online]. Washington, D.C., 2018 [Accessed 2021-4-27]. Available from: https://www.epa.gov/greenvehicles/fast-facts-transportation-greenhouse-gas-emissions

[3] Emissions of air pollutants from transport. European Environment Agency [online]. Copenhagen, 2017 [Accessed 2021-4-26]. Available from: https://www.eea.europa.eu/data-and-maps/indicators/transport-emissions-of-air-pollutants-8/transport-emissions-of-air-pollutants-8

[4] BERNARD, Yoann, Uwe TIETGE, John GERMAN a Rachel MUNCRIEF. Determination of real-world emissions from passenger vehicles using remote sensing data. London, 2018. TRUE.

[5] GHOLAMISHEERI, Masumeh, Indrek S. WICHMAN a Elisa TOULSON. A study of the turbulent jet flow field in a methane fueled turbulent jet ignition (TJI) system. *Combustion and Flame*. 2017, Vol. 183, 194-206. ISSN 00102180. doi:10.1016/j.combustflame.2017.05.008

[6] QIN, Fei, Ashish SHAH, Zhi-wei HUANG, Li-na PENG, Per TUNESTAL a Xue-Song BAI. Detailed numerical simulation of transient mixing and combustion of premixed methane/air mixtures in a pre-chamber/main-chamber system relevant to internal combustion engines. *Combustion and Flame*. 2018, Vol. 188, 357-366. ISSN 00102180. doi:10.1016/j.combustflame.2017.10.006

[7] Desantes, J.M., Novella, R., De La Morena, J., and Pagano lng, V., “Achieving Ultra-Lean Combustion Using a Pre-Chamber Spark Ignition System in a Rapid Compression-Expansion Machine,” SAE Technical Paper 2019-01-0236, 2019. doi:10.4271/2019-01-0236.

[8] Novella, R., Pastor, J., Gomez-Soriano, J., Barbery, I. et al., “Experimental and Numerical Analysis of Passive Pre-Chamber Ignition with EGR and Air Dilution for Future Generation Passenger Car Engines,” SAE Technical Paper 2020-01-0238, 2020. doi:10.4271/2020-01-0238.

[9] Vavra, J., Syrovatka, Z., Vitek, O., Macek, J. et al., “Development of a Pre-Chamber Ignition System for Light Duty Truck Engine,” SAE Technical Paper 2018-01-1147, 2018, doi:10.4271/2018-01-1147.

[10] Vávra, J, Syrovátka, Z, Takáts, M, & Barrientos, E. "Scavenged Pre-Chamber on a Gas Engine for Light Duty Truck." Proceedings of the ASME 2016 Internal Combustion Engine Division Fall Technical Conference. ASME 2016 Internal Combustion Engine Division Fall Technical Conference. Greenville, South Carolina, USA. October 9–12, 2016. V001T03A014. ASME. https://doi.org/10.1115/ICEF2016-9423

[11] Syrovatka, Z., Vitek, O., Vavra, J., and Takats, M., “Scavenged Pre-Chamber Volume Effect on Gas Engine Performance and Emissions,” SAE Technical Paper 2019-01-0258, 2019, doi:10.4271/2019-01-0258.

[12] Syrovatka, Z., Takats, M., and Vavra, J., "Analysis of Scavenged Pre-Chamber for Light Duty Truck Gas Engine," SAE Technical Paper 2017-24-0095, 2017, doi:10.4271/2017-24-0095.

[13] AKSHAY, Kamane. Gaseous Fuel Injection for Engine with a Scavenged Pre-chamber. Prague, 2019. Master’s Thesis. CTU.

[14] WINTER, Vojtech. Intake manifold for experimental spark ignition single cylinder engine. Prague, 2019. Bachelor's Thesis. CTU.

[15] *Šroubení SUPERLOK: Ventile & Fittings Praha* [online]. [Accessed 2021-6-2]. Available from: https://www.ventile.cz/produkty/instrumentace/sroubeni/sroubeni-superlok?manufacturer_id=

[16] TAKÁTS, Michal. *Měření emisí spalovacích motorů*. Praha: České vysoké učení technické, 1997. ISBN 80-010-1632-3.

List of Figures

List of Tables

List of Attachments

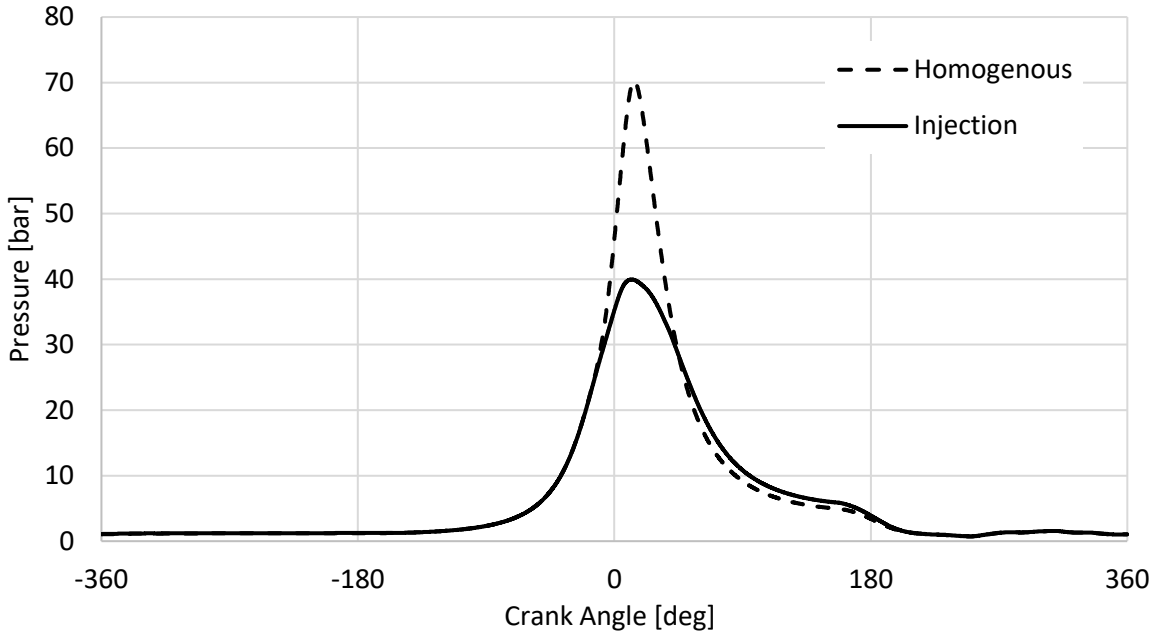

Attachment 1 – Effect of homogeneity on in-cylinder pressure based on CFD simulations

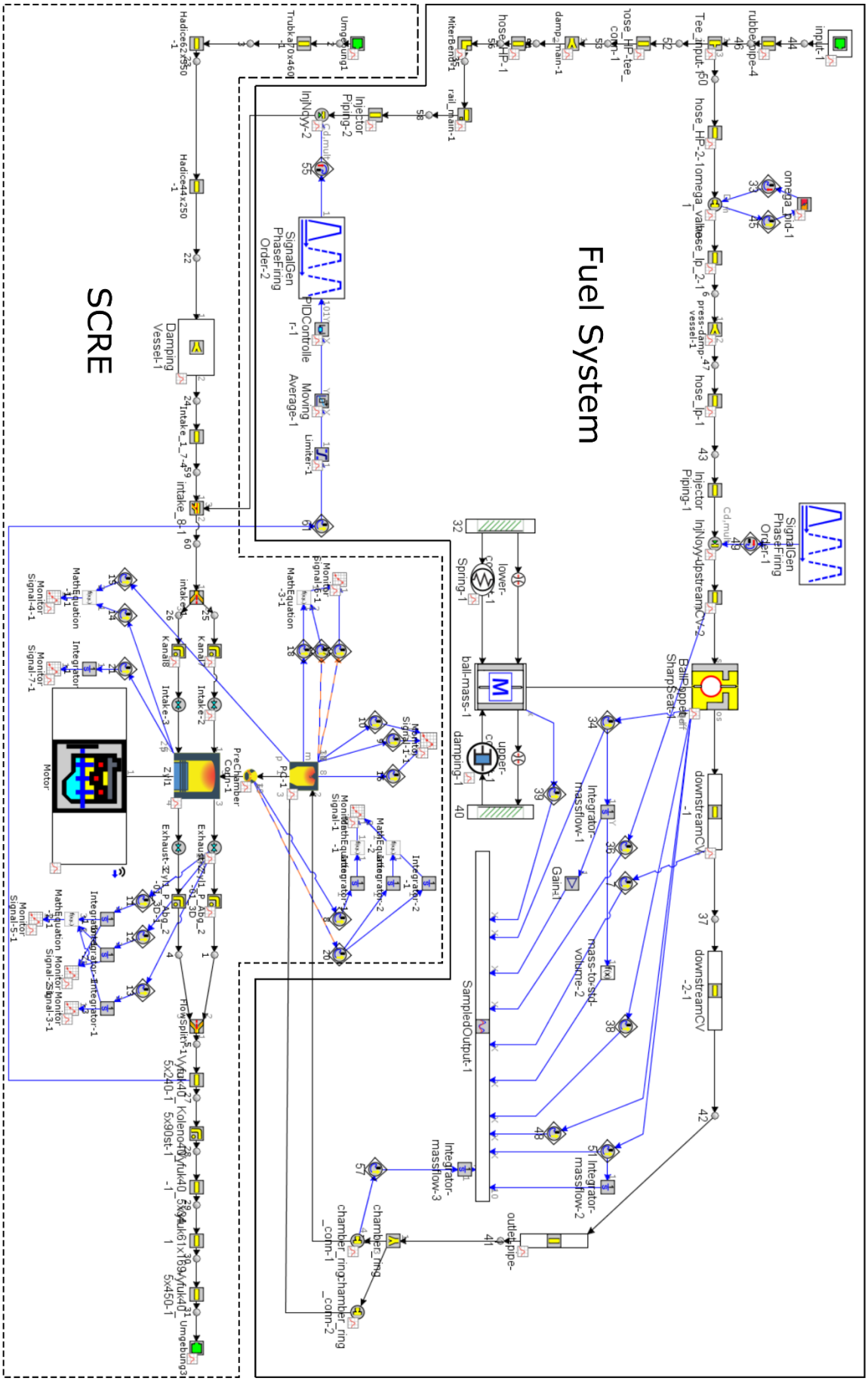

Attachment 24 – 1-D Combined Model Schematics

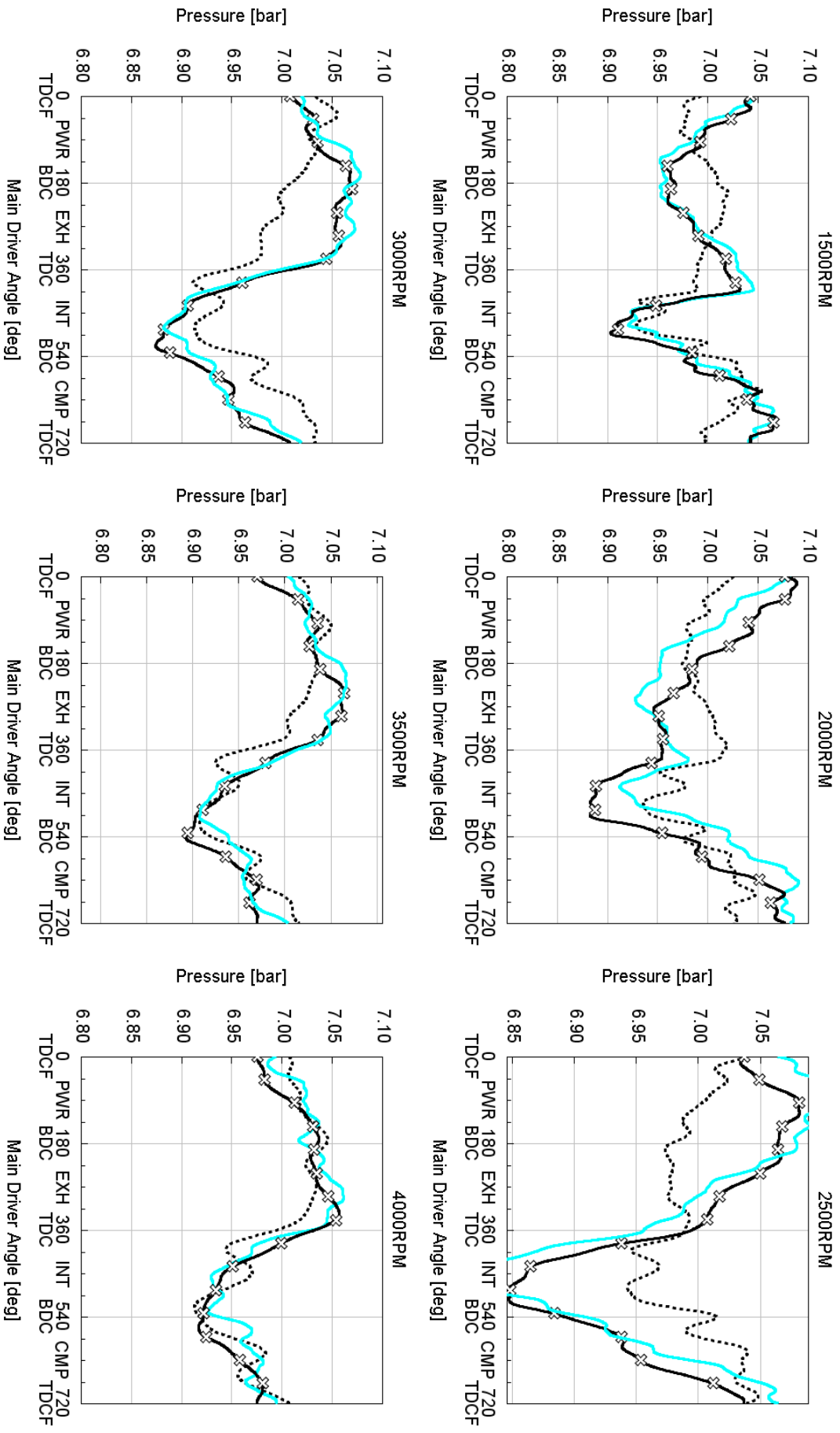

Attachment 25 – p_M predicted with different models at the considered operating points

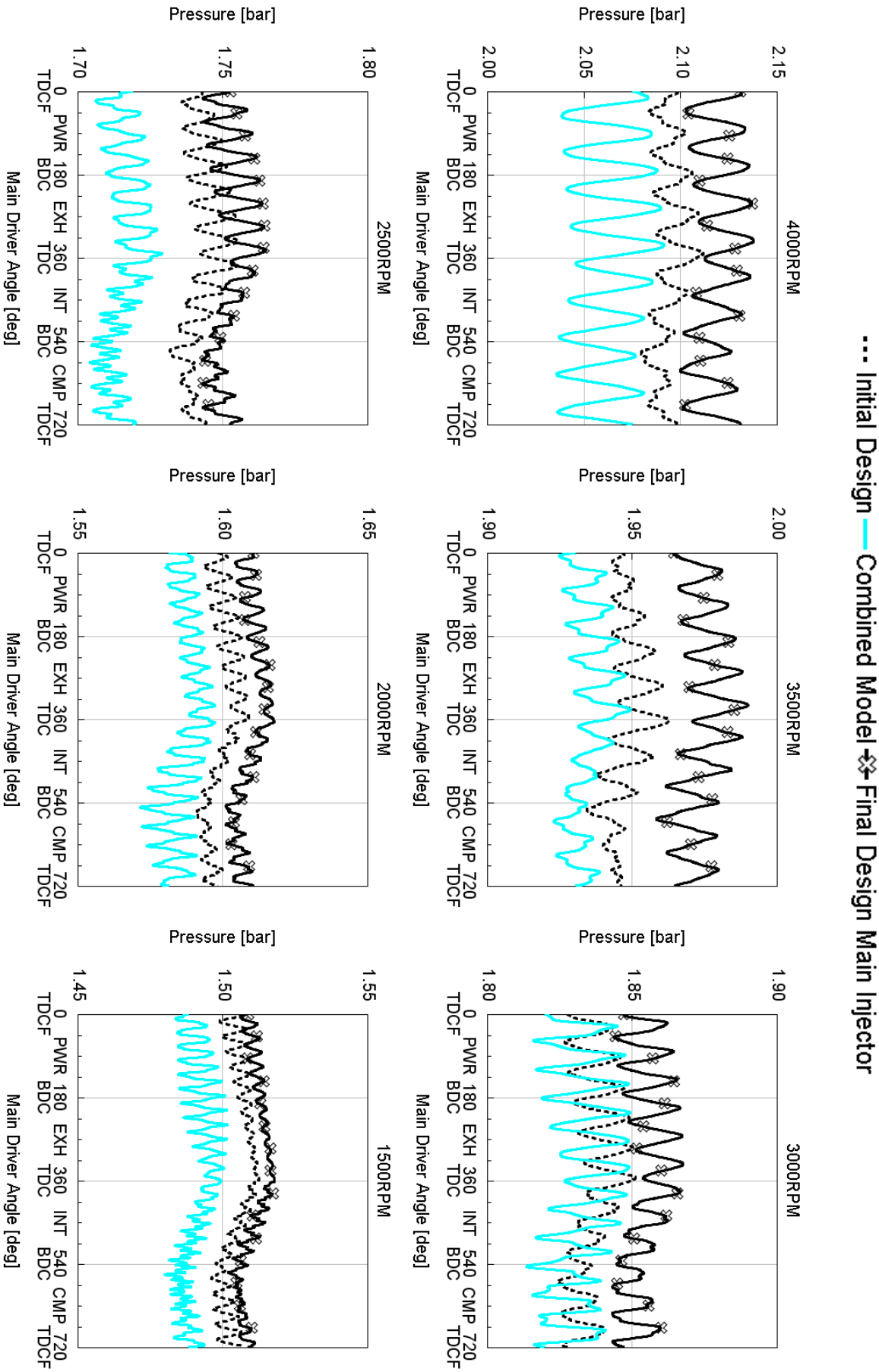

Attachment 26 – p_{Om} predicted with different models at the considered operating points